DESIGN OF HYBRID CABLE-CONSTRAINED PARALLEL MECHANISMS FOR WALKING MACHINES

A Thesis Submitted to
The Graduate School of Engineering and Science of
İzmir Institute of Technology
in Partial Fulfillment of the Requirements for the Degree of

MASTER OF SCIENCE

in Mechanical Engineering

by
Murat DEMİREL

July 2018
İZMİR

We approve the thesis of **Murat DEMİREL**

Examining Committee Members:

Assoc. Prof. Dr. Gökhan KİPER
Department of Mechanical Engineering, İzmir Institute of Technology

---

Prof. Dr. Serhan ÖZDEMİR
Department of Mechanical Engineering, İzmir Institute of Technology

---

Asst. Prof. Dr. Fatih Cemal CAN
Department of Mechatronics Engineering, İzmir Katip Celebi University

9 July 2018

Assoc. Prof. Dr. Gökhan KİPER
Supervisor, Department of Mechanical Engineering, İzmir Institute of Technology

---

Assoc. Prof. Dr. Giuseppe CARBONE
Co-Supervisor, Department of Mechanical Engineering, University of Cassino

---

Prof. Dr. Metin TANOĞLU
Head of the Department of Mechanical Engineering

Prof. Dr. Aysun SOFUOĞLU
Dean of the Graduate School of Engineering and Sciences

ACKNOWLEDGEMENTS

I am very thankful to my supervisor Dr. Gökhan Kiper for his continuous support, valuable advices and patience in every part of this research. Furthermore, I would like to thank to my co-advisor Dr. Giuseppe Carbone and Dr. Marco Ceccarelli for their invaluable guidance during my studies in University of Cassino and South Latium in Italy as an Erasmus exchange student.

A part of this study is carried out at Laboratory of Robotics and Mechatronics (LARM), University of Cassino. During this period, I would like to thank to Dr. Daniel Cafolla and members of LARM for their hospitality and support.

I cannot forget to mention the members of Rasim Alizade Mechatronics Laboratory (RAML) and IzTech Robotics Laboratory (IRL), İzmir Institute of Technology (IzTech). Mr. Emre Uzunoğlu, Mr. Osman Nuri Şahin, Mr. Cevahir Karagöz, Mr. Halil Tetik, Mr. Barış Taner and Ms. Merve Özkahya helped me a lot and I am very thankful for their support.

My deepest gratitude goes foremost to my dear uncle Mr. Bülent Aslantürk for encouraging me in my whole life. Also, I would like to express my deepest appreciation for my beloved parents.

This study has been founded from IzTech Scientific Research Projects program with project number 2016IYTE41.

ABSTRACT

DESIGN OF HYBRID CABLE-CONSTRAINED PARALLEL MECHANISMS FOR WALKING MACHINES

The objective of this thesis study is to propose novel cable-constrained parallel mechanisms for walking machines. According to the literature, hybrid structured parallel mechanisms can overcome mechanical design, control system and workspace limitations compared to other structures.

This thesis study introduces two novel hybrid structured leg mechanisms comprising rigid links and passive cables. Kinematic structure of the proposed mechanisms are ($\underline{UP}$U-2Pa)-(U$\underline{P}$U-2Pa)and ($\underline{U}$U-2Pa)-$\underline{P}$. Both designs have a hip, a knee and a foot platform. Two rotational constraints about horizontal axes are added to the moving platforms by using parallelograms with passive cables. The rotational constraint about the vertical axis is provided by rigid links and joints. Thus, the proposed designs have pure translational motion.

The detailed analysis of the mechanism design with anchored cables is conducted. A CAD model is constructed and a dynamic simulation for human-like gait trajectory is performed in SolidWorks® environment. Once the computed actuator torques and forces are found suitable, a first prototype is built to check the proposed solution. Considering the problems encountered in this first prototype, a second prototype of the ($\underline{U}$U-2Pa)-$\underline{P}$ mechanism is built. The prototype is operated using a real-time PCI controller and experimental results are presented.

The mechanisms presented in this thesis is one of the few cable-constrained parallel manipulator designs in the literature. Such a manipulator design is used for a walking machine for the first time. The prototype and test results are quite satisfactory, so hopefully more detailed research can be conducted on this topic in the future.

ÖZET

YÜRÜME MAKİNALARI İÇİN HİBRİT KABLO KISITLI PARALEL MEKANİZMA TASARIMI

Bu tezin amacı yürüme makineleri için özgün hibrid yapılı kablo kısıtlı paralel mekanizmalar geliştirmektir. Literatür taramasına göre, hibrit yapılandırılmış paralel mekanizmaların diğer yapılara kıyasla mekanik tasarımın, kontrol sistemi ve çalışma uzayı sınırlamalarının üstesinden gelebileceği görülmüştür.

Bu tez çalışmasında önerilen, rijit uzuvlar ve pasif kablolardan oluşan iki özgün hibrit yapıdaki bacak mekanizmalarının kinematik yapıları (UPU-2Pa)-(UPU-2Pa) ve (UU-2Pa)-P şeklindedir. İki bacak tasarımında da sabit taban (kalça), orta platform (diz) ve haraketli platform (ayak) bulunmaktadır. Kablolardan oluşturulmuş pasif paralelogramlar ile hareketli platformların yatay eksenler etrafındaki dönme serbestliği kısıtlanmıştır. Dik eksen etrafındaki dönme serbestliği ise rijit uzuvlar ve mafsallar tarafından kısıtlanlaşmıştır. Böylece, önerilen tasarımlar sadece öteleme hareketine sahip olur.

Bağlantılı kablolarla tasarımı yapılmış mekanizmanın detaylı analizi yapılmıştır. SolidWorks® programı kullanılarak CAD modeli oluşturulmuş ve insan benzeri yürüyüş yörüngesinin dinamik simülasyonu gerçekleştirilmiştir. Hesaplanan eyleyici tork ve kuvvet değerlerinin uygun bulunmasıyla önerilen çözümü kontrol etmek için ilk prototip üretilmiştir. İlk prototipte karşılaşılan problemler düşünüldüğünde, (UU-2Pa)-P mekanizması ikinci prototip olarak üretilmiştir. Bu prototip, gerçek zamanlı PCI denetleyici kullanılarak çalıştırılmış ve deney sonuçları sunulmuştur.

Bu tezde sunulan mekanizmalar, literatürdeki birkaç kablo kısıtlı paralel manipülatör tasarımından biridir. Böyle bir manipülatör tasarımı ilk kez bir yürüyüş makinesi için kullanılmıştır. Prototip ve test sonuçları oldukça tatmin edicidir, bu yüzden gelecekte bu konuda daha detaylı araştırmalar yapılabilir.

TABLE OF CONTENTS

LIST OF FIGURES

LIST OF TABLES

CHAPTER 1

INTRODUCTION

According to *American Heritage College Dictionary* (Mifflin, 1993), a robot is "a mechanical device that can perform a variety of tasks on command or by being programmed in advance". Robotics is a science related with the design, production, theory and applications of robots. Among various types of robots, humanoid robots have received much attention.

This thesis study issues the design of a novel mechanism for biped walking robots. In the following subsections, first kinematic structures of robotic manipulators are briefly presented. Then biped walking machines and their walking modes are explained. After that motivation and aim of the thesis stated. Finally, outline of this thesis presented.

1.1. Kinematic Structures of Robot Manipulators

Manipulators can be classified in terms of their kinematic chain architectures as serial and parallel manipulators (Ceccarelli, 2013). Although most of the existing manipulators are serial anthropomorphic robots, especially ones resembling a human arm, parallel robots are getting popular in the industry. Because parallel manipulators show better performance compared to serial robots in terms of accuracy, rigidity and payload to weight ratio (Merlet, 2006). Also, due to their higher speed and acceleration capacities, they are preferred in applications where process speed is crucial. However, their workspaces are generally smaller compared to serial manipulators of similar size.

Comparison of kinematic architectures of serial and parallel robots can be seen in Figure 1.1. Serial manipulators (see Figure 1.1 (a)) can be modeled as open kinematic chains which links are connected by binary joints. Parallel manipulators (Figure 1.1 (b)) can be modeled as closed kinematic chains. In parallel manipulators the actuated joints can be chosen on the fixed platform of the manipulator. Since actuated joints of the serial manipulators connected consecutively, positioning errors are higher compared to the parallel manipulators.

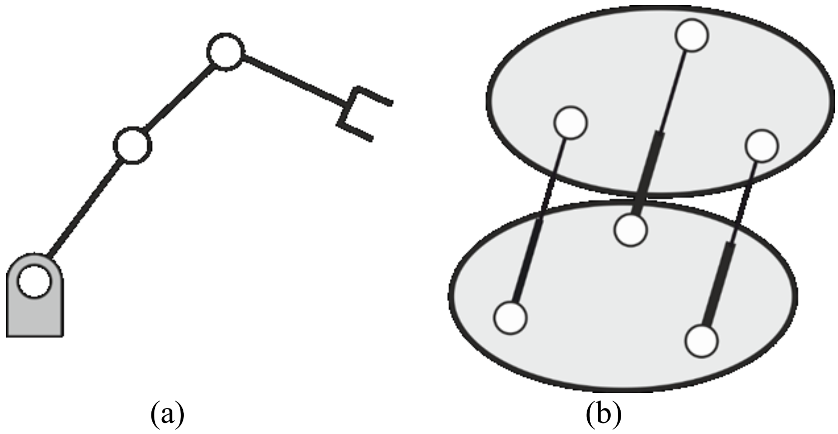

Figure 1.1. Examples of serial and parallel robots, (a) Planar serial robot, (b) Spatial parallel robot.

1.2. Biped Walking Machines

Walking machines are special interest of researchers since the beginning of the technology of transportation machinery due to their better obstacle avoidance capability compared to wheeled systems (Carbone and Ceccarelli, 2005). Figure 1.2 shows the first biped walking machine, WABOT 1, developed at early 70s (Kato, 1973). WABOT 1 was the first robot that can walk few steps. It has limb-control unit, vision unit and a conversation unit (few words in Japaniese). It can measure distances and directions to the objects by using sensors.

Walking machines can operate in two different methods as static walking and dynamic walking. Static walking means that the walking machine is statically stable. In this method, projection of the center of mass (CoM) is kept inside of the foot support area. In other words, if all of the actuators stopped at any moment during the walking, walking machine will be stable. In dynamic walking method, CoM of walking machine can be outside of the support area, while the zero moment point (ZMP) cannot be outside of it (Vukobratović and Stepanenko, 1972). ZMP can be defined as a point in which total moment of biped walking machine on the ground is zero. Static walking has simpler control strategy than dynamic walking. Drawbacks of static walking machines are that their walking speeds are generally slower than dynamic walking machines, and walking machine can only be operated on flat surfaces. On the other hand, dynamic walking machines are faster and can operate on rough surfaces.

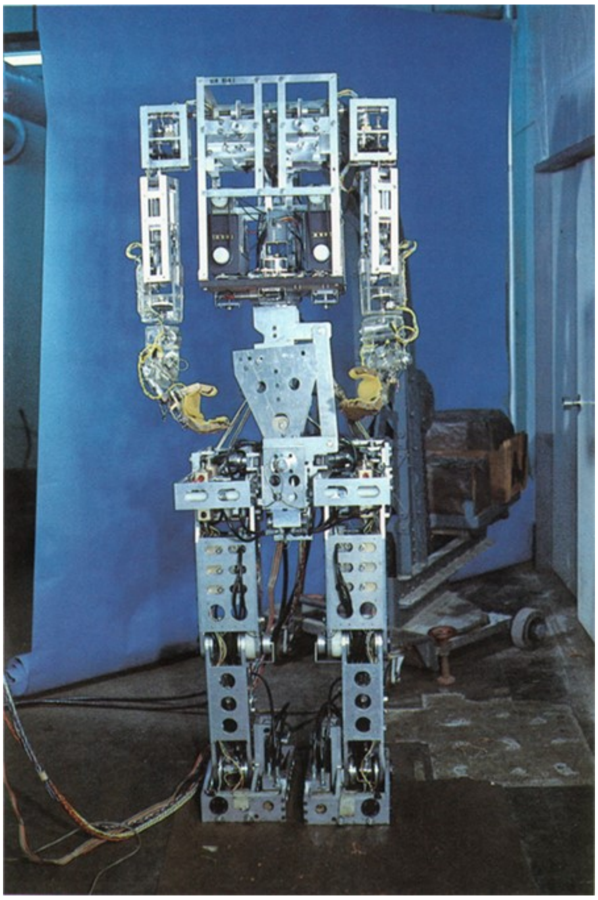

Figure 1.2. First biped walking machine developed in the world.
(Source: Kato and Tsuik, 1972)

1.3. Motivation of The Thesis

Although most of the existing biped walking machines are based on serial kinematic architectures, walking machines with parallel manipulators (PMs) have successful examples as well. If human anatomy is considered, human leg movement can be described as a parallel manipulator because of the muscular system of leg (Ceccarelli and Carbone, 2009). New parallel leg architectures are suggested in (Ceccarelli and Carbone, 2009) which combine rigid links and cables (hybrid structured parallel manipulators). Use of cables enables lightweight design. It is shown that 6 degrees of freedom (dof) of human leg is required for rough terrain adaptability. Less than 6 dof parallel manipulators can be used as leg design for flat surface applications, since orientation dof of leg are not required for this operation. Orientation of the legs can be changed by waist rotation as well. Therefore 3 translational dof is enough for static walking on flat surface. Parallel manipulators (PMs) with 3-dof in translation are called as Translational PMs (TPMs or 3T PMs). Also 4-dof PMs can be considered for walking machines where rotation about a vertical axis is allowed in addition to translations (3T1R PMs).

1.4. Aim of The Thesis

The aim of this work is to propose novel hybrid structured biped walking machines which can perform static walking. In order to design a low-cost and easy-operating walking machine, the proposed walking machines need to have reduced dof (less than 6) leg architecture.

1.5. Outline of The Thesis

This thesis consists of 6 Chapters: Introduction, Literature Survey, Design of The New Hybrid Cable-Constrained Parallel Mechanisms, Performance Analysis of The New Mechanism, Prototype Design and Experimental Validation and Conclusions.

In Chapter 2, literature review of existing 3T PMs, 3T1R PMs, biped walking machines, cable-driven parallel manipulators and hybrid structured parallel manipulators are presented. Later, existing biped walking machines are compared, and possible kinematic structure types are investigated for a new walking machine design.

In Chapter 3, features for walking machine design are explained by investigating human walking and design requirements are given. Then, conceptual designs of two novel hybrid structured biped walking machines are presented with assessed design requirements. At the end of Chapter 3, one of the novel designs is selected.

In Chapter 4, kinematic analysis of the new mechanism has been worked out. A model of the new mechanism is developed in SolidWorks® environment, and workspace of the mechanism is computed. CAD model is tested with simulation of typical human-like gait trajectory. Then, a first prototype has been manufactured and experimental validation of first prototype is presented.

In Chapter 5, a prototype of the new leg mechanism is built and experimental validation of one leg is presented for investigating the operational performance of new walking machine. A prescribed motion of human-like walking gait is designed for operational performance analysis. Then experimental results are presented for a given human-like walking gait.

The conclusions of the thesis are presented in Chapter 6. Contributions of the study are stated, and possible improvements are discussed to utilize the new walking machine design for a humanoid robot.

CHAPTER 2

LITERATURE SURVEY

In this chapter, a literature survey on the existing 3T PMs, 3T1R PMs, biped walking machines, cable-driven parallel manipulators (CDPMs) and hybrid structured parallel manipulators are presented. Firstly, the existing robots are introduced based on their leg architectures. Then, characteristic and walking performances of existing solutions are discussed.

2.1. Translational Parallel Manipulators

The most famous robot with 3 translational dof is Clavel's Delta Robot (Clavel, 1990) shown in Figure 2.1 (a). Delta robots are generally used for pick and place applications in the industry. Each leg of this robot has same kinematic chains RRP_aR where P_a is a planar parallelogram loop. Another type of Delta Robot is achieved by replacing rotary actuators on the fixed platform by linear actuators (called as linear Delta or Linapod) (Beomonte et al., 1996). Linapods are used as an alternative of Cartesian Robots in 3D printing applications. A 3-UPU mechanism designed by Tsai is shown in Figure 2.1 (b) (Joshi and Tsai, 2003). There are other 3-UPU designs differing according to the configuration of the universal joints (Boztaş, 2017). Each leg of the mechanism has 5 dof and restricts one rotational dof of the moving platform (independent from each other). Each prismatic joint is driven by a linear actuator.

Other three examples shown in Figure 2.2 have cylindrical joints in their leg structures. CCR (Figure 2.2 (a)) and CPU (Figure 2.2 (b)) legs have 5 joint dof in each like other examples (Callegari et al., 2005). 3-RPC mechanism shown in Figure 2.2 (c) possesses motions of pure translation (Callegari and Tarantini, 2003). Note that generically a 3-RPC mechanism would be immobile. However, with specific joint configurations, an overconstrained 3-RPC PM can be obtained as a 3T PM. However, with specific joint configurations, an overconstrained 3-RPC PM can be obtained as a 3T PM.

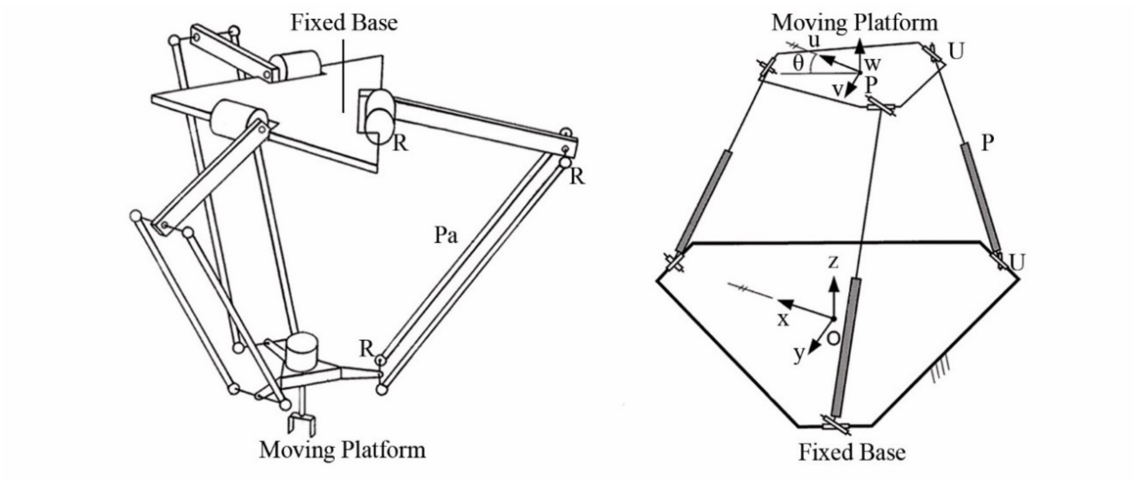

(a) (b)

Figure 2.1. Examples of TPMs (a) Delta robot (Source: Clavel, 1990), (b) 3-UPU mechanism (Source: Joshi and Tsai, 2003).

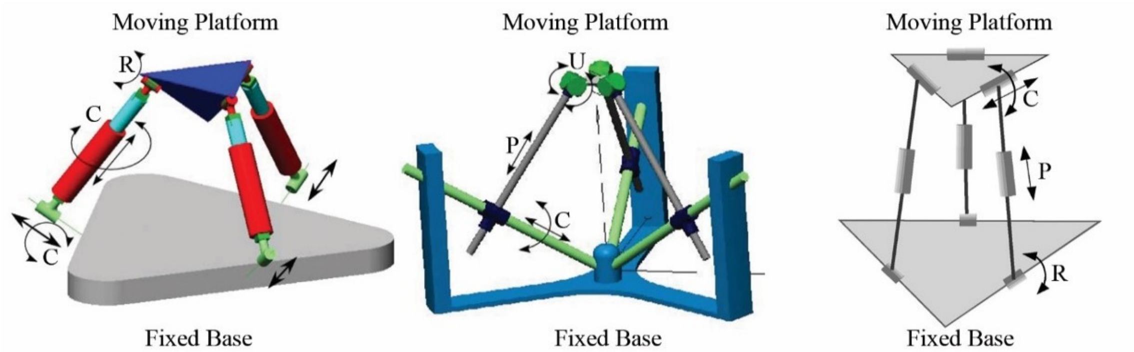

(a) (b) (c)

Figure 2.2. Examples of TPMs with C joint in leg structure (a) 3-CCR Mechanism (Source: Callegari et al., 2005), (b) 3-CPU Mechanism (Source: Callegari et al., 2005), (c) 3-PRC Mechanism (Source: Callegari and Tarantini., 2003).

Legs of the mechanism shown in Figure 2.3 (a) includes parallelogram loops and revolute joints (Tsai et al., 1996) which has same structure with the Delta Robot. Another example is 3-URC mechanism (Di Gregorio, 2004) (see Figure 2.3 (b)). Each leg has three revolute pairs and one passive cylinder pair. Revolute joints attached to the base are actuated. The study shown in Figure 2.3 (c) has RRRRP leg structure with 5-dof legs which do not have rotation singularities (Carricato and Parenti-Castelli, 2003).

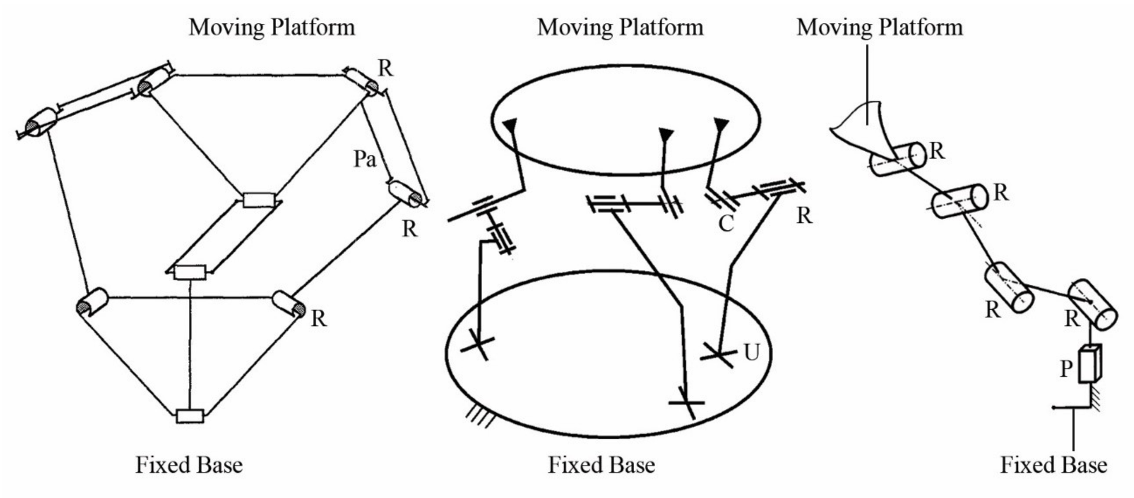

Figure 2.3. Other examples of TPMs (a) 3-RRPaR Mechanism (Source: Tsai et al., 1996), (b) 3-URC Mechanism (Source: Di Gregorio, 2004), (c) 3-RRRRP Mechanism (Source: Carricato and Parenti-Castelli, 2003).

The mechanism shown in Figure 2.4 (a) 3-SPS legs where prismatic joints are actuated and 2- RRPaR passive leg architecture (Romdhane et al., 2002). Another example of an overconstrained 3 TPM is shown in Figure 2.4 (b) as a 3-PRC mechanism, for which each prismatic joint is driven by a linear actuator (Li and Xu., 2006). Other overconstrained TPM shown Figure 2.4 (c) is a 3-CRR mechanism which is driven by linear actuators (Kong and Gosselin, 2002).

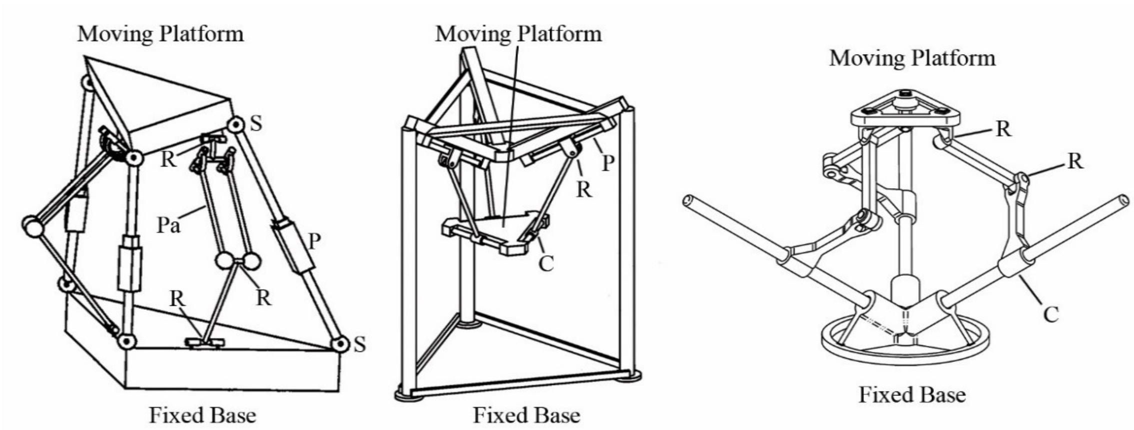

Figure 2.4. Other 3 dof TPMs (a) 3-SPS - 2-RRPaR Mechanism (Source: Romdhane et al., 2002), (b) 3-PRC Mechanism (Source: Li and Xu., 2006), (c) 3-CRR Mechanism (Source: Kong and Gosselin, 2002).

2.2. Parallel Manipulators with Schoenflies Motion

3T1R motion is called the Schoenflies motion. Parallel manipulators with Schoenflies motion (PMSM) have PPPR motion pattern which are controlled by 4 actuated joints. Structural synthesis of PMSMs with 4-legged PPPR motion mechanisms is synthesized in (Kong and Gosselin, 2007), where eleven different configurations are obtained and an example of it 4-RRRRR shown in Figure 2.5 (a). Another example of PMSM with Schoenflies motions is the Isoglide4 which has 3-PRPRR+1-PRPR structure (Gogu, 2007) (Figure 2.5 (b)).

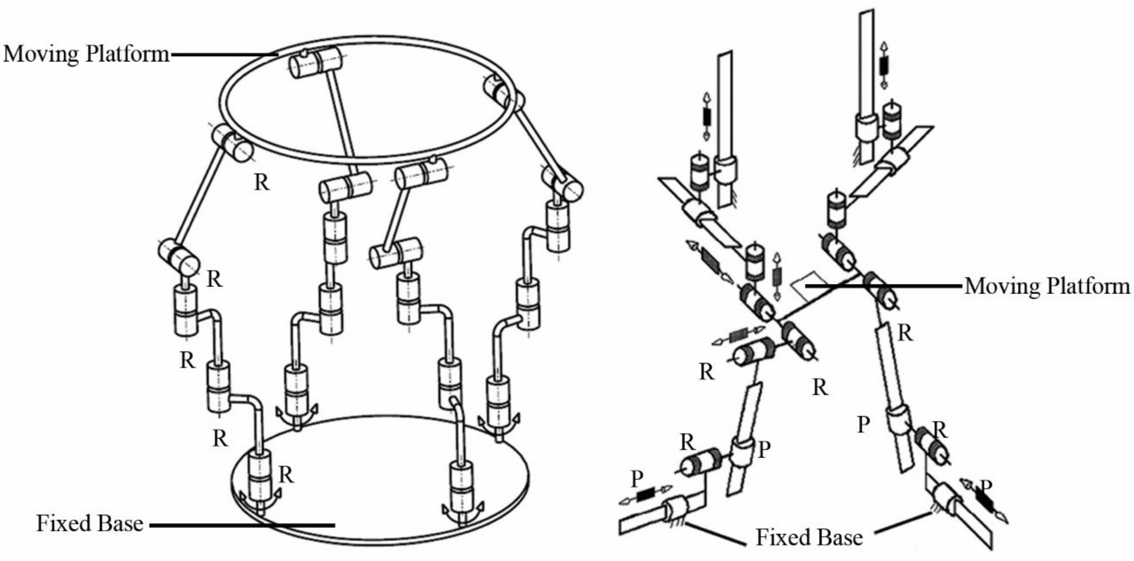

(a) (b)

Figure 2.5. Examples of Parallel Manipulators with Schoenflies motion (a) 4-legged PPPR motion with 4-RRRRR legs (Source: Kong and Gosselin, 2007), (b) 3-PRPRR+1-PRPR PMSM (Source: Gogu, 2007).

Dual4 consists two kinematic chains as RRUR and RRC shown in Figure 2.6 (a). Revolute joints are actuated and both chains are connected to rod (Company et al., 2005). Dual4 can rotate unlimitedly. The RRR parts of the legs can be replaced with RPR or PRR chains to obtain the same motion of the end-effector. Another example of 3T1R PMs is shown below in Figure 2.6 (b) which consists of four hybrid subchains (Kim et al., 2009). Each subchain has 2R-Pa-2R structure.

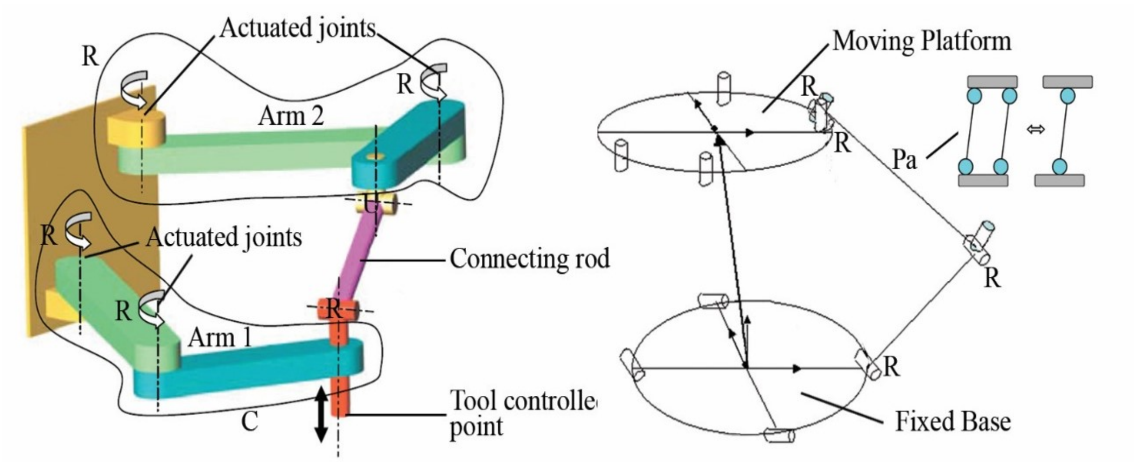

(a) (b)

Figure 2.6. Other examples of PMSM (a) Dual4 (Source: Company et al., 2005), (b) 2R-Pa-2R 3T1R mechanism (Source: Kim et al., 2009).

Some other examples of PMSMs are shown in Figure 2.7. The mechanism in Figure 2.7 (a) has PRRRR legs (Richard et al., 2007). The mechanism in Figure 2.7 (b) has 3UPU structure with one rotary and three prismatic actuators (Lu et al., 2009). The 3T1R mechanism shown in Figure 2.7 (c) has 3-5R structure (Li et al, 2003). First three revolute joints are parallel to the base plane whereas the remaining two joints are perpendicular to them.

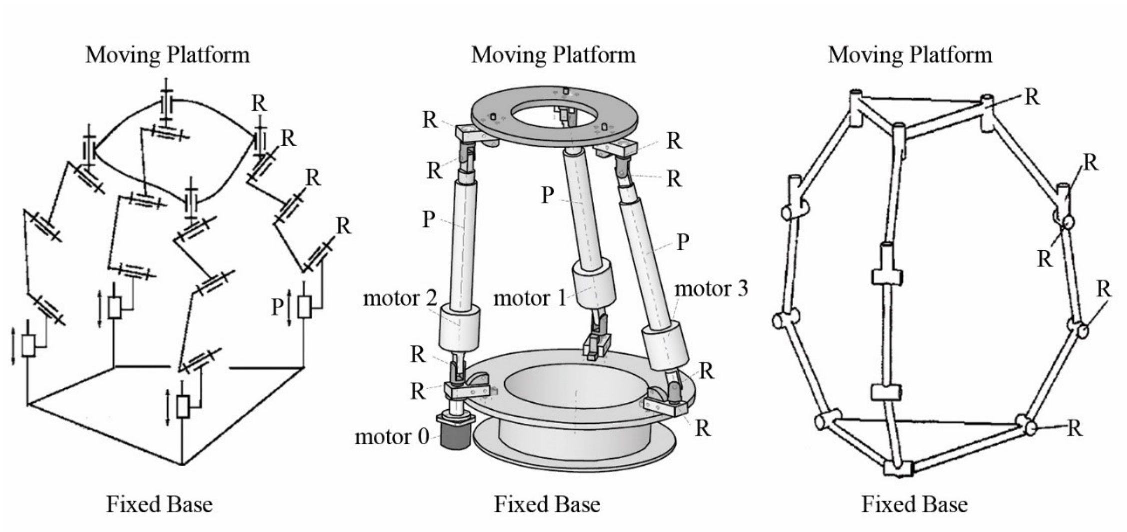

(a) (b) (c)

Figure 2.7. Other examples of PMSM with identical legs (a) 4-PRRRR PMSM (Source: Richard et al., 2007), (b) 3-UPU Mechanism (Source: Lu et al., 2009), (c) 3-5R mechanism (Source: Li et al, 2003).

2.3. Leg Architectures of Existing Biped Walking Machines

In the literature, most of the leg architectures of biped walking machines are based on serial kinematic chains. There are some other machines comprising planar or spatial parallel mechanisms. Examples of serial mechanisms are shown in Figure 2.8. Dof of each leg in Figure 2.8 is 6 and it is described in terms of Hip, Knee and Ankle dof, respectively. Asimo is one of the most famous examples of biped walking machines (Honda Motor Co. Ltd., 2007). Asimo started to develop in 1986 and several models exist. New Asimo shown in Figure 2.8 (a) has 3-1-2 structure, where 3, 1 and 2 are the hip, knee and ankle dof, respectively. It can walk with 2.7 km/h speed. HRP-4C is developed as a cybernetic human which has 3-1-2 leg structure (Kaneko et al., 2009) (Figure 2.8. (b)). It's walking speed is 2.0 km/h. Another example of 3-1-2 structure is WABIAN-2R (WAseda BIpedal humANoid No.2 Refined) shown in Figure 2.8 (c) (Kondo et al., 2008). It can walk with 1.9 km/h speed. BHR (BIT Humanoid Robots) robots are developed by Bejing Institute of Technology (Yu et al., 2014). BHR-5 shown in Figure 2.8 (d) has 3-1-2 structure and this robot is known for playing table-tennis. It can walk with a speed of 1.6 km/h. COMAN (COmpliant HuMANoid Platform) is another 3-1-2 structure which developed by Italian Institute of Technology (Figure 2.8 (e)) (Rocchi et al., 2015). Lola shown in Figure 2.8 (f) has 3-1-2 + 1 passive toe joint architecture and it has maximum 5 km/h walking speed (Richard et al., 2007).

Biped walking machines based on planar and spatial parallel mechanisms are shown in Figure 2.9. EP-WAR (Electro-Pneumatic Walking Robot) is composed of a pantograph and a double articulated parallelogram (Figure 2.9 (a)) (Carbone and Ceccarelli, 2005). Dynamic stability is ensured via the suction cups under the foot. Another example with planar mechanisms, the Chebyshev-pantograph leg is shown in Figure 2.9 (b) (Carbone and Ceccarelli, 2005). Each leg has 1-dof and it's a good example of reduced number of dof to achieve static human walking. WL-16R is based on a type of Gough-Stewart platform (Sugahara et al., 2002) (Figure 2.9 (c)). It is world's first dynamic biped walking machine that can carry a 60 kg adult human. Another example is the 3-UPU mechanism design shown in Figure 2.9 (d) (Wang and Ceccarelli, 2013). It designed to walk in flat surface with a speed of 0.12 km/h and dynamic stability is ensured by rubber spikes under the foot.

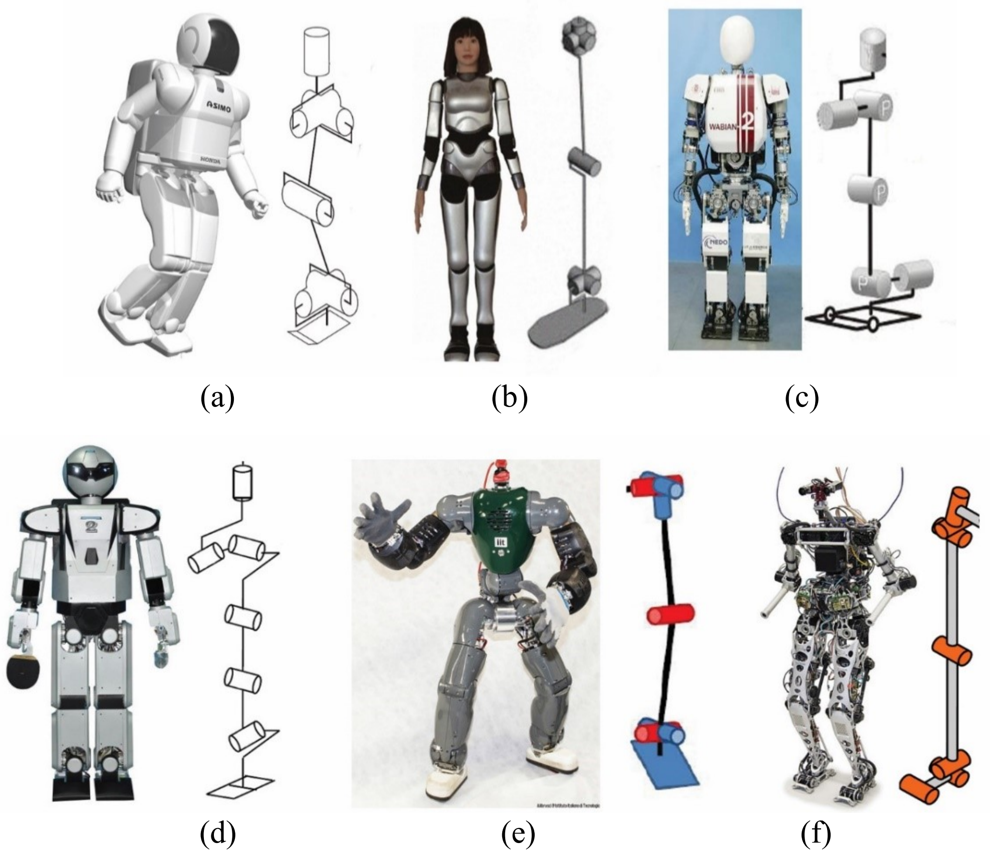

Figure 2.8. Biped walking machines based on serial mechanims (a) Asimo (Source: Asimo, 2018), (b) HRP-4C (Source: Kaneko et al., 2009), (c) WABIAN-2R (Source: Kondo et al., 2008), (d) BHR-5 (Source: Yu et al., 2014), (e) COMAN (Source: Rocchi et al., 2015), (f) Lola mechanism (Source: Richard et al., 2007).

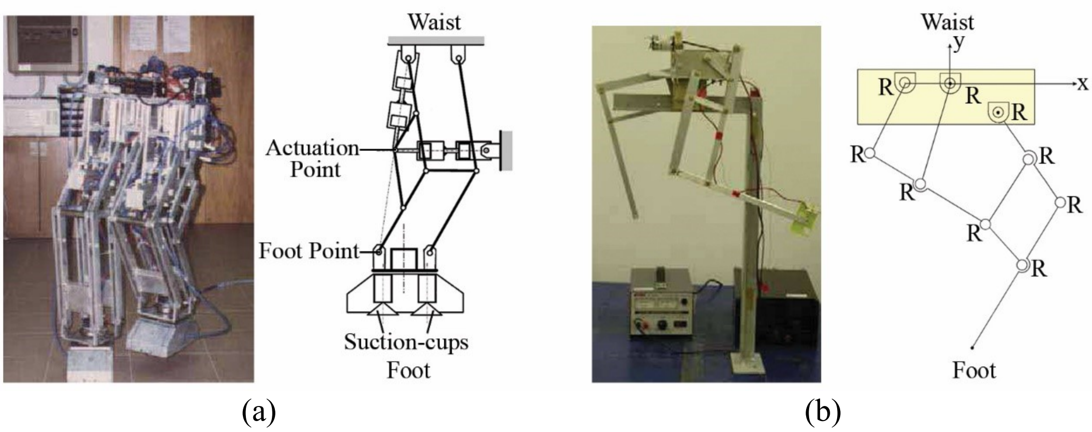

Figure 2.9. Other examples based on linkage mechanisms and parallel mechanisms (a) EP-WAR (Source: Carbone and Ceccarelli, 2005), (b) Chebshev-pantograph leg (Source: Carbone and Ceccarelli, 2005), (c) WL-16R (Source: Sugahara et al., 2002), (d) 3-UPU mechanism (Source: Wang and Ceccarelli, 2013).

(cont. on next page)

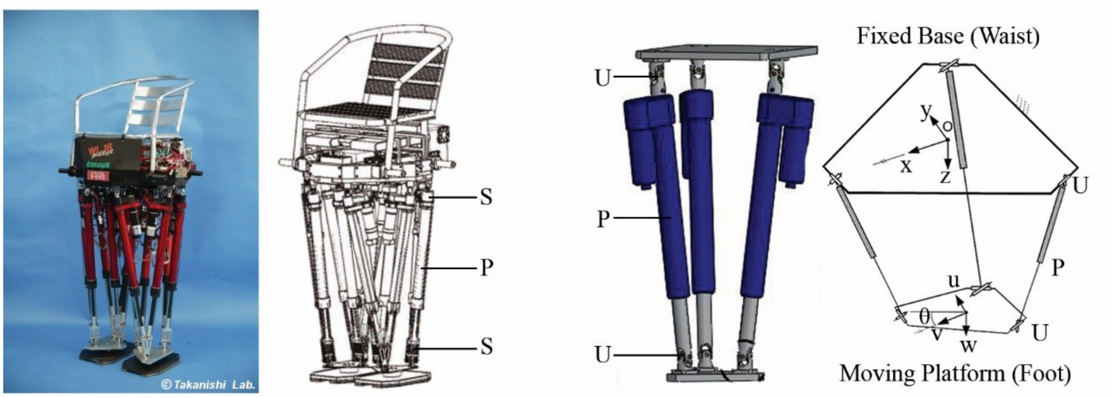

(b) (d)

Figure 2.9 (cont.)

2.4. Cable-Driven Parallel Manipulators

Cable driven parallel manipulators (CDPMs) have cables instead possibly along with some rigid links and position and orientation of the end-effector is controlled by adjusting the cable lengths (Ceccarelli, 2013). CDPMs present several advantages in terms of workspace, payload capacity and dynamic performance because of their efficiency in lightweight and force transmission. Also, their simplicity in structures, reconfigurability, transportability and low costs are other advantages (Behzadipour and Khajepour, 2006). Cables always need to be kept in tension to carry loads and they can only apply pulling action to the end-effector. Thus, in order to have an n-dof CDPM there should be at least n + 1 cables in tension. In some cases, gravity is used instead of a redundant cable necessary to provide tension. In practice, usage of more than one redundant cables is common to have more rigidity. The main drawbacks of cables are ensuring positive tension, collapsing and modeling of them because of the elasticity. The general structure of a spatial CDPM with its components is shown in Figure 2.10.

In the recent decades, several CDPMs were discovered. Robocrane shown in Figure 2.11 (a) is accepted as the first CDPM and it has 6-dof (Albus et al., 1993). It is structure can be considered as similar to Stewart platform with the cables replacing the rigid links. MACARM (Multi-Axis Cartesian-based Arm Rehabilitation Machine) is an example of multi redundant CDPM (see Figure 2.11 (b)) (Mayhew et al., 2005). It is designed for upper limb rehabilitation and it has 8 cables and 6-dof. Two redundant cables are used on this mechanism.

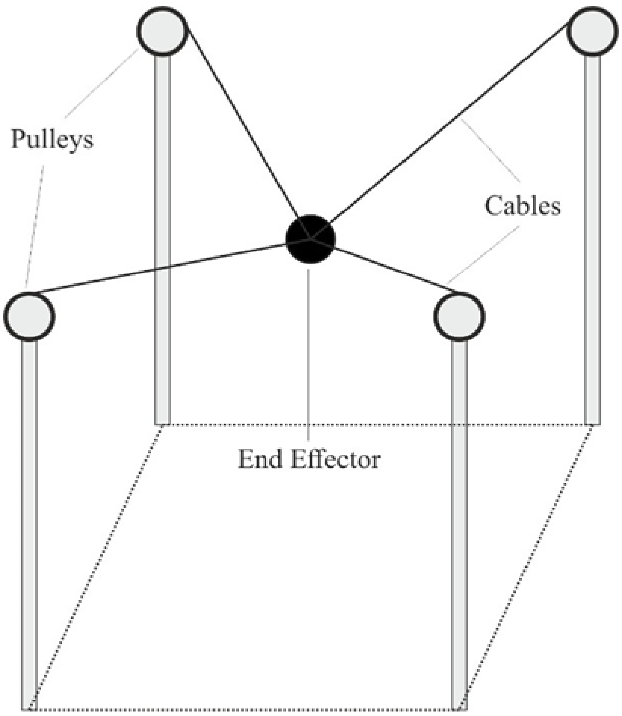

Figure 2.10. General structure of a cable driven parallel manipulator.

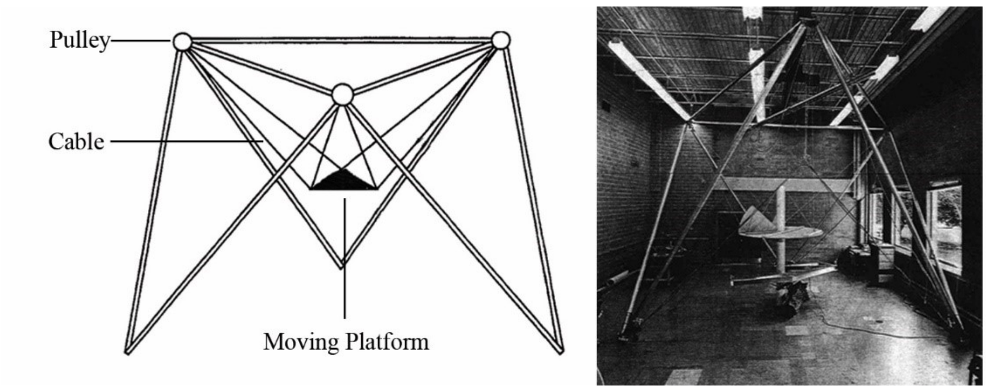

(a)

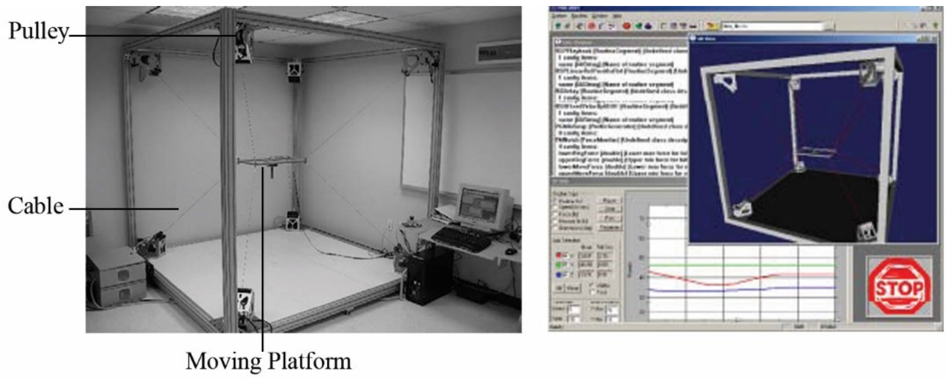

(b)

Figure 2.11. Examples of CDPMs (a) Robocrane first CDPM (Source: Albus et al., 1993), (b) MACARM multi redundant CPDM (Source: Mayhew et al., 2005).

There are two examples of low-cost easy-operation CDPMs designed at Laboratory of Robotics and Mechatronics (LARM), University of Cassino. CaTraSys (Cassino Tracking System) is an example of passive CDPM (Figure 2.12 (a)) (Ottaviano et al., 2010). 6 cables connected to moving platform can track human walking motion. Calowi shown in Figure 2.12 (b) is designed for limb rehabilitation and it consists of four cables (Ottaviano et al, 2007). In this CDPM gravity is used instead of redundant cables.

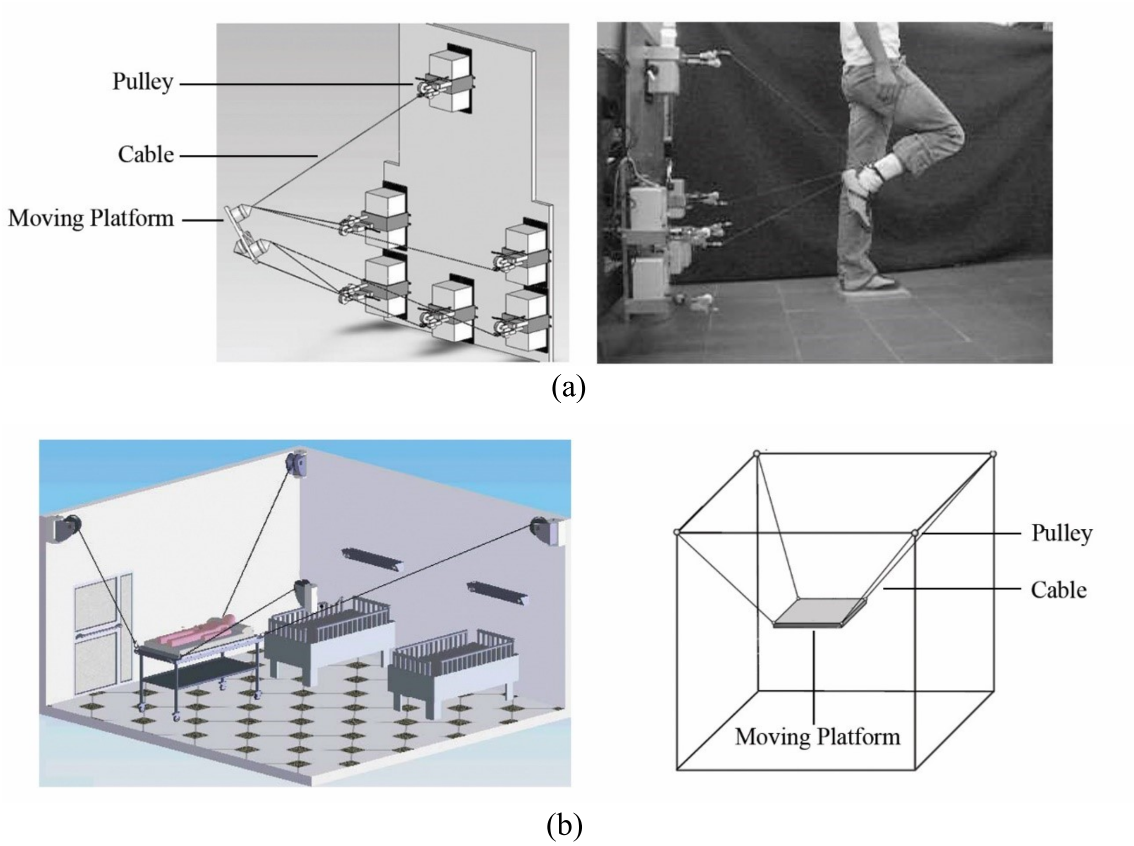

Figure 2.12. Low cost-easy operation CDPM examples of LARM (a) CaTraSys human walking motion tracker (Source: Ottaviano et al., 2010), (b) Calowi limb rehabilitation robot (Source: Ottaviano et al, 2007).

2.5. Hybrid Structured Parallel Manipulators

In the literature, there are few examples of hybrid structures. Betabot is an example of a 3T hybrid manipulator (see Figure 2.13 (a)) (Behzadipour and Khajepour, 2006). It has three parallelogram cable loops and a spine between the base and the end-effector. Cables are considered to be equivalent to SPS legs. Parallelograms eliminate three rotation dofs. Spine is the element which keeps cables in tension by producing force between the base and the end-effector. Actually, it is used instead of a redundant cable. Another example shown in Figure 2.13 (b) is DishBot which has two sets of cables and a spine (Behzadipour and Khajepour, 2006). The first set of cables is active whereas second set is passive. Spine is connected to the base and the end-effector by universal joints. Each passive cable are in series with a pretension spring which produces required force to keep cables in tension. Since length of passive cables are constant, the moving platform is kept parallel to the end-effector. Thus, DishBot has pure translational motion. Figure 2.13 (c) shows C3W4 which is composed of three rigid links (C represents links) and four cables (W represents cables) (Aria et al, 2002). It is designed for heavy material handling inspired from Stewart platform. Each rigid link has SPS structure. It has seven actuators and 6 dof. Other combinations of cables and rigid links (C1W6, C2W5 etc.) are analyzed and a prototype of C3W4 with an extra rod is produced.

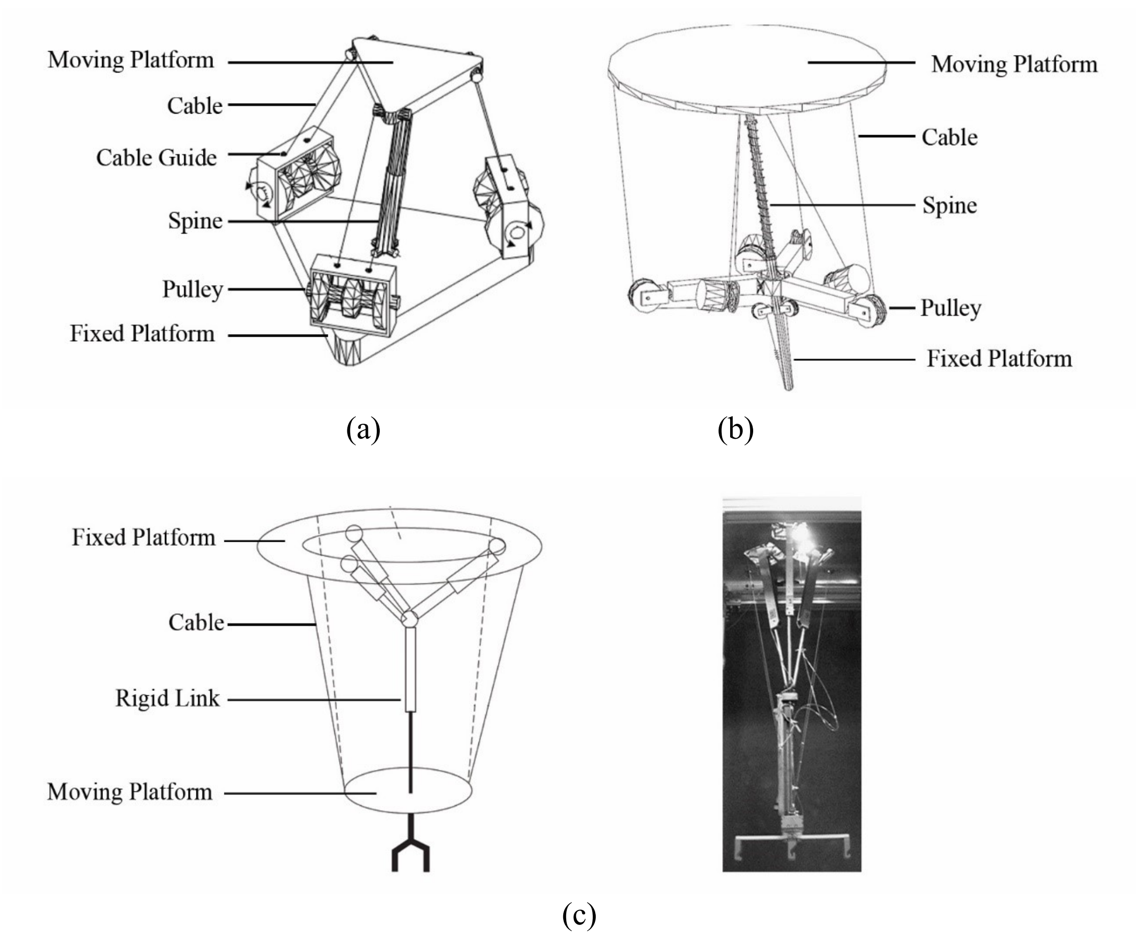

Figure 2.13. Hybrid structure robots (a) Betabot 3T hybrid robot (Source: Behzadipour and Khajepour, 2006), (b) DishBot another 3T hybrid robot with active and passive cables (Source: Behzadipour and Khajepour, 2006), (c) C3W4 6 dof robot for heavy material handling (Source: Aria et al, 2002).

2.6. Comparison of Existing Biped Walking Machines with Possible Kinematic Structure Types for a New Walking Machine

Different types of manipulators are discussed in the previous sections. Existing biped walking machines are compared according to their leg structures in Table 2.1. Serial mechanisms with 6 dof legs have larger workspace than other types, but their payload/weight ratio is lower due to the serial architecture. Also, due to complex joint designs (e.g. 3 dof hip joint) their mechanical designs are complex. Since they have mostly 6 dof legs, their control systems are more complex, and their costs are higher. Due to their larger workspace, serial manipulators are more stable for dynamic walking.

Planar linkage type of biped walking machines are mostly based on 1-dof legs with pantograph linkages. These type of biped walking machines are good in terms of simpler mechanical design, simpler control system and low cost. But they have a predetermined trajectory and therefore low stability. They can only walk with static walking mode. Also, their payload/weight ratio is lower like serial mechanisms.

There are few examples of biped walking machines based on spatial parallel mechanisms with 6 dof legs. Payload/weight ratio of biped walking machines based on spatial parallel mechanisms is the highest. They have better stability than planar parallel types. Spatial parallel mechanisms have limited workspace than serial ones. Since they have 6 dof legs, their mechanical design and control system are complex and their costs are high.

Table 2.1. Comparison of existing biped walking machines.

	Serial Mechanisms (6 dof legs)	Planar Parallel Mechanisms	Spatial Parallel Mechanisms (6 dof legs)
Workspace	Large	Limited	Limited
Payload/Weight Ratio	Low	Low	High
Control System	Complex	Simple	Complex
Stability	High	Low	High
Mechanical Design	Complex	Simple	Complex
Cost	High	Low	High

As mentioned before, hybrid structured parallel walking machines comprising cables and rigid links with less than 6 dof legs still need to be investigated (Ceccarelli and Carbone, 2009). Reduced dof hybrid structured parallel walking machines can overcome limited workspace, complex mechanical design, and complex control system problems of spatial parallel mechanisms. Also, they can be more efficient than rigid serial and parallel solutions in terms of mass, inertia, and cost. Various types of kinematic structures can be utilized to design hybrid structured parallel mechanisms where the cables can be passive or active. Also, more than one rigid link can be used depending on required rigidity.

CHAPTER 3

DESIGN OF THE NEW HYBRID CABLE-CONSTRAINED PARALLEL MECHANISMS

In this Chapter, new hybrid cable-constrained PMs are proposed as low-cost and easy-operation design. As oppose to a cable-driven PM, a cable-constrained PM has unactuated cables. In such a PM, cables are just used to constrain the motion of some of the links.

In the following sections, firstly, human walking is briefly examined. Then, design criteria of the new mechanisms are stated. According to these design features two novel cable-constrained hybrid structured parallel mechanisms are proposed. Their kinematic structures are explained, and conceptual designs are presented. Finally, feasibility of the new mechanisms is discussed.

3.1. Features for Walking Machine Design

In order to design easy-operation and low-cost mechanisms for walking, human walking should be understood, and design features of the new mechanisms are decided accordingly.

3.1.1. Human Walking

Locomotion is a process that an animal moves itself from one geographic position to another and human walking is an activity of locomotion where firstly human body is supported by one leg and then the other (Rose, 1994). During walking, one of the legs is always on the ground and supports the human body. Each leg becomes a support leg in sequence. If one leg is on the ground, this phase is called as single support phase. Two legs are transiently on the ground during support leg change and it is called as double support phase. In order to proceed with details of the human walking, fundamental three reference planes and their axes are shown in Figure 3.1 as sagittal plane, frontal plane, and transverse plane.

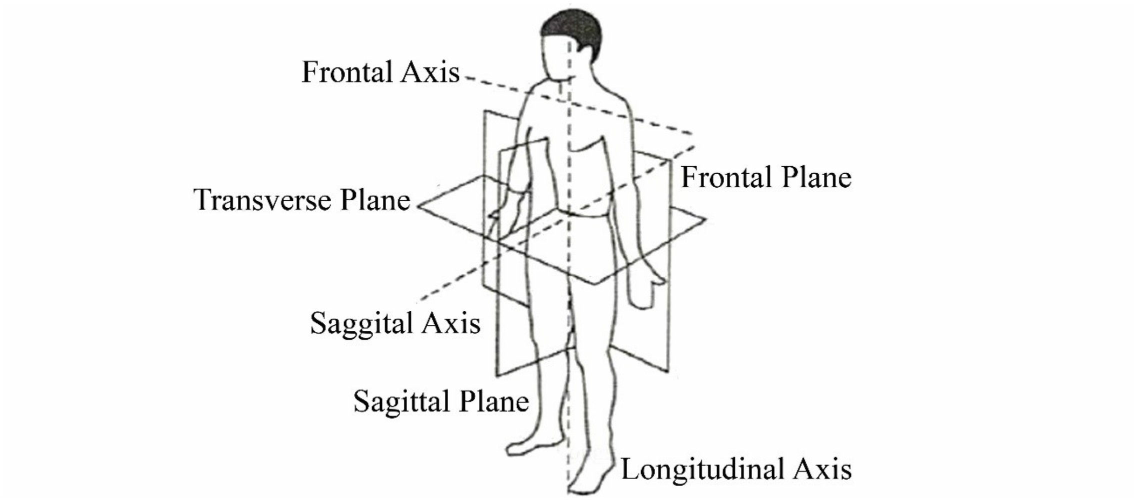

Figure 3.1. Fundamental reference planes for human body.
(Source: Sato et. al., 2010)

A typical human walking gait has 1.0 m step length and step lift up to 0.5 m (Medved, 2000). Path of CoM during a human walk in frontal plane is shown in Figure 3.2, where Figure 3.2 (a) shows the path in sagittal plane and Figure 3.2. (b) is in transverse plane (Saunders et. al., 1953). Path of the CoM is a low amplitude sine-like curve in the sagittal plane and a relatively high amplitude sine-like curve in the transverse plane. It can be seen that human body tries to balance the CoM on support leg.

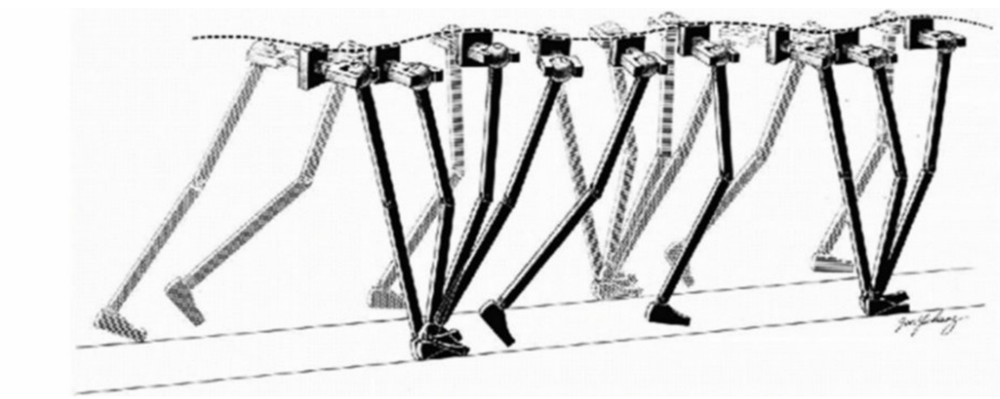

(a)

Figure 3.2. CoM path of human body during walking in frontal plane (a) sagittal plane, (b) transverse plane (Source: Saunders et. al., 1953).

(cont. on next page)

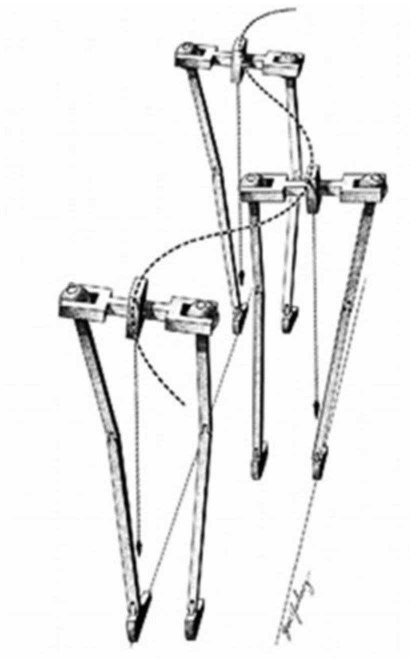

(b)

Figure 3.2 (cont.)

Walking cycle can be defined in two phases, firstly stance phase and then swing phase. Stance phase means foot is on the ground and swing phase means it is not. Walking cycle of human is shown in Figure 3.3 (Rose, 1994). Stance phase includes 62% of the walking gait and rest is swing phase. Two types of events occur during walking as foot strike and foot off.

The gait is started with double leg support at the time of right foot strike (initial double support). After 12% of the motion, the left foot lifts off (opposite foot off) and the gait continues with single support leg (single limb stance) for 38% of the motion. This period ends as the left foot strike time (opposite foot strike). Then second double leg support period continues until the right foot lifts off for another %12 of the motion. Stance phase also ends with this event.

Swing phase starts with the right foot off and ends with right foot strike. This phase is divided into three periods in Figure 3.3 as initial swing, mid swing, and terminal swing. The initial swing period starts with right foot off up to foot clearance. After that, the gait continues with mid swing period up to lower leg become in vertical position (tibia vertical). Then, rest of the gait is called as terminal swing period and it is ended by right foot strike.

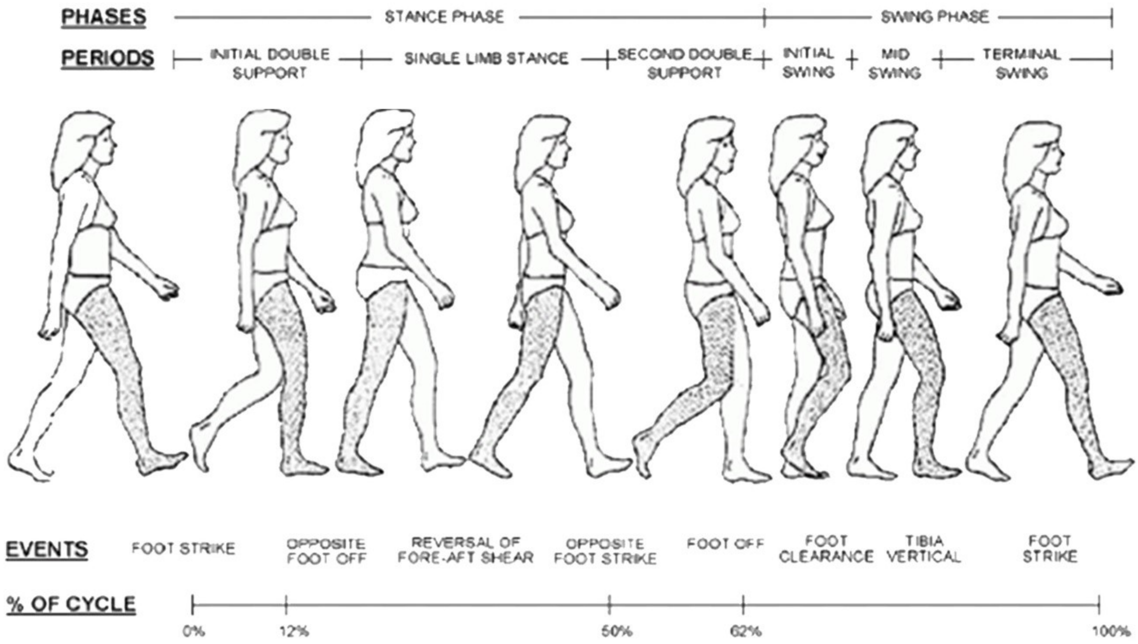

Figure 3.3. Walking cycle of a human.
(Source: Rose, 1994)

Hip, knee and ankle motions in sagittal plane is shown in Figure 3.4 (Rose, 1994). Figure 3.4 shows the gate cycle when the hip, the knee and the ankle move by 40°, 60° and 35° of rotation, respectively. While positive values indicate flexion, negative values represent extension in Figure 3.4. These motion data acquired from 36 people of subject for 10 sets of experiments.

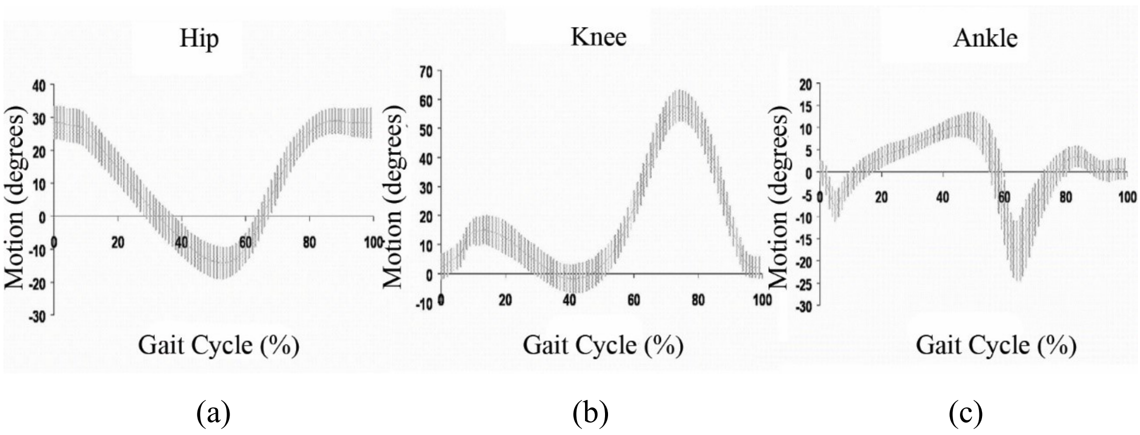

Figure 3.4. Motions in sagittal plane (a) hip motion (b) knee motion (c) ankle motion.
(Source: Rose, 1994)

3.1.2. Design Features of the New Mechanisms

As previously stated, reduced dof hybrid structured parallel mechanisms can overcome limited workspace, complex control system, high inertia and high cost problems of legs comprising spatial parallel mechanisms with 6 dof. Also, various types of kinematic structures can be utilized to design hybrid structured parallel mechanisms.

Since orientation dofs of walking machines are required for rough terrain adaptation and turning requirement of foot can be solved by waist rotation (Ceccarelli and Carbone, 2009), 3 dof TPM leg structure is suitable for new mechanisms. New mechanisms should be able to operate in static walking mode on flat surface applications and can accomplish fundamental walking functions, just as, straight walking, direction change and crossing over obstacle.

Cables used in hybrid structured parallel mechanisms can be active or passive, i.e., mechanisms can be cable-driven or cable-constrained. Since redundant cable(s) are required to provide tension, cable-constrained mechanisms are preferred over cable-driven mechanisms in this thesis so that there is no actuation redundancy.

Considering the above-mentioned statements, design criteria of the new mechanisms are determined as:

- Structure: hybrid cable-constrained parallel mechanism
- Dof of each leg: 3 dof TPM
- Walking mode: static walking
- Operation environment: flat surface
- Walking functions: straight walking, side walking and crossing over obstacles
- Application field: humanoid robots

3.2. Conceptual Design of the New Mechanisms

In order to have pure translational motion in a parallel mechanism, orientation dofs of moving platform should be restricted. It is known that parallelogram loops are used to provide rotational constraint to the moving platform, such as in the Delta Robot

(Clavel, 1990), and cables can used to form parallelograms, such as in the Betabot (Behzadipour et al., 2006). Parallelograms composed of passive cables are used to eliminate two rotation dof on the mechanisms proposed in the following two sections. Two different mechanisms are presented as Design I: a mechanism with cables and pulleys and Design II: a mechanism with anchored cables.

3.2.1. Design I: Mechanism with Cables and Pulleys

Kinematic structure of the first design is (UPU-2Pa)-(UPU-2Pa) (two parallel loops serially attached to each other) as shown in Figure 3.5 where underlined joints represent actuated joints. This mechanism consists of a fixed platform (hip), a middle platform (knee), a moving platform (foot), four rigid links and two parallelograms. Two rigid links form a P-joint (P_1) and connect the hip to the knee by two U-joints (U_H and U_K) at each end. Similarly, P_2 connects the knee to the foot by two U-joints (U_K and U_F). Two P-joints (P_1 and P_2) have reciprocating motion (translation in opposing directions by same amount of distance) and they can be actuated by a single actuator. P-joints (P_1 and P_2) allow translation along z-direction. Rotation axes of U-joints (U_H, U_K and U_F) are perpendicular and coincident. They allow rotation about x- and y-directions. U_H is actuated by two rotary actuators. Parallelograms are composed of passive cables and twelve pulleys (P_{H1-4}, P_{K1-4} and P_{F1-4}). Each pulley is connected to the associated platforms by a passive R-joint.

$U_H P_1 U_K$ leg constrains rotation of the knee platform with respect to the hip platform about z-direction. Similarly, $U_K P_2 U_F$ constrains rotation of the foot platform with respect to the knee platform. Two parallelograms with the blue R-joints constrain rotation of the knee and foot platforms about x-direction. Likewise, the two parallelograms with the green R-joints constrain rotation of the platforms about y-direction. Thus, proposed mechanism has knee and foot platforms with pure translational motion.

An example of a parallelogram loop is shown in Figure 3.6. The cable length on both sides of the parallelograms are kept constant (a + b remains constant). The motions of the P-joints (P_1 and P_2) should be adjusted such that the cable lengths remain constant.

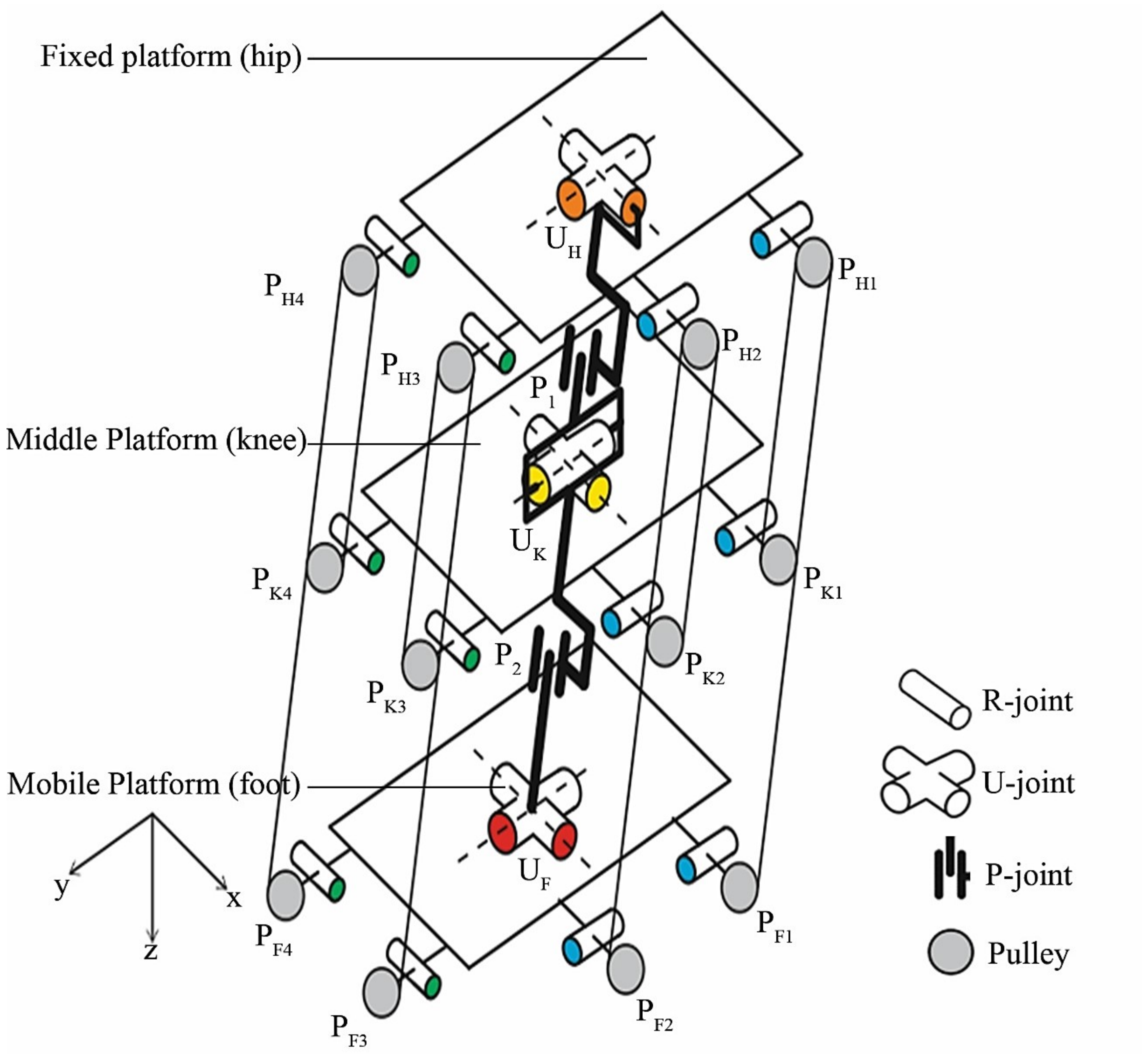

Figure 3.5. Kinematic structure of Design I.

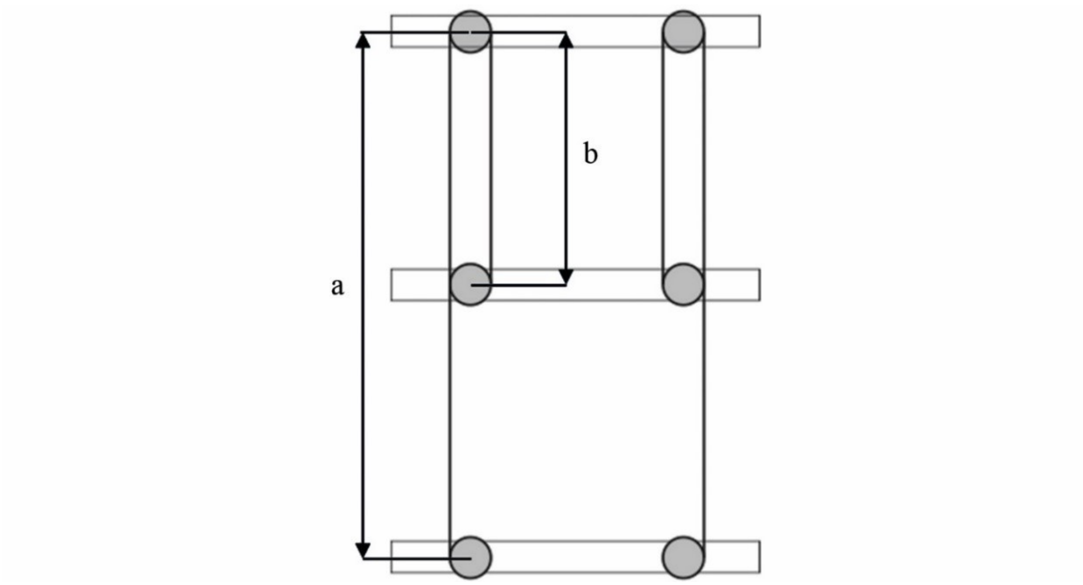

Figure 3.6. An example of parallelogram composed of passive cables.

A conceptual design of cables used with pulley solution is shown in Figure 3.7. The CAD model of the Design I is constructed in Solidworks Environment. In order to simulate the mechanism in Solidworks, belt module is used to model cables. Since a belt module needs to be closed loop, extra pulleys are added to the hip and the knee platforms (two pulleys per each side of the platforms). But in practice, 6 pulleys are enough to obtain the two parallelograms as in Figure 3.6. The design consists of hip, knee and foot platforms, two ball screws and nuts. The ball screws and nuts are used to obtain reciprocating motion of the knee and the foot platforms with respect to the hip platform. An actuated U-joint (U_H) is realized with a gimbal design ($Gimbal_H$) indicated with orange. The gimbal design is actuated by two rotary actuators indicated with black boxes. A passive U-joint (U_K) is presented with another gimbal design ($Gimbal_K$). The last passive U-joint (U_P) is selected as a commercial U-joint (U_F) product design. Since mass of the cables and their connection parts are almost negligible, four different sets of cables can be used on all sides of the platforms to keep the platforms parallel to each other.

Details of the U-joints are shown in Figure 3.8. The actuated gimbal design consists of two rotary parts ($Gimbal_{H1}$ and $Gimbal_{H2}$) which are connected to the rest of the mechanism with a rigid link (Figure 3.8 (a)). $Gimbal_{H1}$ rotates the link about the x-direction where $Gimbal_{H2}$ rotates it about the y-direction. Rigid link-$Gimbal_{H2}$ contact has considerable amount of friction. Although friction is a drawback of this design and several types of actuated gimbal mechanisms exist, two rotary actuators have independent motion in this design and they do not carry the weight of each other. A closer view of $Gimbal_K$ is shown in Figure 3.8 (b). $Gimbal_K$ connects the 2nd nut to the knee and allows rotation about x- and y-directions. The pulleys (Figure 3.8 (c)) have same amount of rotation about the same directions as $Gimbal_H$ and $Gimbal_K$: P_{H1-2}, P_{K1-2}, P_{F1-2} rotate with the same amount of rotation of $Gimbal_{H1}$ whereas P_{H3-4}, P_{K3-4} and P_{F3-4} rotate with the same amount of rotation of $Gimbal_{H2}$.

The two ball screws are used to obtain reciprocating motion between the knee and the foot platforms. 1st ball screw is a hallow shaft ball screw and is connected to $Gimbal_K$ with the 1st nut. Motion of a rotary actuator is transmitted to the 1st ball screw which results in the translational motion in the knee platform by the help of parallelograms. The 2nd nut is fixed at the end of the 1st ball screw and transmits motion to the foot platform with reverse rotation of 2nd ball screw. Motion of the ball screws in two different positions can be seen in Figure 3.9.

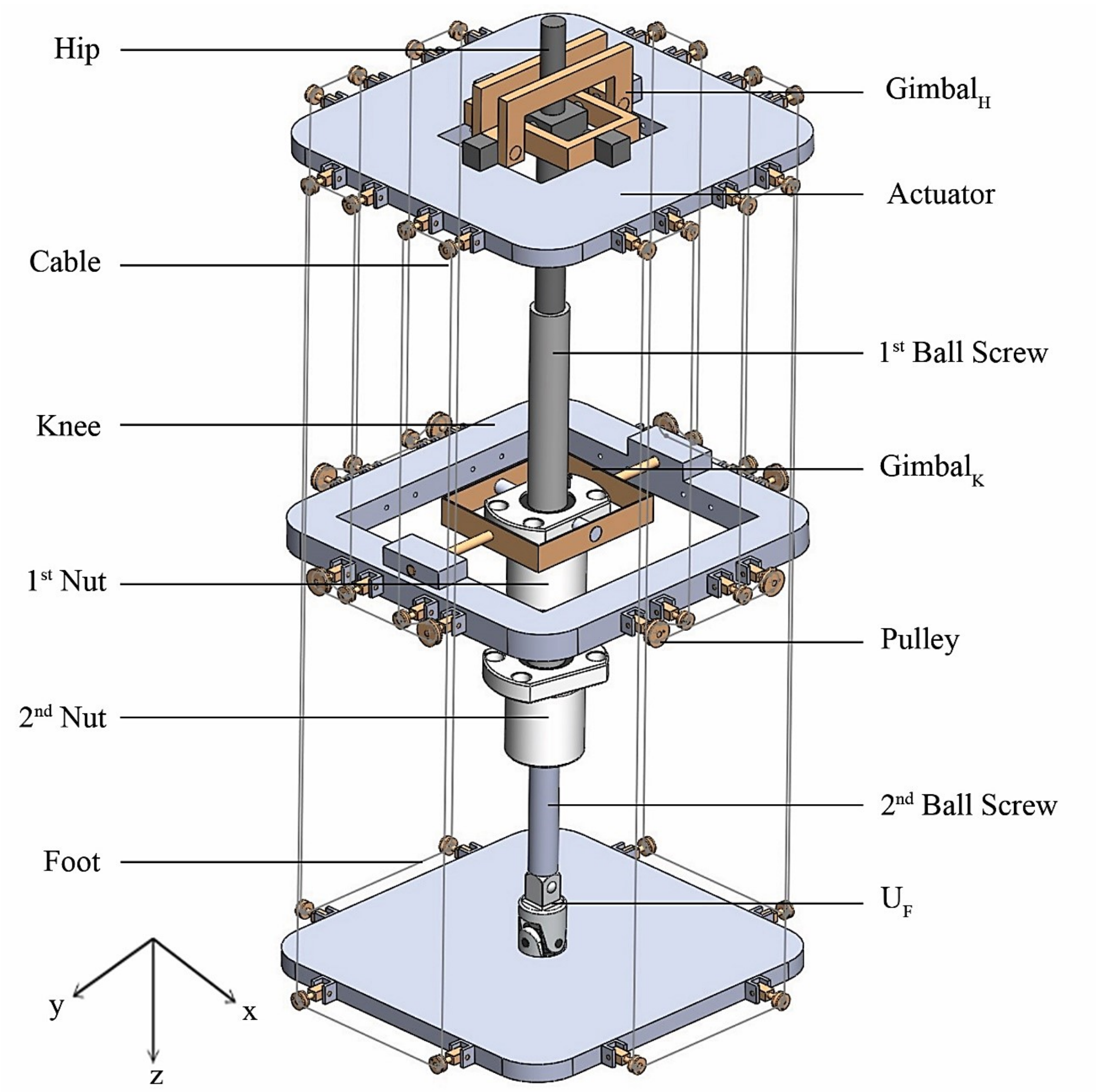

Figure 3.7. CAD model of the Design I.

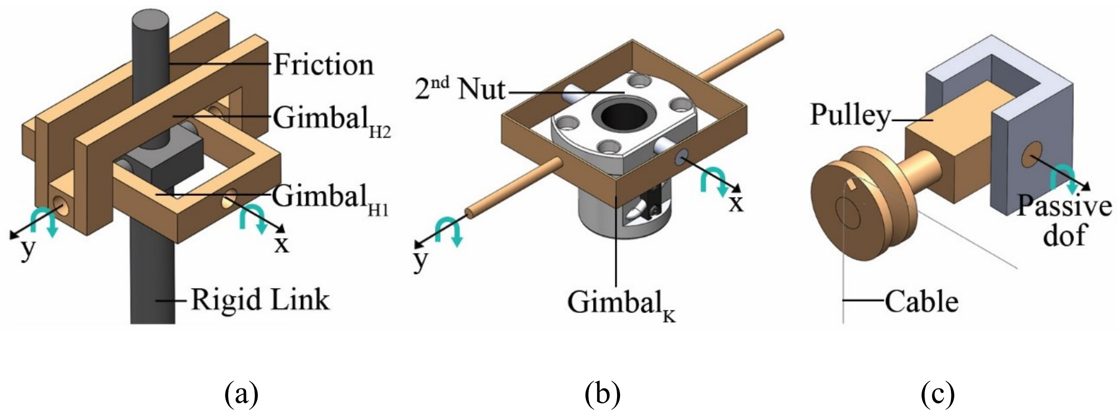

Figure 3.8. Details of the conceptual design (a) gimbal$_H$, (b) gimbal$_K$, (c) pulley.

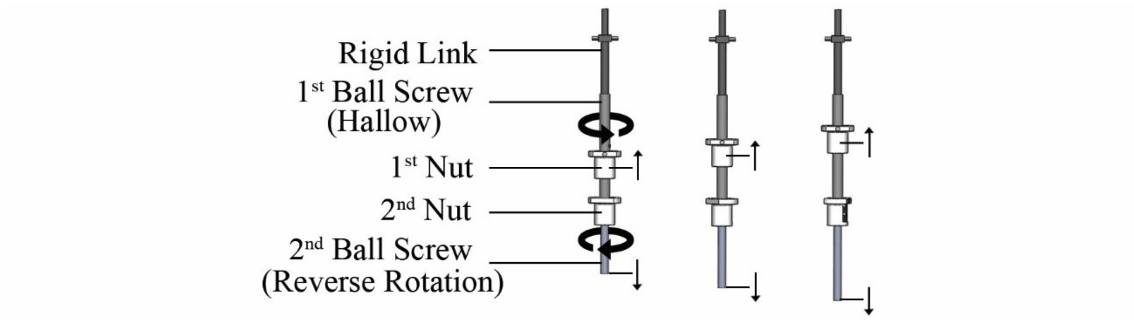

Figure 3.9. Two ball screw solution to obtain reciprocating motion.

Independent motions of Design I in four different positions according to Gimbal$_{H1}$ angle (θ_{H1}), Gimbal$_{H2}$ angle (θ_{H2}) and ball screw stroke (s) are shown in Figure 3.10. θ_{H1} is measured about x-direction, whereas θ_{H2} is about y-direction and s is along z-direction in ball screws axes. Home position of Design I is shown in solid model where $\theta_{H1} = 0°$, $\theta_{H2} = 0°$ and s = 0 mm. Motion of Gimbal$_{H1}$ shown in red is for $\theta_{H1} = 30°$. Blue indicated model shows motion of the Gimbal$_{H2}$ for $\theta_{H2} = -30°$. Furthermore, motion of the ball screws shown in black is for s = 100 mm. It can be seen that passive rotation of the pulleys depends on θ_{H1} and θ_{H2}. Also, how total length of the cables are kept constant with reciprocating motion can be seen from this figure.

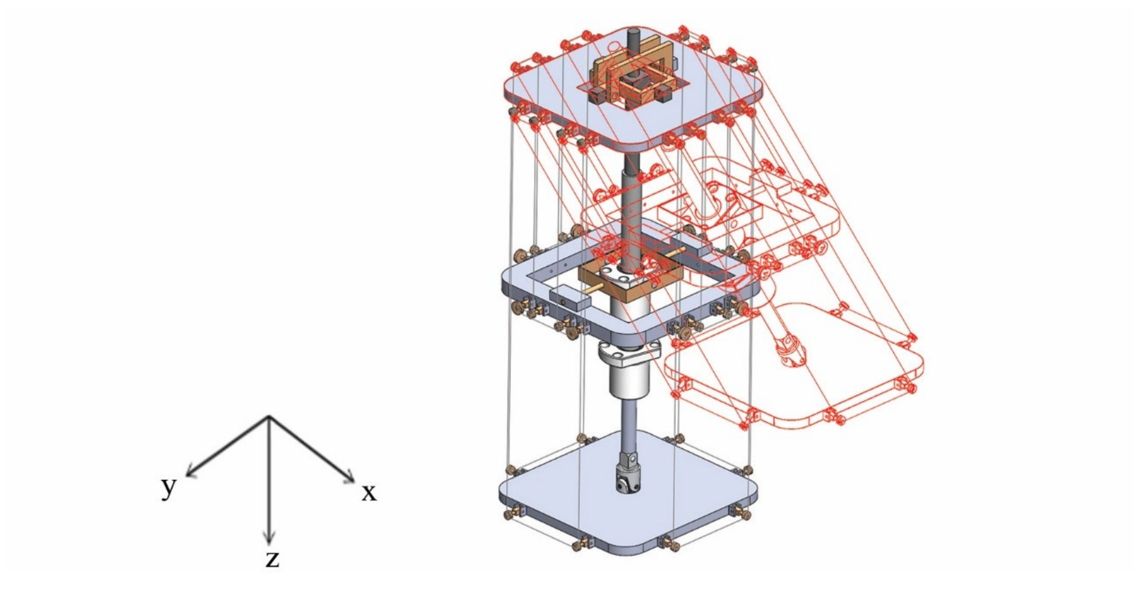

(a)

Figure 3.10. Independent motions of the Design I (a) $\theta_{H1} = 30°$, (b) $\theta_{H2} = -30°$, (c) s = 100 mm.

(cont. on next page)

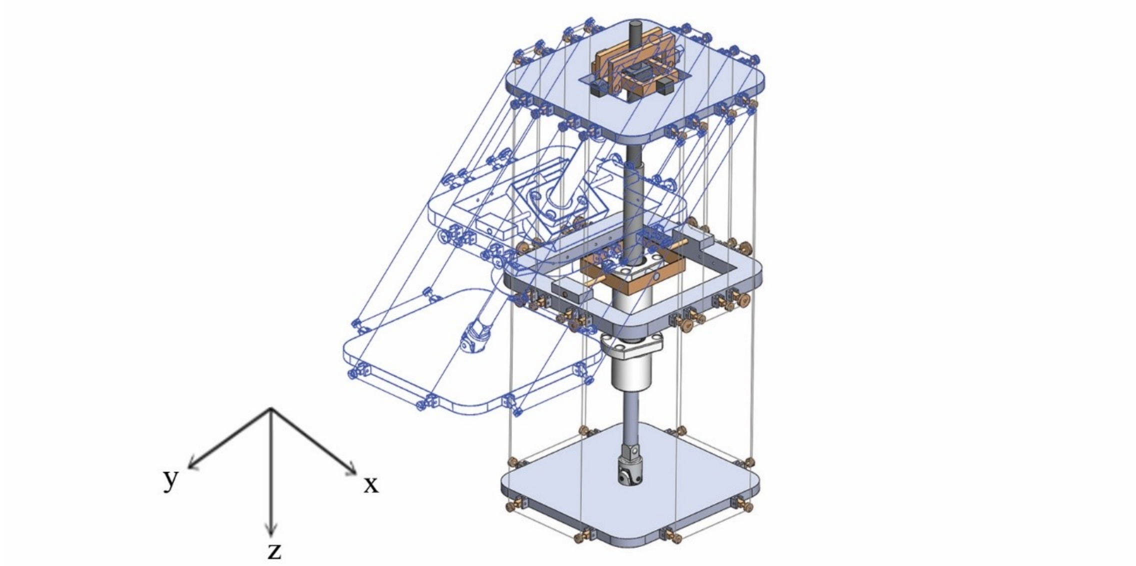

(b)

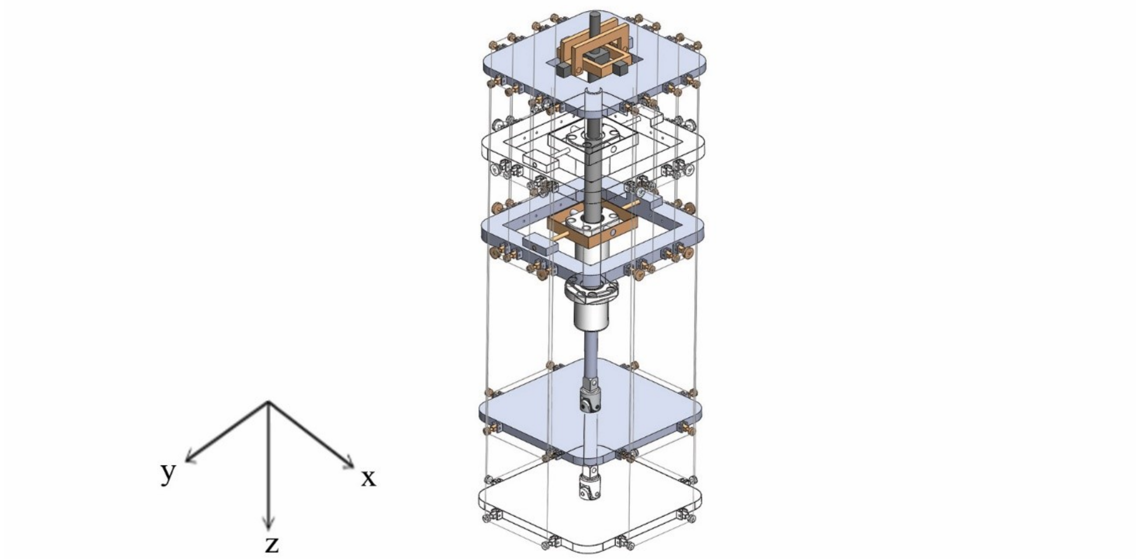

(c)

Figure 3.10 (cont.)

3.2.2. Design II: Mechanism with Anchored Cables

Kinematic structure of the second design is (UU-2Pa)-P as shown in Figure 3.11. This mechanism consists of a hip platform, a knee platform and a foot platform. A rigid link (thigh) connects the hip to the knee by two U-joints (U_H and U_K) at each end where U_H is actuated by two rotary actuators. The shank composed of two links connects the knee to the foot by an actuated P-joint. Rotation axes of U_H and U_K are about x- and y-directions. The P joint allows translation in z-direction. Two parallelograms include four passive cables which are anchored from points (A_{H1-4} and A_{K1-4}). Since cables needs to be in tension during the motion of the mechanism, each cable is equivalent to a rigid link and it has a S-joint at each end. That is, each cable is considered as a rigid SS linkage. U_HU_K leg constrains rotation of the knee with respect to the hip about z-direction. Two parallelograms each of which containing a pair of passive cables constrain the rotation about x- and y-directions. The P joint between the knee and foot platforms allows only translational motion. Hence, all orientation dof of the foot are constrained, and proposed mechanism possess pure translational motion.

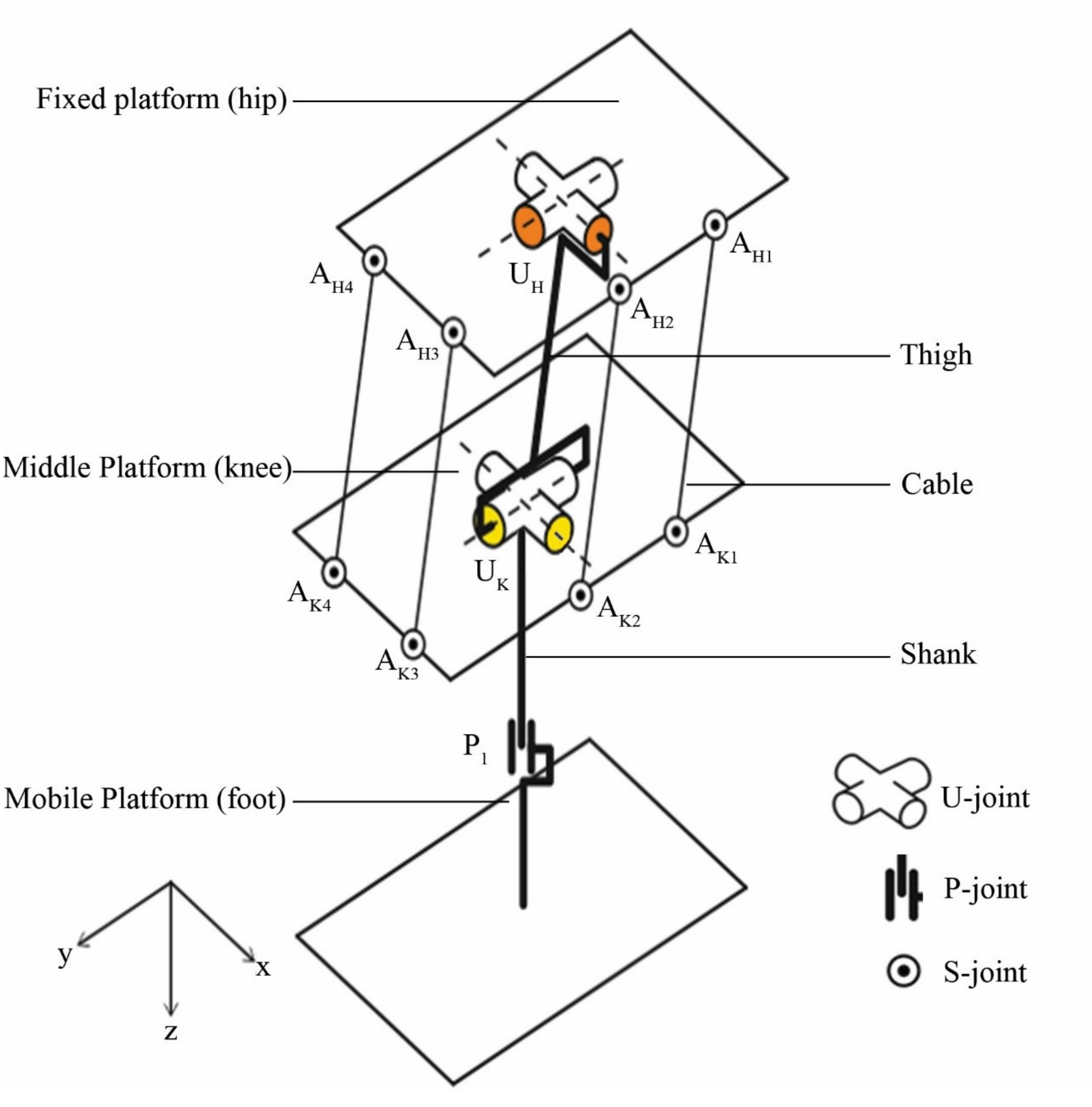

Figure 3.11. Kinematic structure of the Design II.

A conceptual design of cables anchored without pulley solution is shown in Figure 3.12. The CAD model includes three platforms (the hip, the knee and the foot). This time, cables are modeled as rigid links with circular cross section and are anchored with S-joints (point to point mate). Although three cables are enough to form two parallelograms (one of the cables is shared), eight cables are used to form two pairs of opposite parallelograms on each side of the thigh. Same actuated gimbal design ($Gimbal_H$) as the one in Design I is used. This gimbal is actuated by two rotary actuators indicated as black boxes in Figure 3.12. A passive U-joint ($Gimbal_K$) is used on the knee platform. The thigh link is connected to the hip with $Gimbal_H$ and to the knee with U_K. A linear actuator is used as the shank.

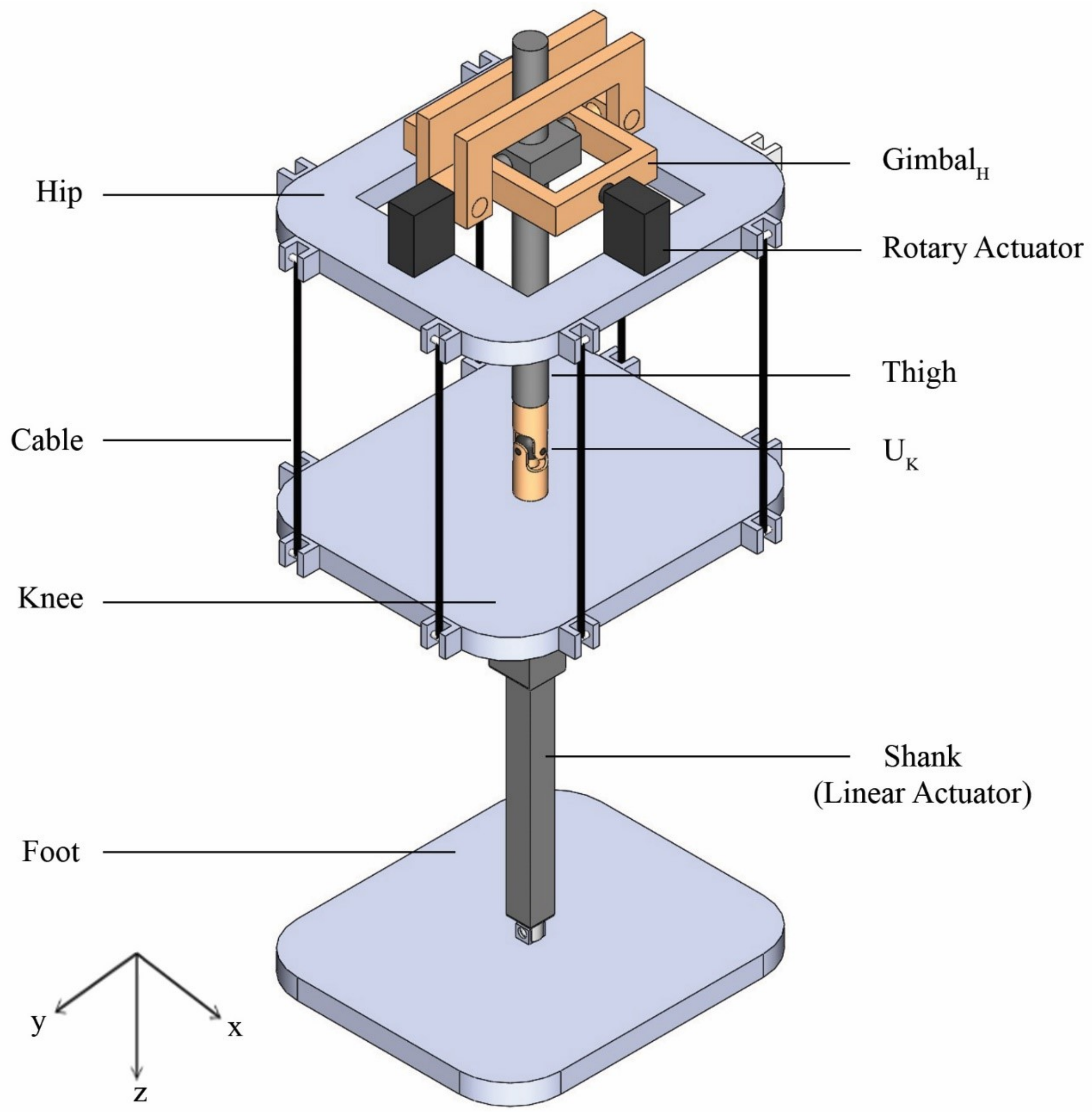

Figure 3.12. CAD model of the Design II.

Independent motions of Design II, in four different positions according to Gimbal$_{H1}$ angle (θ_{H1}), Gimbal$_{H2}$ angle (θ_{H2}) and linear actuator stroke (s) is shown in Figure 3.13. θ_{H1} is measured about x-direction, whereas θ_{H2} is about y-direction and s is along z-direction. Home position of the Design II is shown as a solid model where $\theta_{H1} = 0°$, $\theta_{H2} = 0°$ and s = 0 mm. Motion of the Gimbal$_{H1}$ is shown in red where $\theta_{H1} = 30°$. Blue model shows motion of the Gimbal$_{H2}$ at $\theta_{H2} = -30°$. Furthermore, motion of the linear actuator is shown for s = 50 mm.

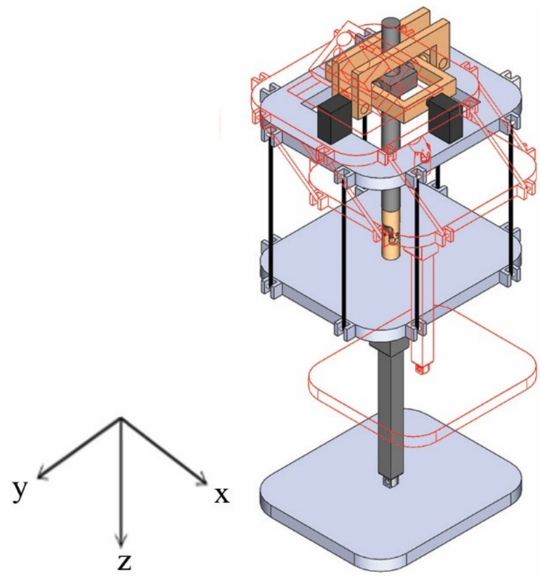

(a)

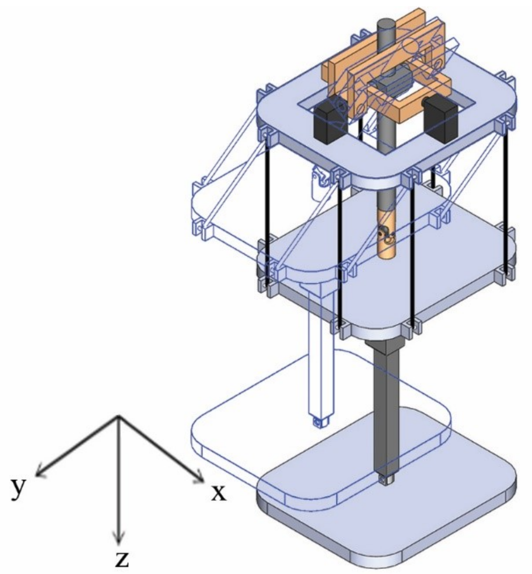

(b)

Figure 3.13. Independent motions of the Design II in different positions.

(cont. on next page)

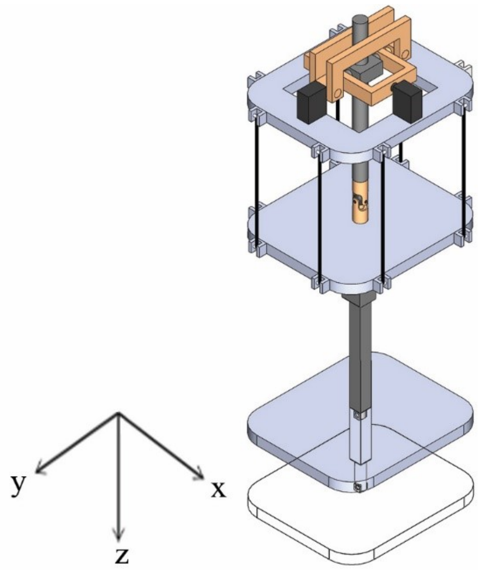

(c)

Figure 3.13 (cont.)

3.3. Feasibility of the New Mechanisms

Two different novel hybrid cable-constrained parallel mechanisms with three translational dofs are proposed in the previous sections. In Design I, cables are used with pulley and two pulleys per each side of the platforms are connected to the three platforms (the hip, the knee and the foot). Also, two ball screws are used to obtain reciprocating motion between the knee and the foot platforms. On the other hand, cables of Design II are anchored at the hip and the knee platforms and there is no cable on the foot platform. In addition to that, reciprocating motion is not required. A linear actuator is enough to translate the foot along the z-direction. Design II has simpler mechanical structure than Design I due to direct connection of cables and linear actuator solution. Since the selected mechanism is to be used as a leg design for a biped walking machine, relative positions of the links during motions of the mechanisms are also important. Design II is favorable in this sense, because thigh and shank links are not concentric during the motion of the mechanism. If human walking is considered, Design II is a more “human-like” design for walking operation. According to these comparisons Design II: mechanism with anchored cables solution is found more feasible for a biped walking machine.

CHAPTER 4

PERFORMANCE ANALYSIS OF THE NEW MECHANISM

In this chapter, performance analysis of the selected leg mechanism is presented. Firstly, kinematic analysis of the mechanism is worked out. CAD model of a first prototype is constructed in SolidWorks® environment. Workspace of the CAD model is computed according to the joint limits. Kinematic simulation of the leg mechanism for human-like walking gait is carried out using SolidWorks® Motion Analysis Toolbox. Once the simulation values are found acceptable, a first prototype is built to check the feasibility of the new mechanism. The content of this Chapter is published as (Demirel et.al, 2018) except workspace and experimental validation sections. Also, kinematic analysis section is more detailed in this Chapter.

4.1. Kinematic Analysis of the New Mechanism

Kinematic analysis allows to determine and design motion characteristics of manipulators (Ceccarelli, 2013). The ($\underline{U}$U-2Pa)-$\underline{P}$ mechanism is depicted in Figure 4.1. The upper leg includes a rigid binary link (thigh) which has two U-joints (U_H and U_K) at each end and it connects the hip to the knee. Length of the thigh is defined as l_T. Rotation axes of U_{H1} (orange) and U_{K1} (green) are about x-direction, whereas the axes of U_{H2} (blue) and U_{K2} (yellow) are about y-direction. Joint parameters of U_{H1}, U_{H2}, U_{K1} and U_{K2} are θ_{H1}, θ_{H2}, θ_{K1} and θ_{K2}, respectively. Four passive cables ($C_{1\text{-}4}$) in equal length (l_C) form two parallelograms together with two adjacent sides of the hip and the knee platforms. These cables are equivalent of rigid SS linkage when the cables under tension and the deformations of the cables under tension are ignored. Cables are anchored at points $A_{H1\text{-}4}$ and $A_{K1\text{-}4}$ and these points represent S-joint centers. Lower leg comprises two links connected with a P-joint with joint variable s that translates along the z-direction. The knee and foot platforms of the ($\underline{U}$U-2P_a)-$\underline{P}$ mechanism possess pure translational motion due to rotation constraints provided by the UU connection, parallelograms and the P joint.

U_{H1}, U_{H2} and P joints are actuated by two rotary actuators and a linear actuator, respectively.

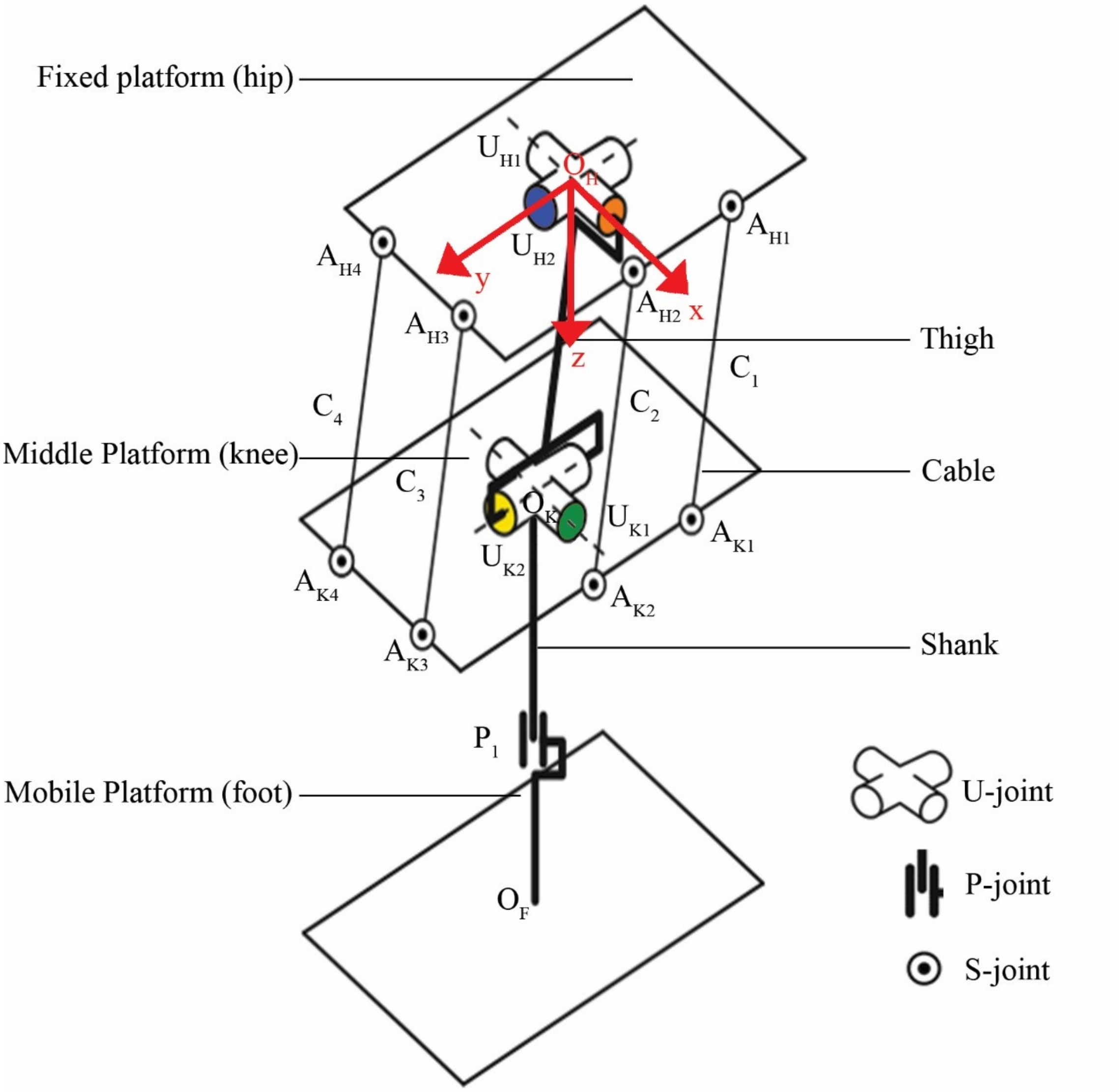

Figure 4.1. Kinematic model of the (UU-2Pa)-P mechanism.

The proposed design can be idealized by an extendable link (in z-direction) attached to a two dof pendulum (Figure 4.2). The link and joint parameters are illustrated in Figure 4.2. Knee point (O_K) in fixed reference frame $O_H(x, y, z)$ is at $P_K\,(0, 0, l_T)$ when $\theta_{H1} = 0$ and $\theta_{H2} = 0$. The thigh link rotates by θ_{H1} about the x-direction and by θ_{H2} about the y-direction. Foot point (O_F) is just translated from O_K by an amount of s along z-direction. Position of $O_F(O_{Fx}, O_{Fy}, O_{Fz})$ in $O_H(x, y, z)$ frame is calculated by using direct kinematics equations Equations (4.1)-(4.2) depending on actuated joint angles θ_{H1}, θ_{H2}

and displacement s. Note that s can be defined as $s = l_s + \Delta s$ considering the initial length l_s due to the constructional design of the shank.

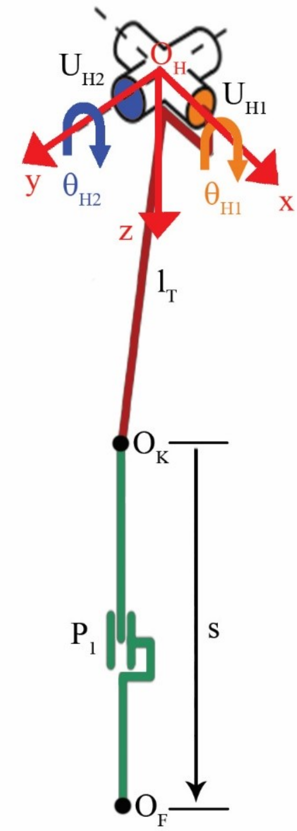

Figure 4.2. UP kinematic chain with link and joint parameters.

$$\begin{bmatrix} O_{Fx} \\ O_{Fy} \\ O_{Fz} \end{bmatrix} = \begin{bmatrix} 1 & 0 & 0 \\ 0 & \cos\theta_{H1} & \sin\theta_{H1} \\ 0 & -\sin\theta_{H1} & \cos\theta_{H1} \end{bmatrix} \begin{bmatrix} \cos\theta_{H2} & 0 & -\sin\theta_{H2} \\ 0 & 1 & 0 \\ \sin\theta_{H2} & 0 & \cos\theta_{H2} \end{bmatrix} \begin{bmatrix} 0 \\ 0 \\ l_T \end{bmatrix} + \begin{bmatrix} 0 \\ 0 \\ s \end{bmatrix} \quad (4.1)$$

Performing the multiplications in Equation (4.1):

$$O_{Fx} = -l_T \sin\theta_{H2} \ , \ O_{Fy} = l_T \sin\theta_{H1} \cos\theta_{H2} \ , \ O_{Fz} = l_T \cos\theta_{H1} \cos\theta_{H2} + s \quad (4.2)$$

θ_{H1}, θ_{H2} and s values can be calculated by inverse kinematics equation (4.3) for given position of the foot point O_F in fixed reference frame. Position level kinematics of the leg mechanism is straight forward so that proposed mechanism is computational efficient for position level kinematics. Velocity and acceleration level kinematics can be performed by taking derivatives of equation (4.2).

$$\theta_{H2} = \sin^{-1}\left(\frac{-O_{Fx}}{l_T}\right) \ , \ \theta_{H1} = \sin^{-1}\left(\frac{O_{Fy}}{l_T \cos\theta_{H2}}\right) \ , \ s = O_{Fz} - l_T \cos\theta_{H1} \cos\theta_{H2} \quad (4.3)$$

4.2. CAD Model of the First Prototype

A 3-D model of the proposed leg mechanism is constructed in SolidWorks® environment (Figure 4.3 (a)). The main specifications of the proposed mechanism are listed in Table 4.1. l_s is the shortest distance in between the knee and the foot platforms. Dimension parameters are indicated and listed in Figure 4.3 (b), Figure 4.3 (c) and Table 4.2. Note that this is a scaled model compared to a typical human leg size. The distance between the actuated U-joint center and the anchor points of cables (A_{H1}, A_{K2}, etc.) are called as d_{UH}, d_{UK} and they should be equal to each other so that the cable lengths are kept constant. Eight cables are used in the CAD model. Masses of cables are negligible, therefore, additional cables do not contribute as additional mass in the simulation. Since cables are passive, they can be fixedly attached to the platforms without pulleys. Cables are modeled as links with circular cross-section and their length is kept constant assuming they are always in tension.

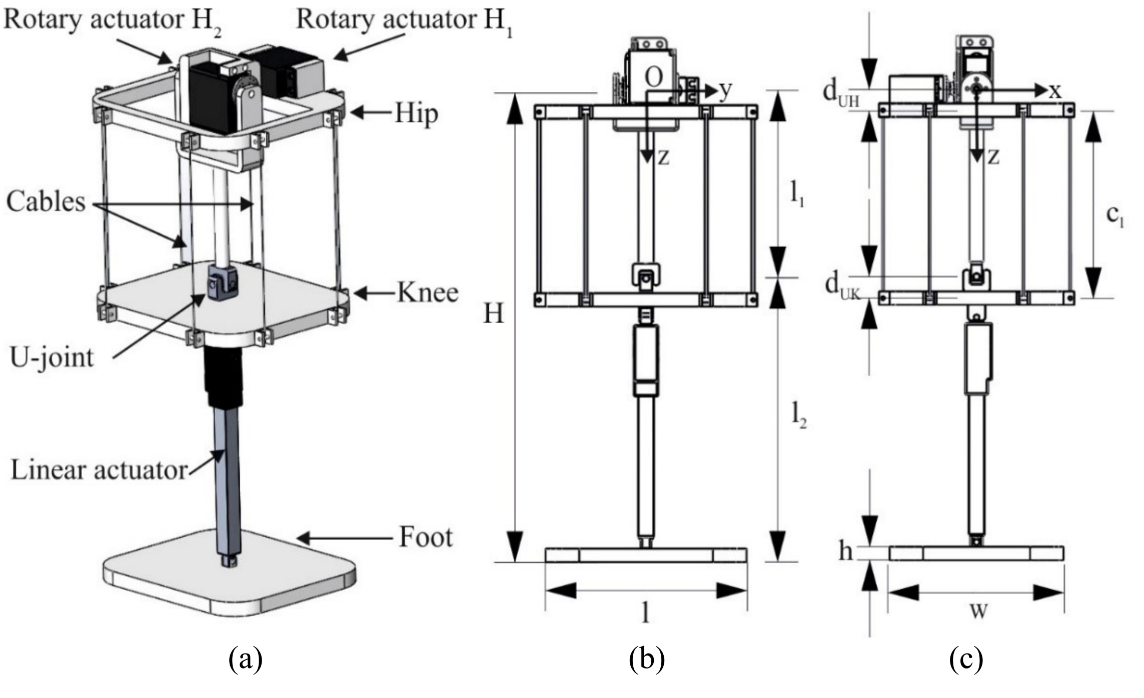

(a) (b) (c)

Figure 4.3. Proposed leg mechanism; (a) CAD model, (b) dimension parameters of the CAD model from sagittal view (yz plane) and (c) front view (xz plane).

Table 4.1. Main specifications of the proposed mechanism in Figure 4.3.

DOF	Mass (kg)	Size (mm)	Step size (mm)	Step cycle (s)
3	0.75	150 × 130 × 351	200 × 50	1

Table 4.2. Dimension parameters (in mm) of the model in Figure 4.3.

l	w	h	l_1	l_2	d_u	c_l	H
150	130	10	140	211	11	140	351

Mass centers of each platform are set in geometric center of the platforms. Mass values of each component are listed in Table 4.3 for the hip platform (m_H), the knee platform (m_K), the foot platform (m_F), the universal joint (m_U), thigh (m_T), the rotary actuators (m_A each) and the linear actuator (m_L). The torques of the rotary actuators are denoted as τ_{H1} and τ_{H2}, where the force of the linear actuator is F_L. The proposed model is designed with light-weight materials for the platforms (ABS) and commercial products (U-joint, linear actuator and rotary actuators). These components are modelled properly in the 3-D model for static walking simulation.

Table 4.3. Mass values (in grams) of the model in Figure 4.3.

m_H	m_K	m_F	m_U	m_L	m_A
95	195	195	12	74	80

4.3. Dynamic Simulation of the First Prototype for Human-Like Walking Gait

The aim of this simulation is to confirm feasibility of the proposed hybrid leg architecture to be used for a walking machine. First, the kinematic analysis for a human-like walking trajectory is carried out for the simulation. This trajectory is a planar ovoid curve as shown in Figure 4.4 (a) and it is composed of two phases called as swinging and supporting phases. The lateral motion of the mechanism is not considered in this simulation, i.e. $\theta_{H2} = 0$. The straight-line segment represents the supporting phase where the curved segment represents the swinging phase. Two length parameters are enough to describe step cycle as step length (S_L) and step height (S_H). Walking gait of foot point O_F is defined as A-B-C-D-A for 1 s step cycle. Displacement of the foot point is shown in Figure 4.4 (b) for a walking cycle with S_L = 200 mm and S_H = 50 mm. Static walking simulation requires only motions of the rotary actuator H_1 (θ_{H1}) and linear actuator (s). θ_{H1} and s values are calculated by using inverse kinematics Equations. (4.3).

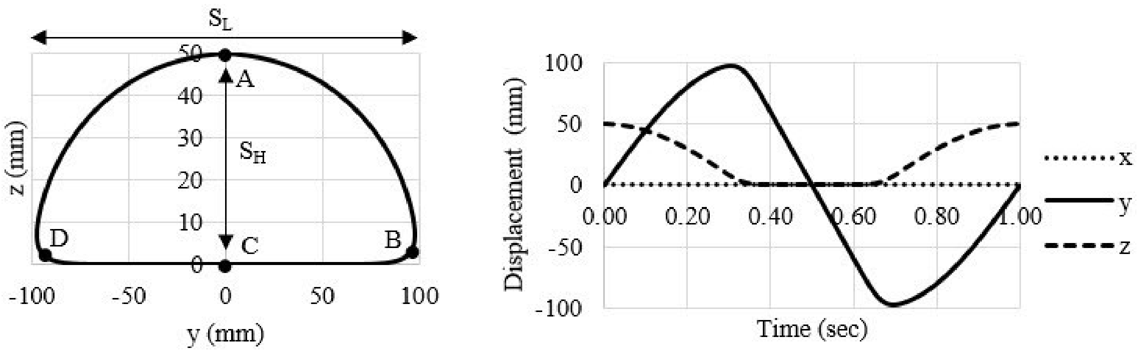

Figure 4.4. Walking cycle (a) ovoid curve cycle for S_H=50, S_L=200 mm, (b) displacement of foot point O_F.

For three steps of walking cycle in 3 seconds, input position data of rotary actuator H_1 and linear actuator are shown in Figure 4.5. $\Delta\theta_{H1} = \pm 42^{\circ}$ and Δs = 0-72 mm. Simulation of three steps is performed in SolidWorks® environment by using the Motion Analysis toolbox. This toolbox uses MSC ADAMS® solver. Sagittal view snapshots of the first step cycle for points A (t = 0 s), B (t = 0.33 s), C (t = 0.5 s), D (t = 0.66 s), A (t = 1 s) are shown in Figure 4.6.

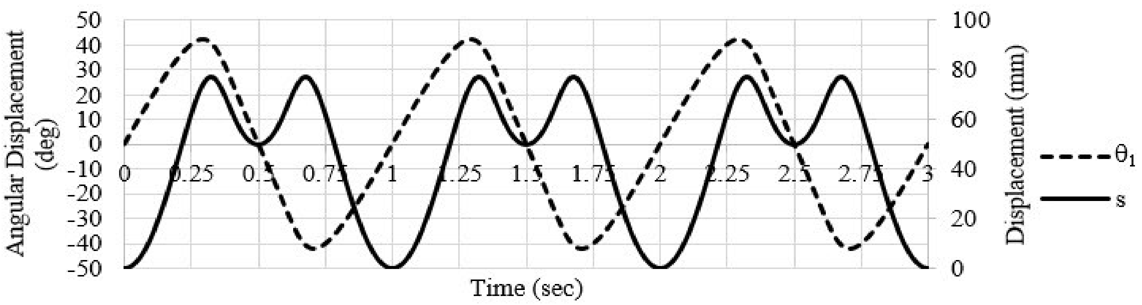

Figure 4.5. Input angular displacement of rotary actuator H_1 (θ_1 vs time) and input displacement of the linear actuator (s vs time).

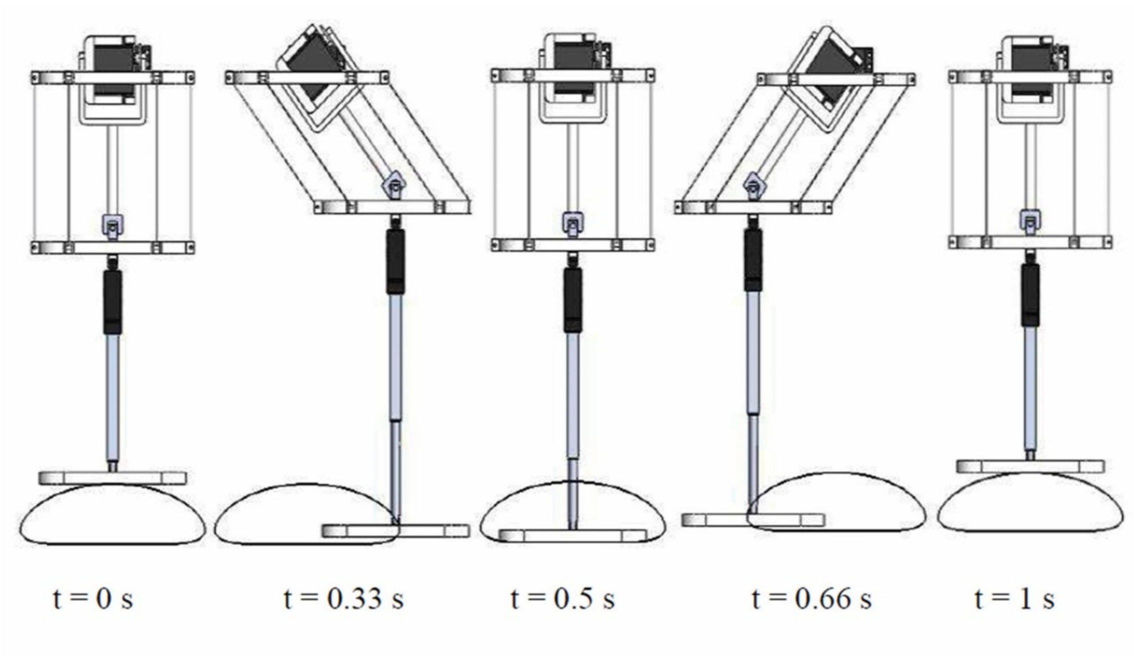

Figure 4.6. Snapshots of the simulated motion in yz-plane.

The gravitational and inertial forces and moments are effective in the simulation, while external and friction forces are not modeled. Computed τ_{H1} and F_L values are shown in Figure 4.7. Maximum torque and force values of actuators occur at the step phase changes, point B and D: τ_{1max} = 0.271 N·mm and F_{Lmax} = 2.6 N. Computed joint reaction forces of hip joint U_{H1} and knee joint U_{K1} in x-, y- and z-directions are shown in Figure 4.8. Some numerical errors can be seen in Figure 4.8 (a) for F_{UH1Z}. Maximum joint reaction forces are about 6 N in all revolute joints. Since total weight of the mechanism is about 7.5 N, the computed reaction forces are reasonable.

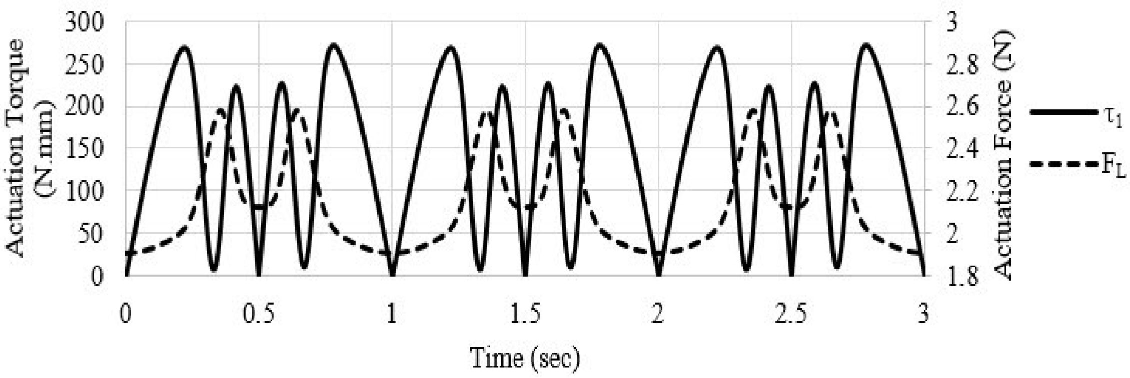

Figure 4.7. Computed actuation torque of rotary actuator H_1 (τ_1) and force of linear actuator (F_L).

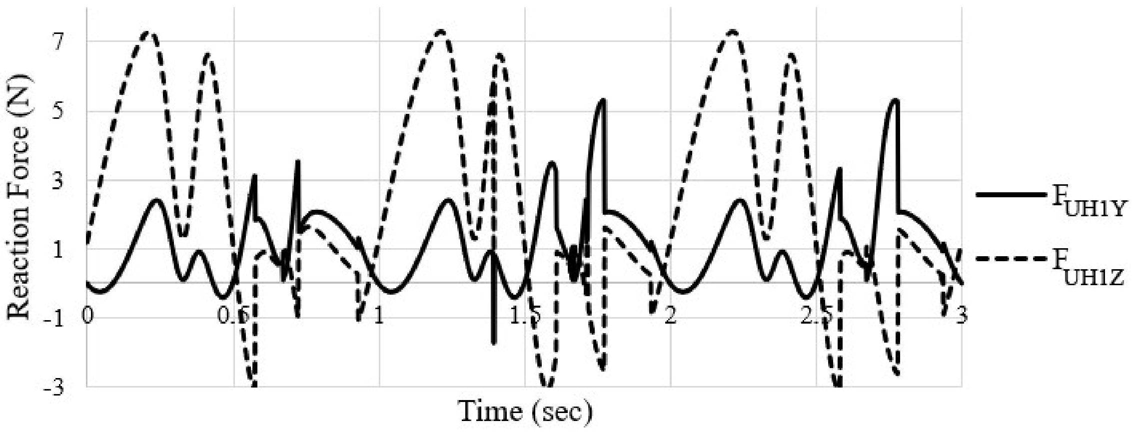

(a)

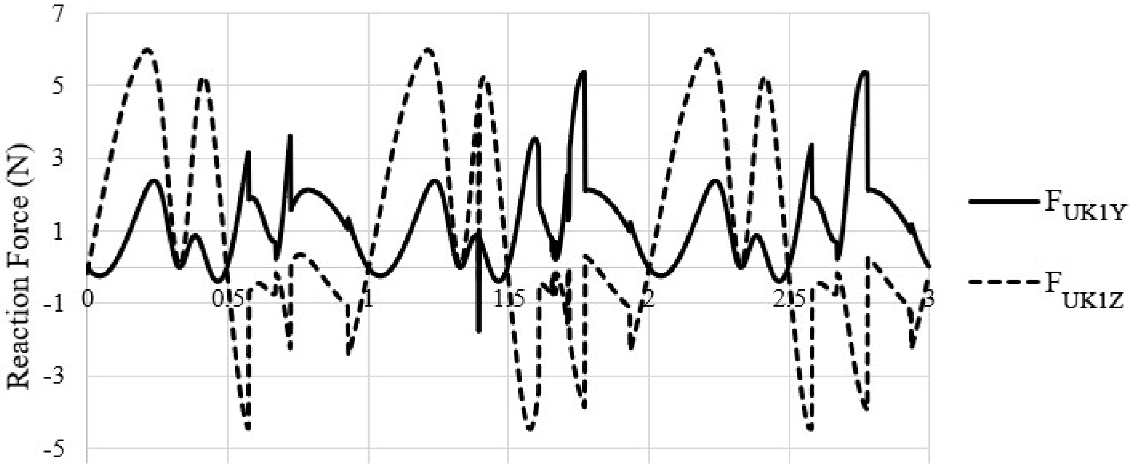

(b)

Figure 4.8. Computed reaction forces of (a) the hip joint U_{H1}, (b) the knee joint U_{K1}.

As mentioned before, mass centers of the platforms are coincident with the geometric centers of the platforms. Acceleration values of these points in y- and z-directions are shown in Figure 4.9. Maximum speed and acceleration values of center of masses of the knee and the foot are computed as V_{KY} = 611 mm/s, V_{KZ} = 305 mm/s, a_{KY} = 6669 mm/s^2, a_{KZ} = 5287 mm/s^2 and V_{FY} = 611 mm/s, V_{FZ} = 204 mm/s, a_{FY} = 6669 mm/s^2, a_{FZ} = 2044 mm/s^2. Since there is only translational motion in z-direction between the knee and the foot platforms, a_{KY} and a_{FY} values are equal during the simulation. Maximum values occur in step phase changes (point B and D) again. These sudden changes are due to inertial effects of the mechanism.

Simulation results show that the proposed leg mechanism is able to accomplish human-like foot step trajectory. Computed torque and force values of the actuators and reaction forces ensure feasibility of the proposed design as a low-cost design.

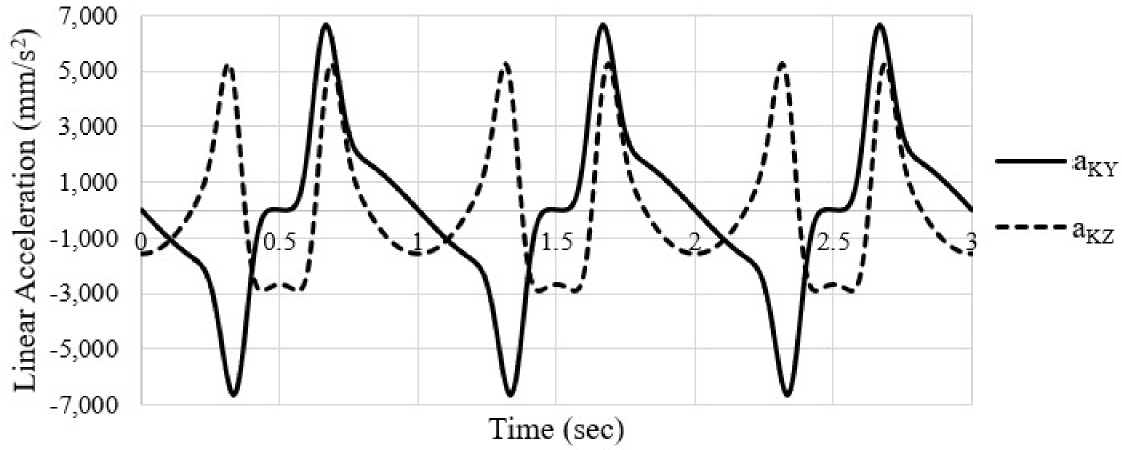

(a)

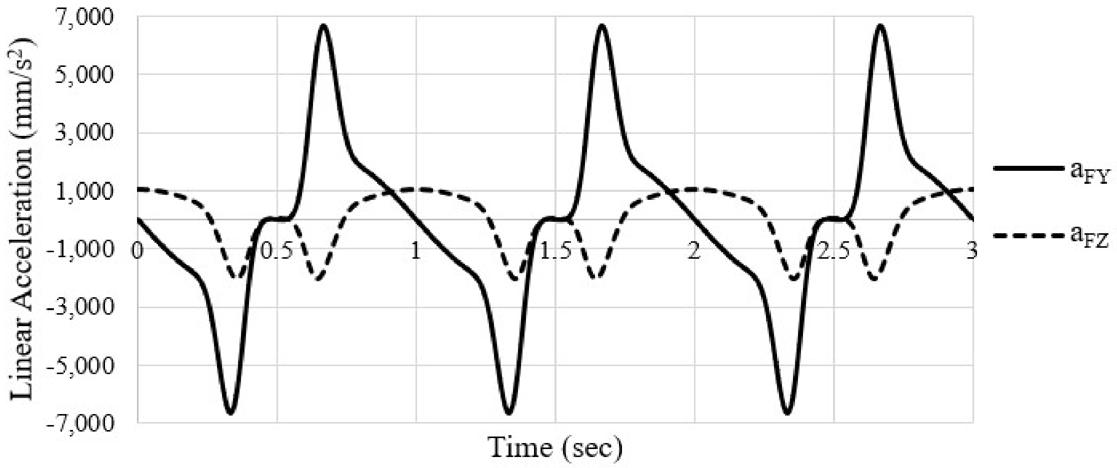

(b)

Figure 4.9. Computed center of mass accelerations in O_X and O_Z direction; (a) the knee point, (b) the foot point.

4.4. Experimental Validation of the First Prototype

As mentioned in Section 4.3, components of the CAD model are selected from available products in the market and 3D printed ABS platforms. The hip, knee and shank joints are available products in the market. Metal cables are connected to the platforms using electric terminal connectors. Cables are guided by holes (same diameter with cables). Cables are covered with compression springs and plastic pipes. Two SpringRC SM-S4315M analog DC servo motors and a Firgelli L16-P linear actuator with 100 mm stroke and potentiometer feedback are used as actuators. An Arduino Mega 2560 R3 board is used as a controller. Components of the first prototype are shown in Figure 4.10.

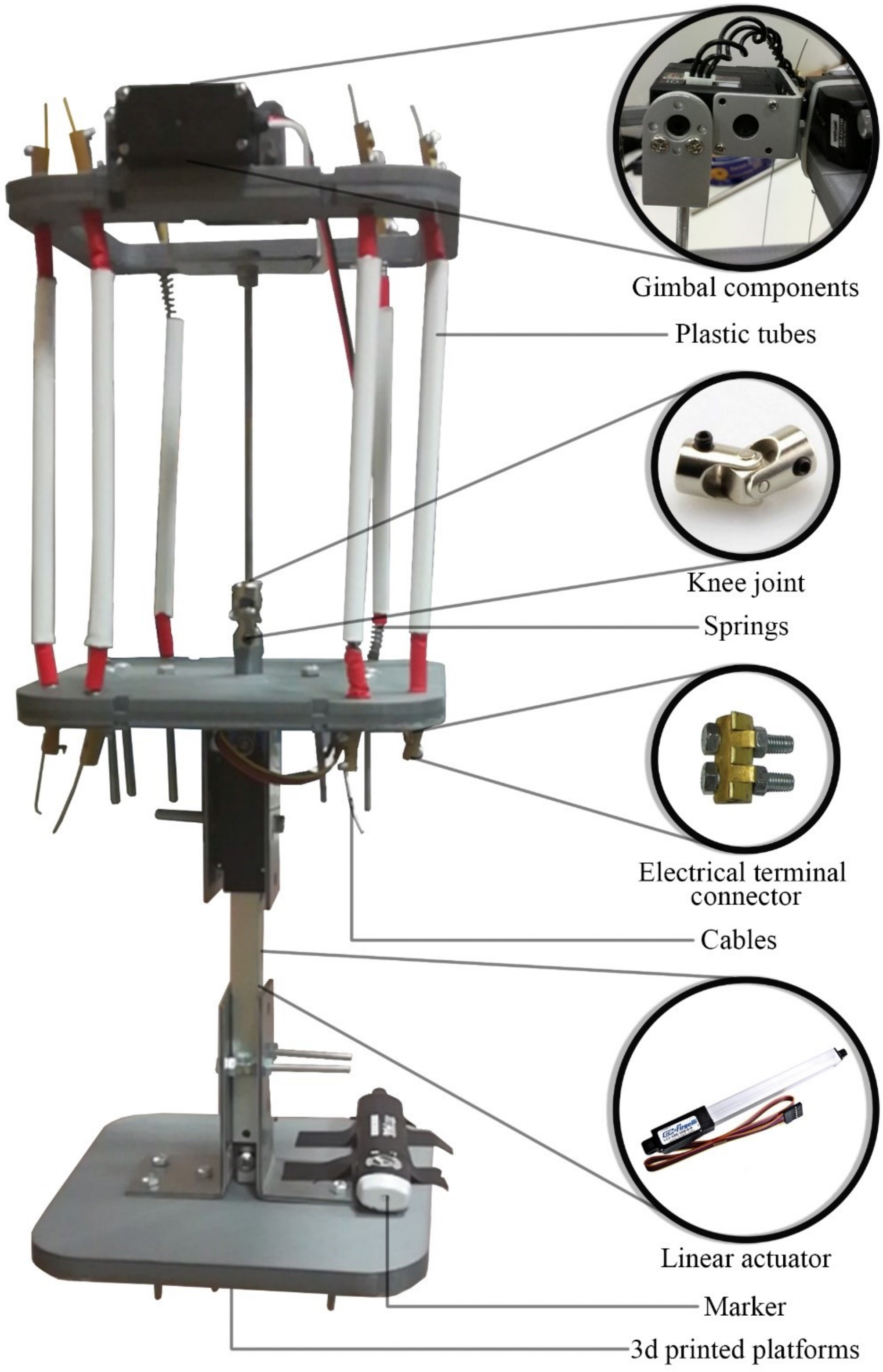

Figure 4.10. Details of the first prototype.

A triangular trajectory with corners A-B-C is selected for the walking gait and point-to-point control is applied to the motors. Figure 4.11 shows snapshots of motion of the prototype. A board marker attached on the foot platform draws on a graph paper to track position of the foot. Unfortunately, marker shakes too much so the platform cannot properly track a smooth trajectory. Accuracy of the prototype is not good, but repeatability of it is good. Repeatability can be better understood from the taken videos.

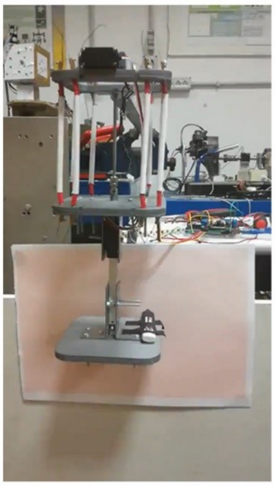

(a)

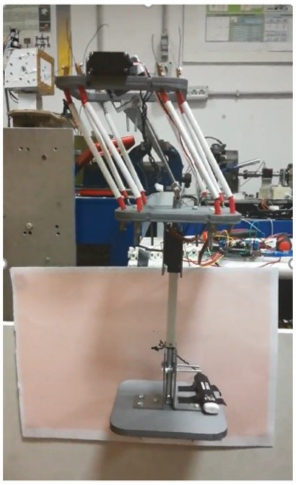

(b)

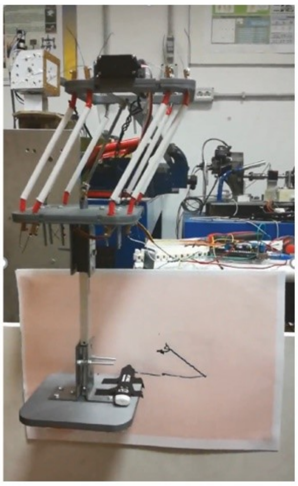

(c)

(d)

Figure 4.11. Snapshots of motion of the first prototype (a) point A, (b) point B, (c) point C, (d) point A again.

This prototype is built to discover potential future problems in the real prototype and check feasibility of the kinematic structure. As it can be seen from the snapshots, cables and thigh link keeps orientation of the knee platform constant with respect to the hip platform. The most challenging part of this prototype was assembling. While connecting cables it was difficult to keep them in equal length and tension. Cables should be carefully connected by using a jig design. Better jig design means, less assembly error. Initially, cables were connected without springs. Since many redundant cables are used, it is observed that many of them lose tension during motion. Compression springs are used to keep cables in tension. In order to prevent buckling of the springs, plastic pipes are used around them. Several design problems are discovered by building such a first prototype. A second prototype is designed afterwards.

CHAPTER 5

PROTOTYPE DESIGN AND EXPERIMENTAL VALIDATION

A new prototype of the ($\underline{U}U$-$2P_a$)-$\underline{P}$ mechanism is presented in this Chapter. As presented in previous Chapters, the proposed leg mechanism is suitable for a biped walking machine with static walking operation. A first prototype verified the feasibility of the design and a new prototype is designed based on the conceptual design in Chapter 3. Firstly, the new prototype's design and manufacturing process is presented. Then, experiment setup of the prototype is presented. A 5^{th} order walking gait is planned for the experiments. After that, the prototype is operated for the planned trajectory. Output shaft angles are measured using rotary magnet encoders. Finally, experimental results are stated and discussed.

5.1. Prototype Design

Design and prototyping of the proposed leg mechanism are presented in this Section. Aluminum profiles are used to form the hip, the knee and the foot platforms. A slider crank mechanism is designed to achieve the translational motion between the knee and the foot platforms. Cables are guided by holes on the platforms and some pulleys. The cables on two opposite sides of the platforms are constructed in a rectangular loop in order to equate the tension and length of parallel cables in a loop. The tension of the cables is controlled by a turn. Many parts of the prototype are selected as available products in the market. Stepper motors are used as actuators. Components of the gimbal design presented in Chapter 3 is produced by using a CNC milling machine. Laser cut acrylic plates are used to connect components on the hip and the knee platforms and also for guiding the cables. 3D printed parts are used as sensor holders and as supports of the cable guiding acrylic plates.

5.1.1. Mechanical Design

The CAD model of the leg mechanism is illustrated in Figure 5.1. Since the linear actuators available in the market are mostly designed for high force and low speed applications, a slider-crank mechanism is used instead. This time, cables are guided by pulleys. Two sets of cables on the two opposite sides of the hip and the knee platforms form four parallelograms on each side of the platforms.

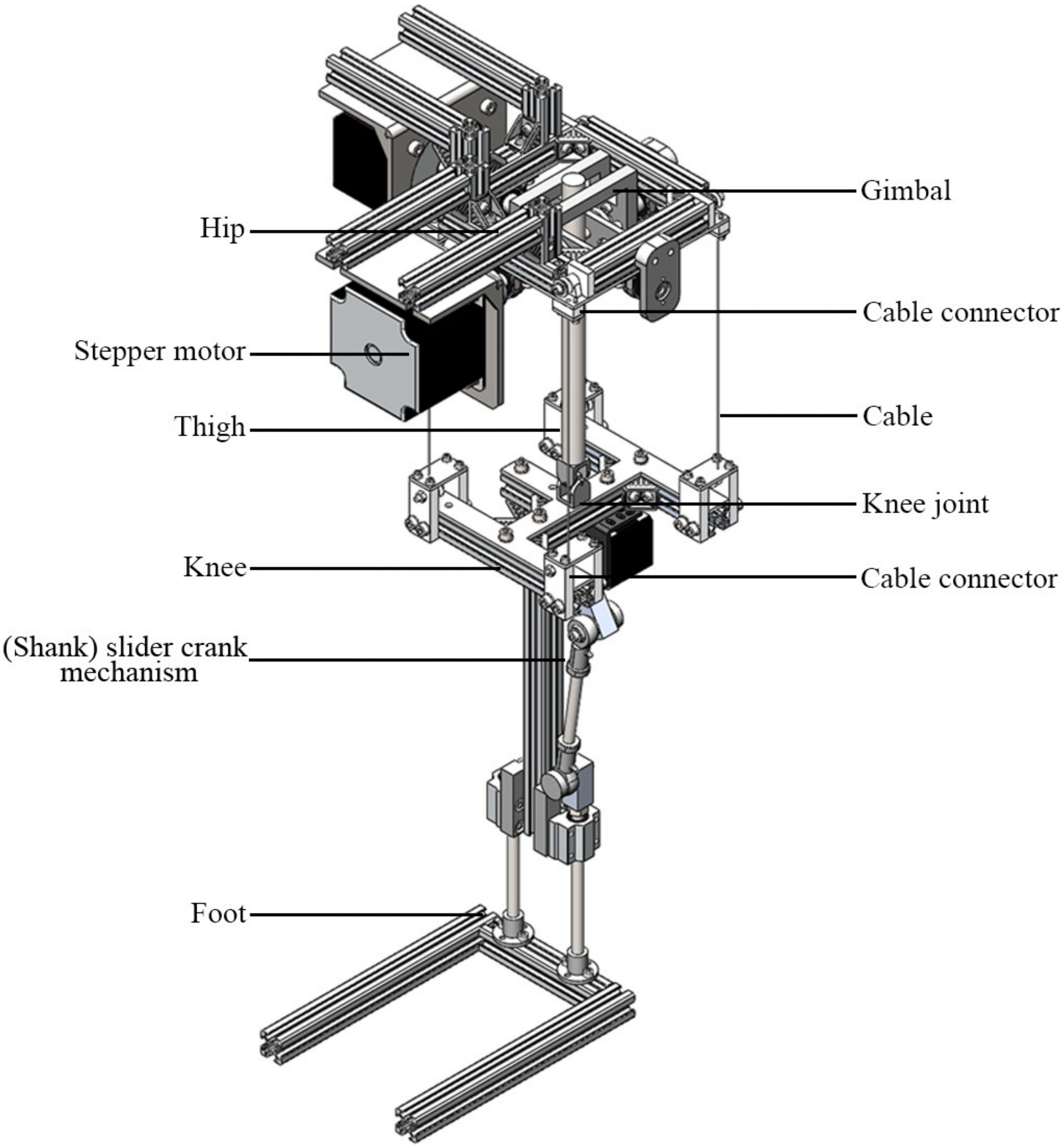

Figure 5.1. Mechanical design of the leg mechanism.

The main specifications and dimension parameters are listed in Table 5.1 and Table 5.2 by referring dimensions shown in Figure 5.2. 3-dof leg mechanism is designed for 200x50 mm step length and height ($S_H x S_L$). m_L is the total mass of the mechanism without actuators. Dimensions are determined according to 200x50 mm step. Square platforms have a side length of l_P for the hip and the knee platforms. Length of thigh link (l_T) is determined according to 30° rotation of θ_{H1}. Also, the maximum value of Δs is calculated as 80 mm for this step size. Thus, crank (l_C) and coupler (l_{CO}) lengths of the slider-crank mechanism are designed for this stroke. Coupler/Crank ratio (l_C/l_{CO}) is selected as 2.

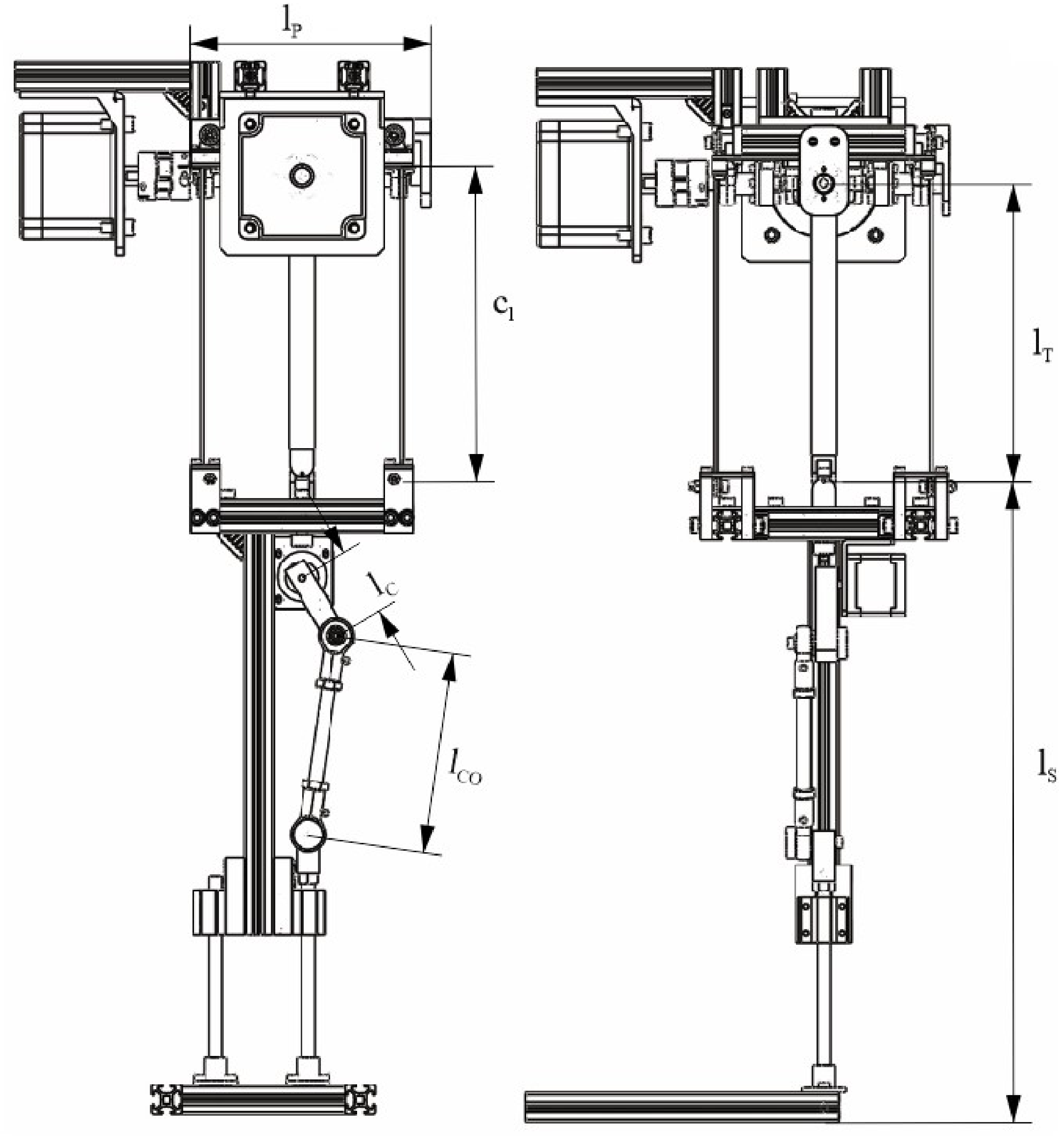

Figure 5.2. Dimension parameters of the leg mechanism.

Table 5.1. Main specifications of the leg mechanism.

DOF	m_L (kg)	Step size (mm)	Step cycle (s)
3	10.84	200 × 50	8

Table 5.2. Dimension parameters (in mm) of the leg mechanism.

l_P	c_l	l_T	l_C	l_{CO}	l_S
150	200	200	65	135	353

Mass values of each component are listed in Table 5.3 for the hip platform (m_H), the knee platform (m_K), the foot platform (m_F), thigh (m_T), the rotary actuators (m_{H1}, m_{H2} and m_S) and the slider-crank mechanism without actuator (m_{Sl}). Overall mass of the mechanism is about 10.84 kg.

Table 5.3. Mass values (in grams) of the model in Figure 5.1.

m_H	m_K	m_F	m_T	m_{H1}	m_{H2}	m_S	m_{Sl}
2425	685	453	350	2800	2800	1100	231

5.1.2. Purchased and Manufactured Components

Purchased components in the prototype are shown in Figure 5.3. Platforms are composed of aluminum profiles and connection components are shown in Figure 5.3 (a). Stepper motors are used as actuators (see Figure 5.3 (b)). Two rotary actuators (Oriental Motor Pk E 4.5A) on the hip rotates the gimbal components. Another stepper motor (Shinano SST59D-5150) actuates the slider-crank mechanism. Stepper motors on the hip are connected to the gimbals by steel shafts, couplings and flanges (Figure 5.3 (c)). Linear (SC8UU) and two types of pillow block bearings (KP008 and PK008) are used to connect the shafts to the platforms (Figure 5.3 (d)). Turnbuckles are used to tensioning cables and they consist of two opposite threads (right- and left-hand threads) at each end (Figure 5.3 (e)). Pulleys (V624zz) are selected as V-groove bearings and the knee joint (KP008) is a passive universal joint (Figure 5.3 (f)). Female rod end bearings (PHS08A) are used to connect links of the slider crank mechanism. Eccentricity due to manufacturing in the slider crank mechanism can be compensated with these bearings. Most of the components obtained from the market (shaft connectors, bearings, etc.) are selected from Do-It-Yourself 3D printer components. These components are useful and easily accessible for low-cost prototypes.

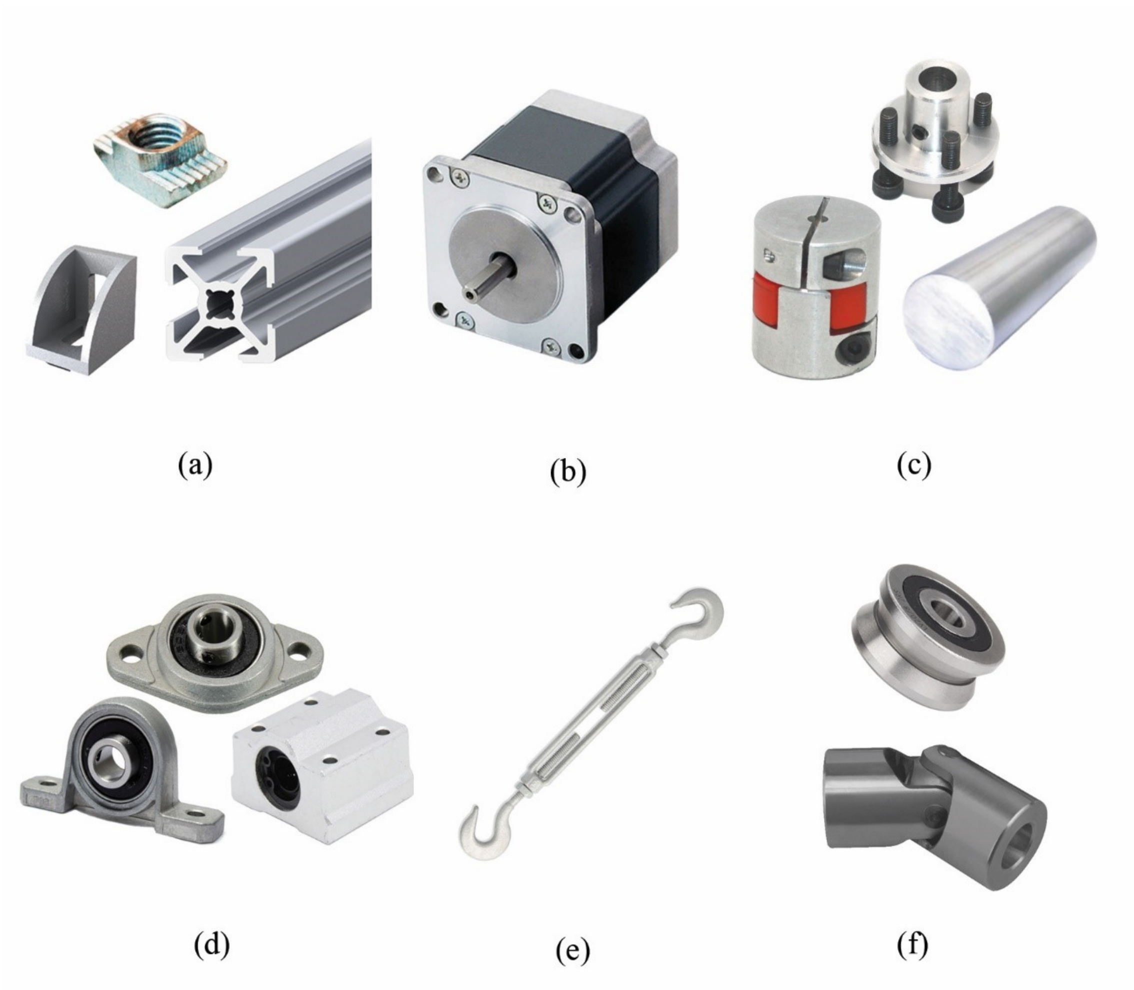

Figure 5.3. Purchased components in the leg mechanism (a) aluminum profiles and connection components, (b) stepper motors, (c) shafts, couplings and flanges, (d) linear and pillow block bearing, (e) v-groove pulleys, (f) knee joint.

Manufactured components of the leg mechanism are shown in Figure 5.4. Components of $Gimbal_H$ are shown in Figure 5.4 (a). Delrin components are produced by using a CNC Milling Machine at Metal Cutting Laboratory, Mechanical Engineering Department, IzTech. Acrylic plates and cable guides shown in Figure 5.4 (b) are cut by using a laser cutter in the Architecture Department, IzTech. The big plates are used to precisely locate the components attached to the hip and knee platforms. Cable connectors, sensor holders and linear bearing connectors are produced from ABS+ and PLA+ materials by using a 3D Printers at IzTech (Figure 5.4 (c)). The thigh link and shafts used to connect rod ends are steel shafts machined with a lathe (Figure 5.4 (d)).

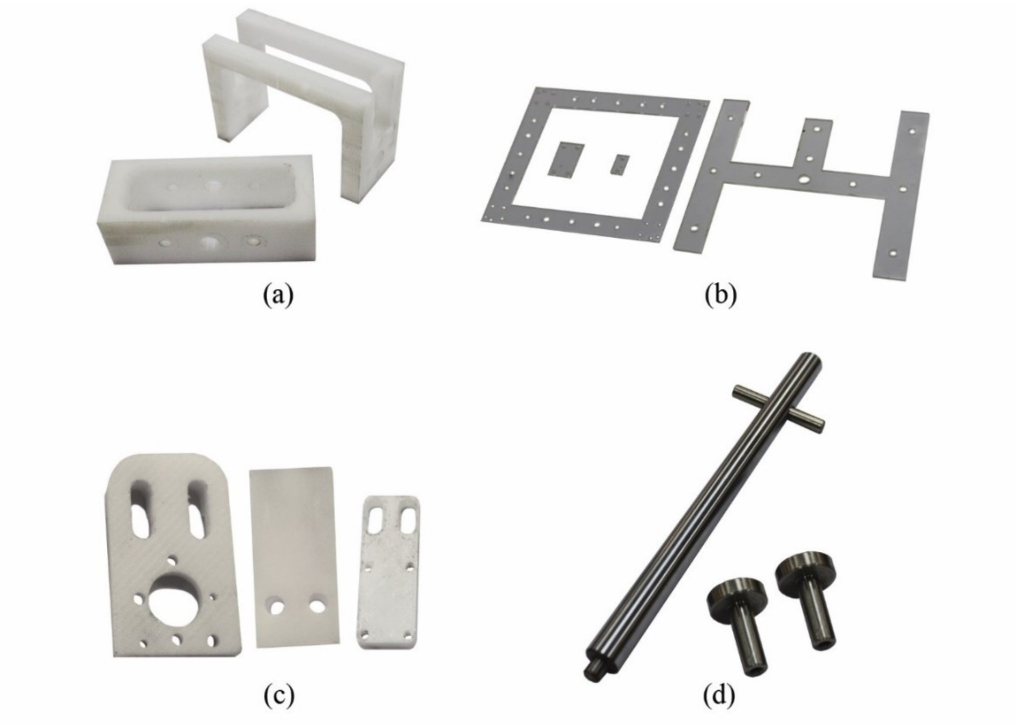

Figure 5.4. Manufactured components in the leg mechanism (a) gimbal_H components, (b) acrylic covers, (c) 3D printed components, (d) thigh link and shafts.

5.1.3. Assembled Prototype

The prototype of the leg mechanism is shown in Figure 5.5. Firstly, aluminum profiles of the platforms connected, and pulley connectors are mounted at the corners of the platforms. Acrylic plates are used to attach the bearings and the knee joint on the hip and the knee platforms. The thigh link is connected to the gimbal and the knee joint. A simple jig is used to keep the hip and the knee platforms parallel to each other. Cables are guided with holes on small acrylic plates and pulleys and tensioned with turnbuckles on the knee platform and a screw on the hip platform. The stepper motor of the lower leg is mounted on the knee platform. The slider-crank mechanism components are assembled.

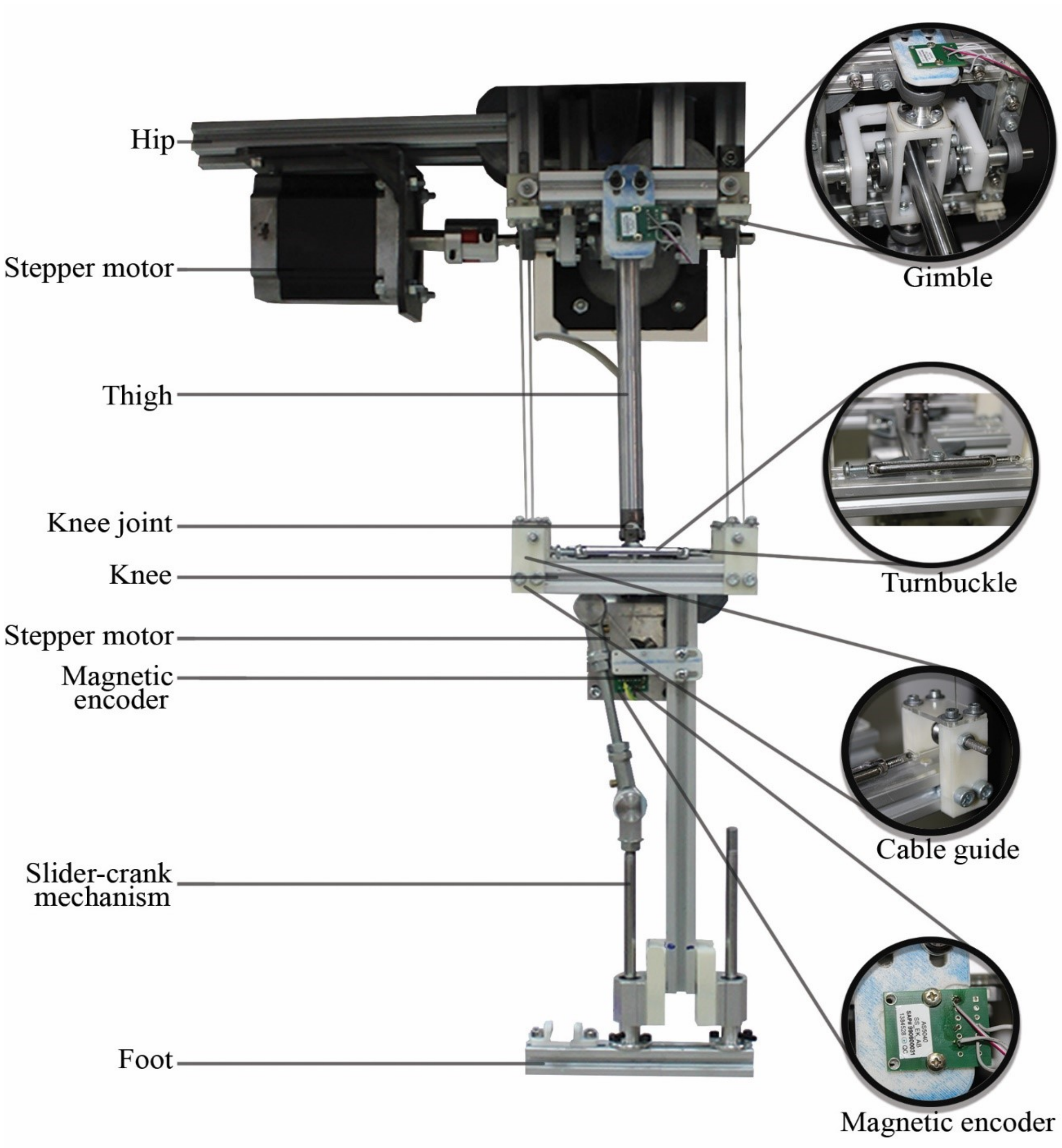

Figure 5.5. Prototype of the leg mechanism.

5.2. Experimental Validation

In this section, experimental validation of the built prototype is presented. Magnetic encoders attached on the actuated shafts and connected to a real time PCI controller card together with the stepper motor drivers. 5th order polynomials are used for the stepper motor inputs. Open loop velocity profile control of the leg mechanism is coded in Matlab/Simulink® environment and the control commands are sent to the PCI controller. Finally, experimental results presented.

5.2.1. Experimental Setup

Figure 5.6 shows experimental setup of the proposed leg mechanism. A Humosoft PCI card (MF 624) is used as controller. The leg mechanism is actuated by two high torque (6.2 N·m) stepper motors (Oriental motor, Pk299.E.4.5A) and a low torque (1.5 N·m) stepper motor (Shinano SST59D-5150). Two magnetic encoders (AS5048B) are used with magnets connected on input shafts. Stepper motors are actuated by two types of stepper drivers (DQ258M and DM278M). A black fixed reference frame is constructed to fix mechanism. A water gage is used for leveling the hip platform and the stepper motors on the black fixed reference frame. A white cardboard connected on the back side of the fixed frame. Planned trajectory printed out and fixed on the cardboard to track trajectory of the foot point with a laser.

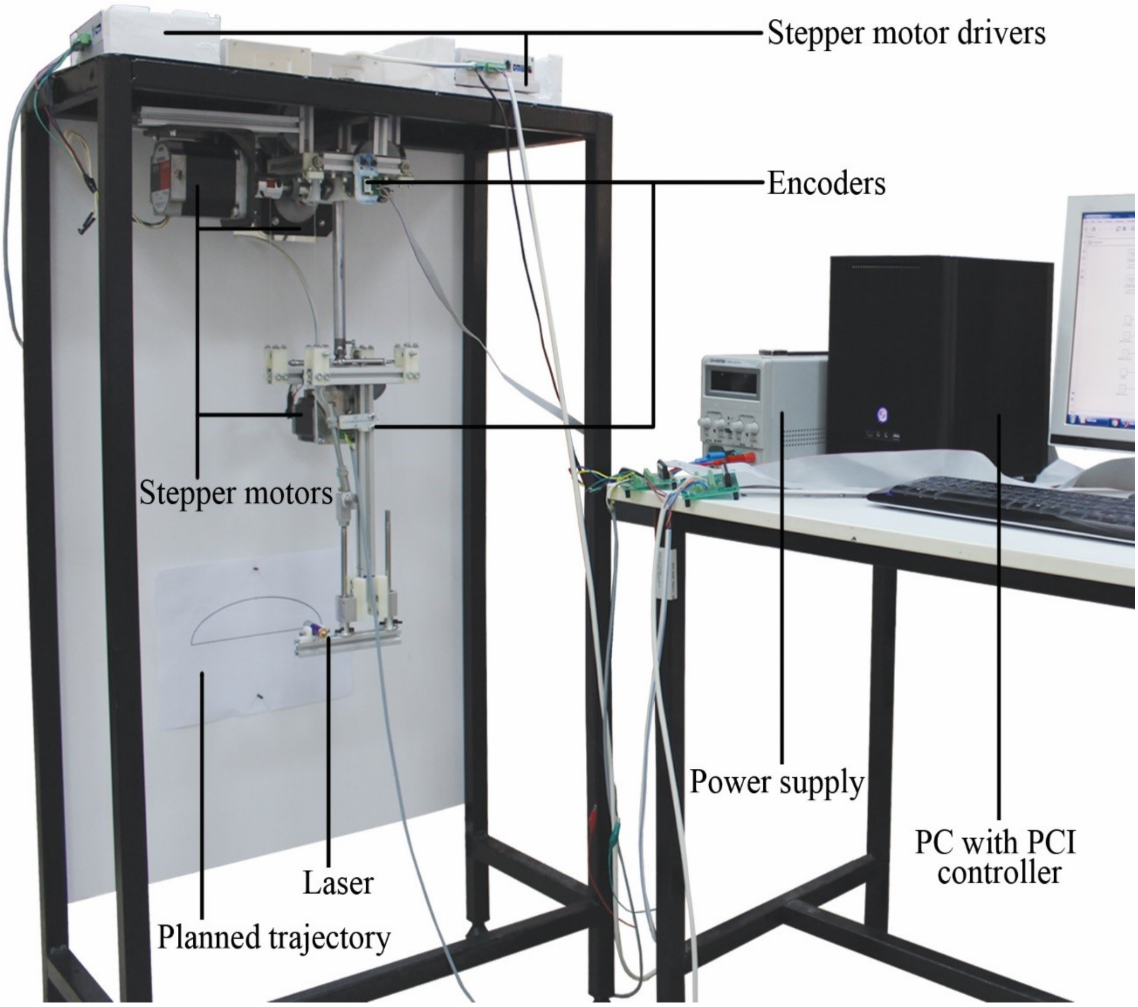

Figure 5.6. Experimental setup of the leg mechanism.

5.2.2. Simulink Model for Experiments

Stepper motors drivers require digital pulse and direction signals. Humosoft PCI controller's frequency and digital outputs used to generate pulse and direction signals, respectively. Also, incremental encoder channels are connected to the magnetic encoders. A Simulink model is prepared for Humosoft PCI controller to run at 10 kHz (Figure 5.7). Speed of the stepper motors are controlling by changing frequency of the pulse signals. Absolute of input pulse signal is input of the frequency output block. Direction signals are toggling from 0 (low) to 1 (high) according to sign of pulse signal. Inputs of each motor multiplied by a gain according to micro step setting of corresponding drivers. Encoder data is multiplied with 360/1024 for mapping 10-bit data into degrees.

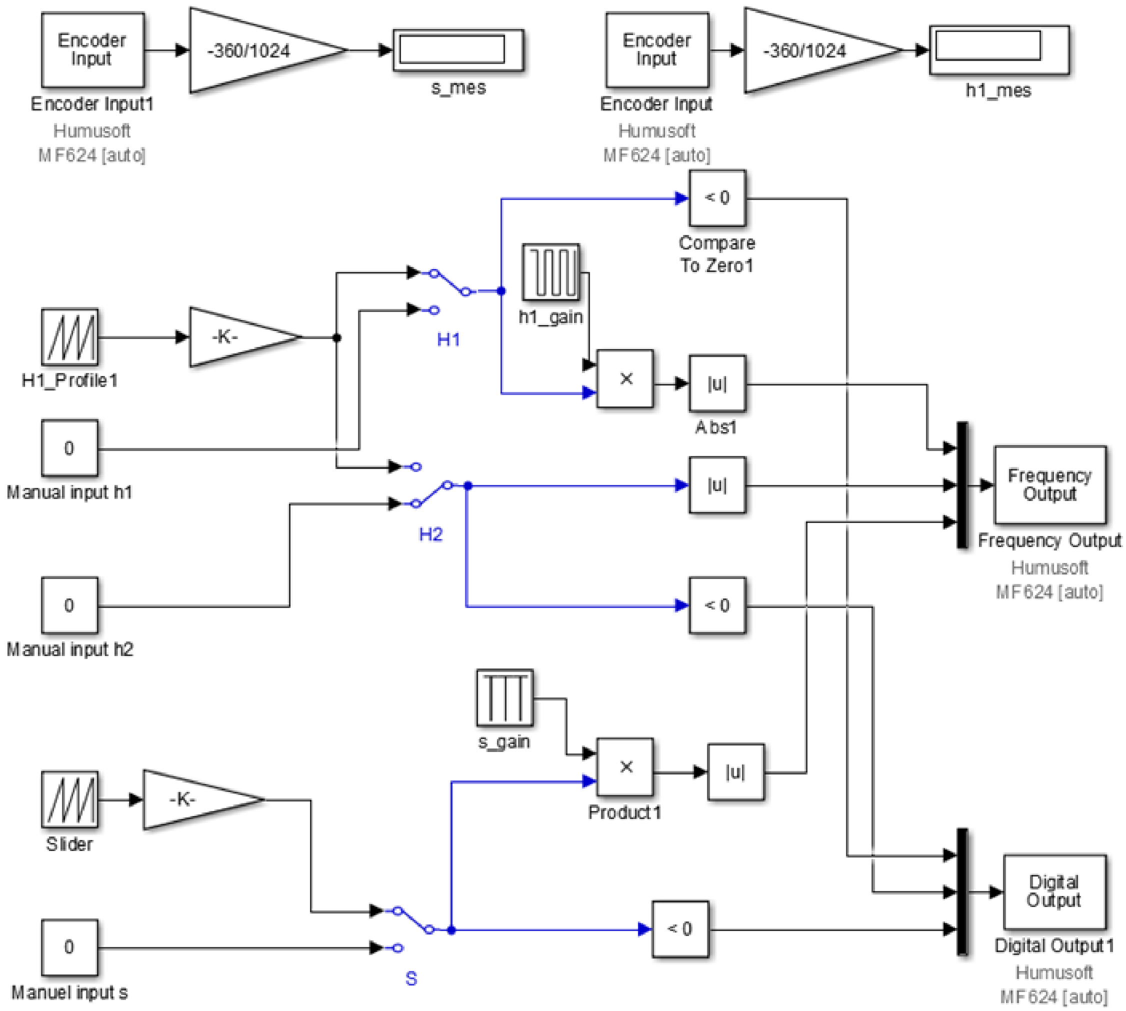

Figure 5.7. Simulink model for the experiments.

5.2.3. Walking Gait Planning for Experiments

A 5th order spline is used for the actuator inputs for the human-like walking gait in sagittal plane. This polynomial is calculated according to the following equation:

$$q(t) = a_0 + a_1 t + a_2 t^2 + a_3 t^3 + a_4 t^4 + a_5 t^5 \tag{5.1}$$

where

$$a_0 = q_i \tag{5.2}$$

$$a_1 = \dot{q}_i \tag{5.3}$$

$$a_2 = \frac{1}{2}\ddot{q}_i \tag{5.4}$$

$$a_3 = \frac{1}{2dt^3}\left[20(q_f - q_i) - \left(8\dot{q}_f + 12\dot{q}_i\right)dt - \left(3\ddot{q}_f - \ddot{q}_i\right)dt^2\right] \tag{5.5}$$

$$a_4 = \frac{1}{2dt^4}\left[30(q_f - q_i) - \left(14\dot{q}_f + 16\dot{q}_i\right)dt - \left(3\ddot{q}_f - 2\ddot{q}_i\right)dt^2\right] \tag{5.6}$$

$$a_5 = \frac{1}{2dt^5}\left[12(q_f - q_i) - \left(6\dot{q}_f + 6\dot{q}_i\right)dt - \left(\ddot{q}_f - \ddot{q}_i\right)dt^2\right] \tag{5.7}$$

q_i and q_f represent the initial and final position values. Velocity and acceleration values of corresponding position variables are indicated with single dot and double dots, respectively.

Trajectory of the foot point defined as combination of a half ellipse and a straight line (Figure 5.8). 200 x 50 mm (S_L x S_H) human-like walking gait planned for 8 s step time (S_t) sagittal plane motion. Half ellipse segment corresponds to swinging phase of the walking, where straight line segment corresponds to stance phase. The foot point follows A-B-C-A sequence with respect to time values listed in Table 5.4. Position level kinematic analysis is performed in Chapter 4. However, s value should be recalculated according to crank angle θ_s (equation 5.8).

$$\theta_S = \cos^{-1}\left(\frac{l_C^{\,2} + s^2 - l_{CO}^{\,2}}{2 l_C s}\right) \tag{5.8}$$

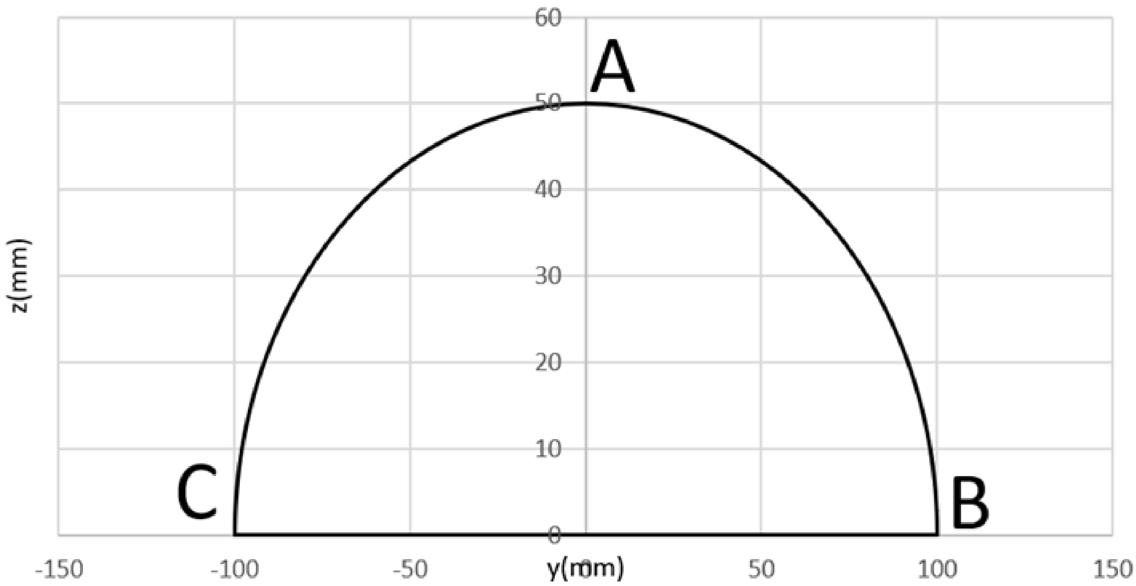

Figure 5.8. Trajectory of the foot point in sagittal plane (yz plane).

Table 5.4. Step sequence of the foot point.

Time	Position
0	A
2	B
6	C
8	A

Angular displacements of the actuated hip joint (θ_{H1}) and the slider-crank mechanism (θ_S) is computed in 3 segments which are AB (0-2 s), BC (2-6 s) and CA (6-8s) segments. AB and CA segments represents half ellipse part, while BC segment is linear part. Velocity and acceleration values at points A, B and C is 0. Velocity profiles of the actuated joints are shown in Figure 5.9 for a single step. Other actuated hip joint has no motion (θ_{H2}=0) during the planned trajectory.

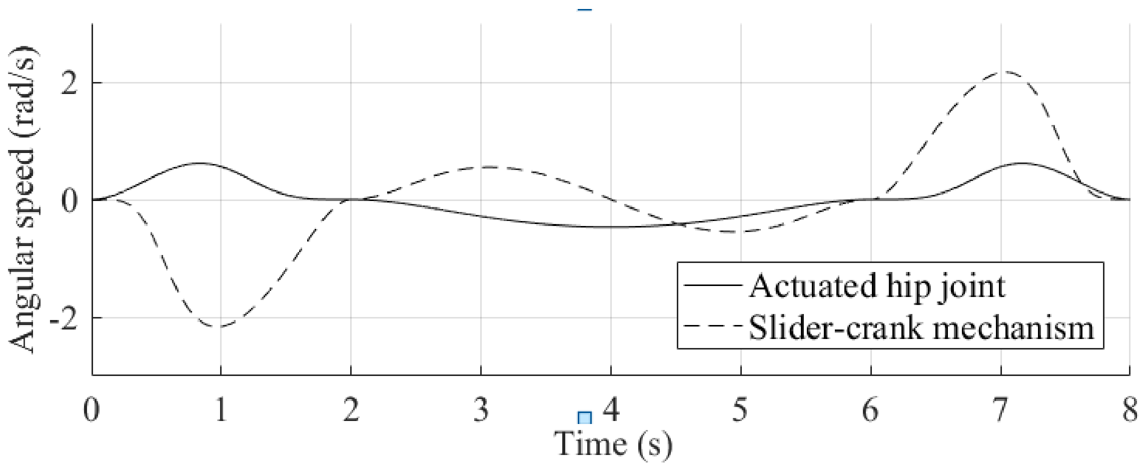

Figure 5.9. Velocity profiles of the actuated joints.

5.2.4. Experimental Results

The leg mechanism is operated for the prescribed trajectory presented in Section 5.2.3. A walking trajectory is traces three times (3 steps) and angular displacements of the actuated shafts are measured using rotary magnet encoders. This test is repeated 3 times to check for repeatability. Frequency of the input data and PCI controller is set to 10 kHz during the experiments. Snapshots of the first step are shown in Figure 5.10.

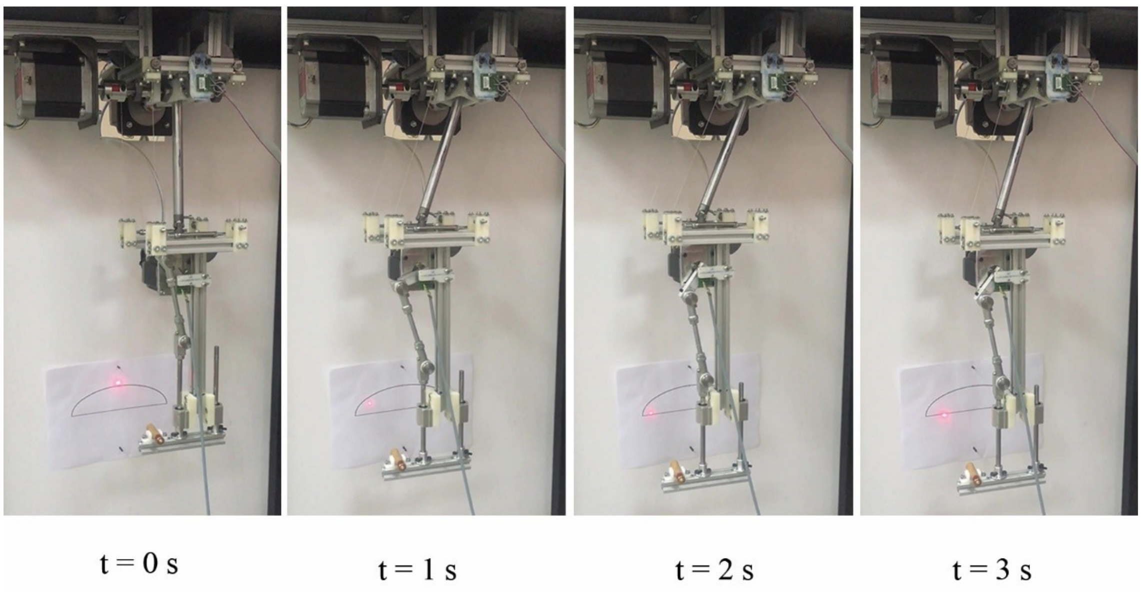

Figure 5.10. Snapshots of the first step.

(cont. on next page)

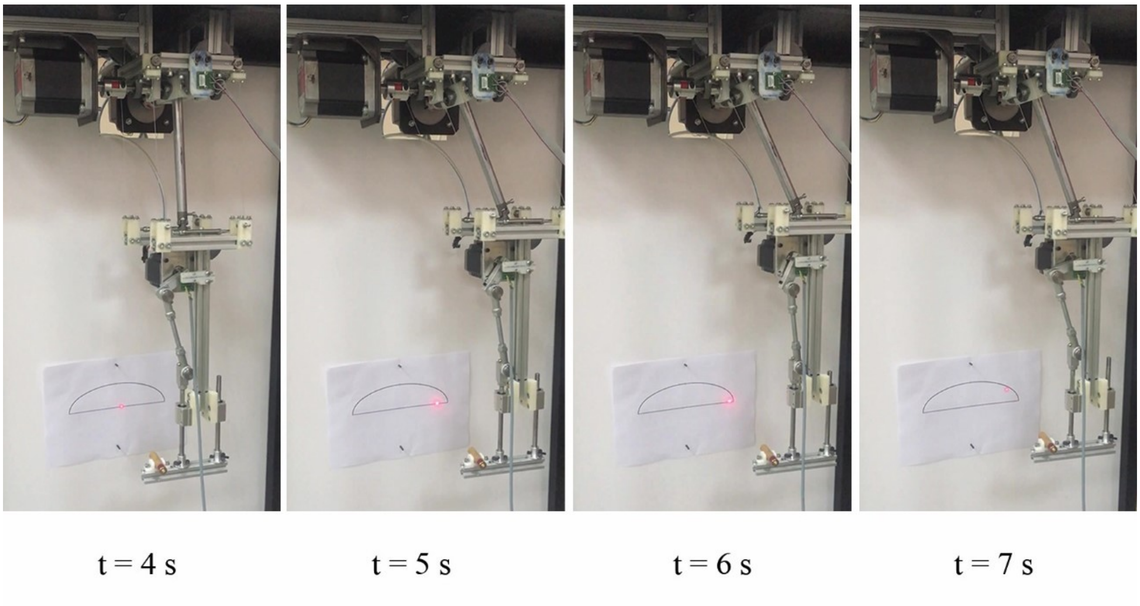

Figure 5.10 (cont.)

Desired and measured angular displacements of the actuated joints (θ_{H1}, θ_S, θ_{H1mes}, θ_{HSmes}) for 3 sets of 3 steps of walking is shown in Figure 5.11. Repeatability of the motion is satisfactory, but accuracy is not. The maximum error for the hip joint is $\Delta\theta_{H1}$ = 4.34°, whereas for the slider crank mechanism it is $\Delta\theta_S$ = 3.51°.

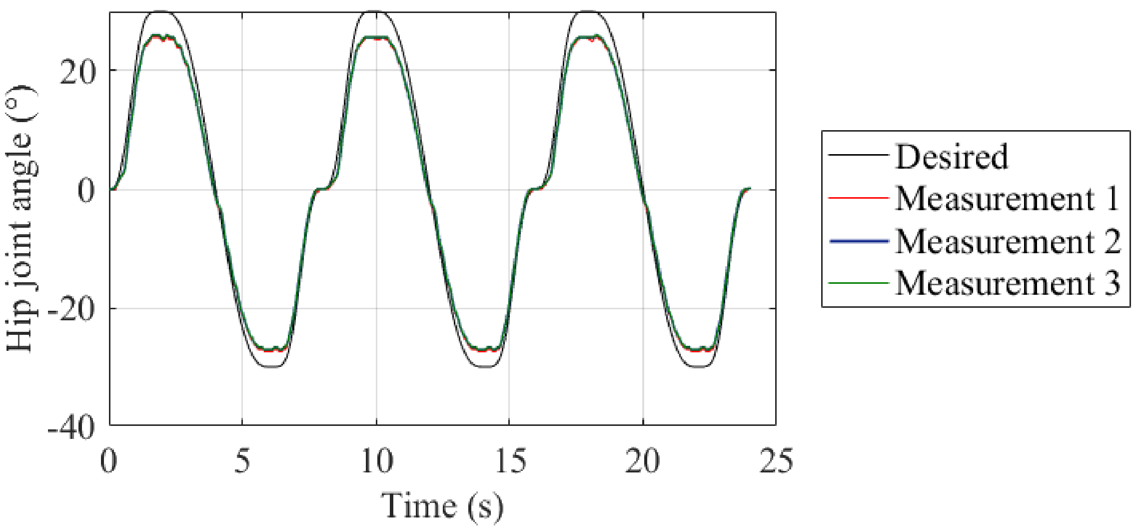

(a)

Figure 5.11. Desired and measured angular displacements of the actuated joints (a) hip joint (θ_{H1}), (b) slider-crank mechanism (θ_S).

(cont. on next page)

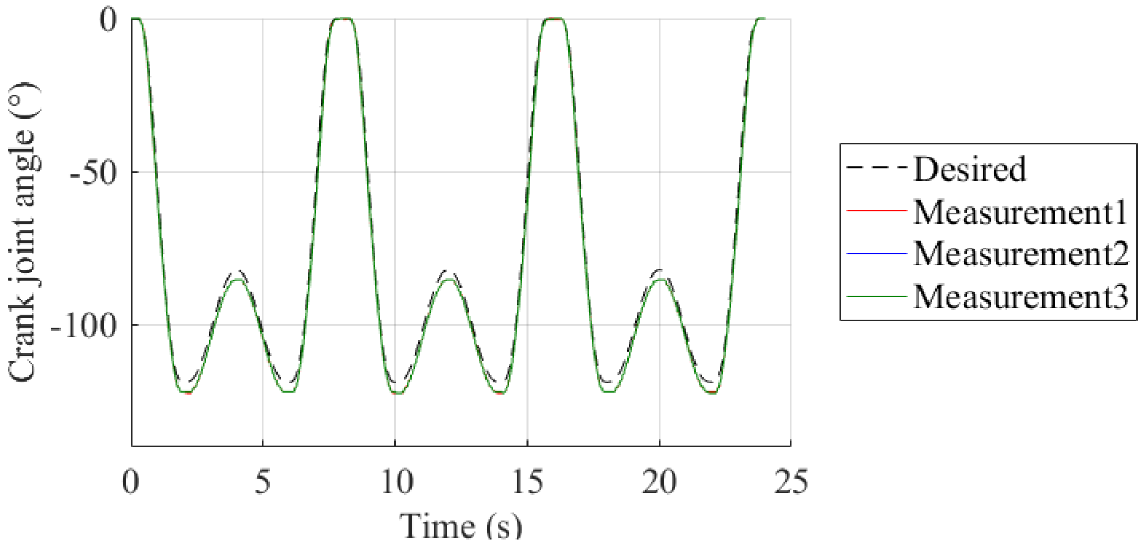

(b)

Figure 5.11 (cont.)

To decrease the angular error values, encoder data are collected, and input velocity profiles are amplified by proportional gains (H_{1Gain} and s_{Gain}). H_{1Gain} and s_{Gain} values are tuned based on the previous 3 sets of encoder measurements. The mechanism is operated for another 3 steps with proportional gains. Snapshots of the amplified input motion are shown in Figure 5.12.

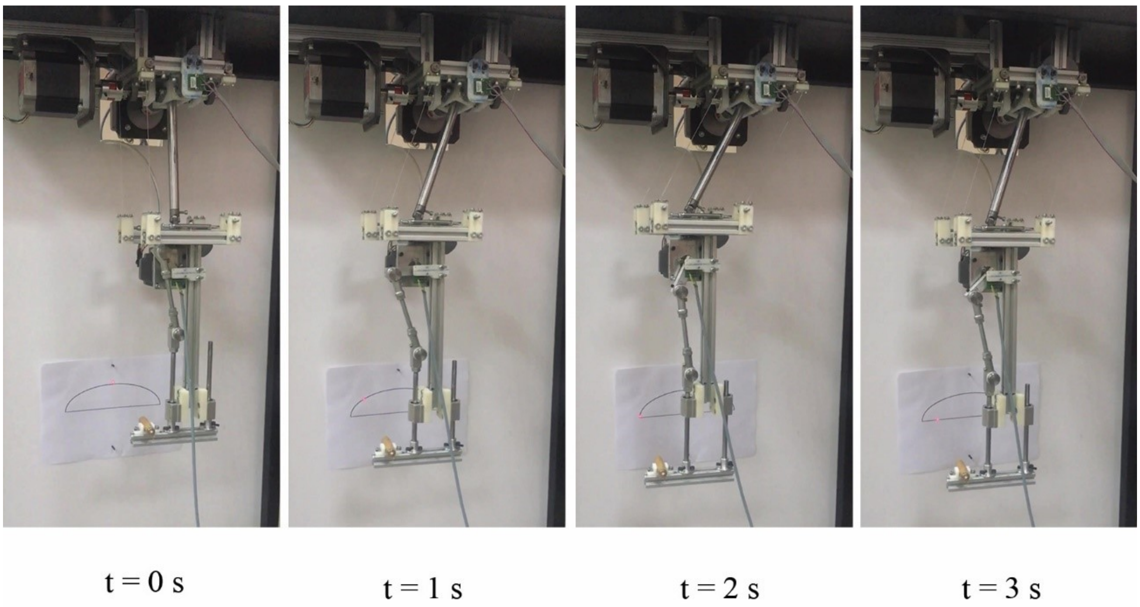

Figure 5.12. Snapshots of amplified input motion.

(cont. on next page)

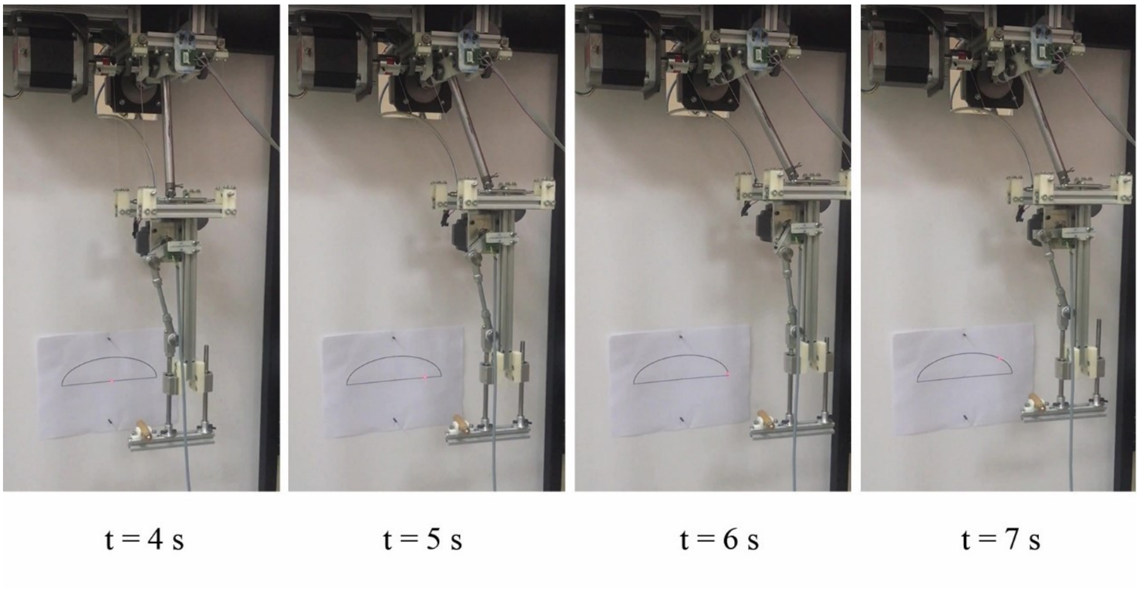

Figure 5.12 (cont.)

The desired and measured angular displacements of the actuated joints (θ_{H1}, θ_S, θ_{H1mes}, θ_{HSmes}) for 3 steps of walking are shown in Figure 5.13. Maximum errors of the hip joint are $\Delta\theta_{H1M1}$ = 0.93°, $\Delta\theta_{H1M2}$ = 1.28° are $\Delta\theta_{H1M3}$ = 1.29° for measurement 1, measurement 2 and measurement 3, respectively. Maximum errors measured from the slider-crank mechanisms are $\Delta\theta_{SM1}$ = 1.4°, $\Delta\theta_{SM2}$ = 0.86° are $\Delta\theta_{SM3}$ = 0.82°. The mechanism accomplished the AB and BC segments successfully but there is still error during the CA segment. The tracking is much better in the tuned version.

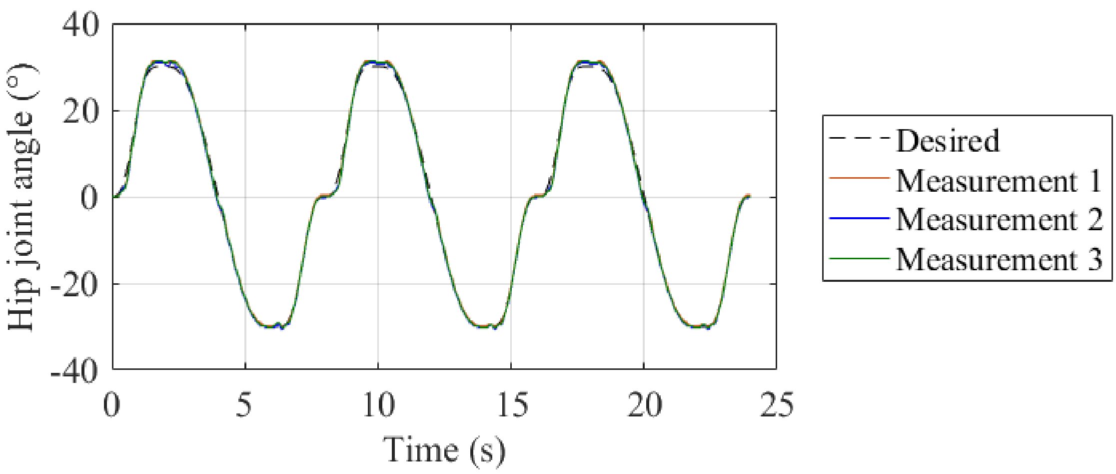

(a)

Figure 5.13. Desired and measured angular displacements of the actuated joints for amplified input (a) hip joint (θ_{H1}), (b) slider-crank mechanism (θ_S).

(cont. on next page)

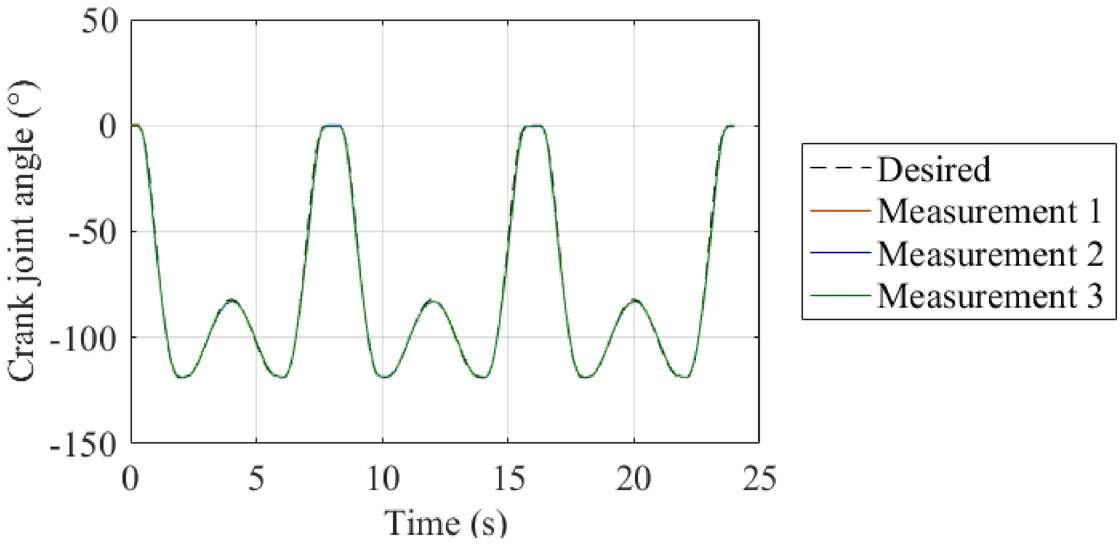

(b)

Figure 5.13 (cont.)

Desired and computed position (according to mean of encoder data of the tuned tests) of the foot point is shown in yz plane in Figure 5.14. (a). The errors in y- and z-directions are shown in Figure 5.14 (b). The maximum error between the desired and the computed position is 9.65 mm in the y-direction and 3.81 mm in the z-direction. The mechanism accomplished the AB and BC segments successfully but still there is error during the CA segment. Vibration has an important role on these errors.

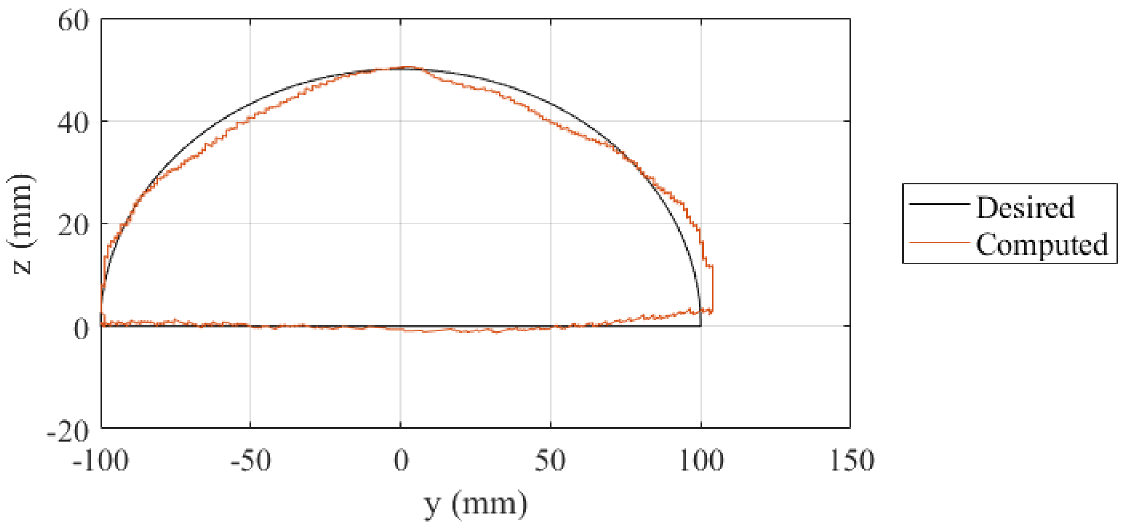

(a)

Figure 5.14. Desired and computed positions of the foot point according to encoder data (a) sagittal plane (yz plane), (b) y and z errors.

(cont. on next page)

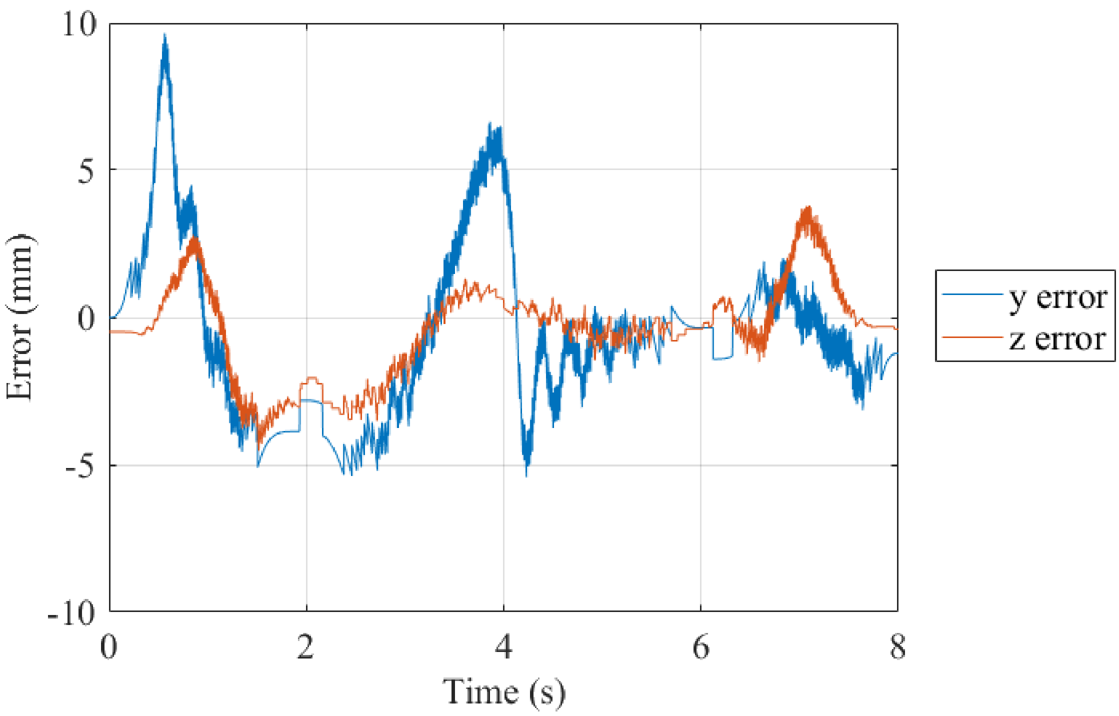

(b)

Figure 5.14 (cont.)

In order to analyze the motion of the foot, first 500 snapshots are obtained from an 8 s video. Then, these images are processed with a macro in Adobe Photoshop CC®. The macro gets raw image and eliminates all data except laser data by decreasing brightness and increasing contrast of the image. Figure 5.15 (a) and (b) shows an example of raw and processed image. Figure 5.16 shows trajectory of the foot point according to laser point data. The measured trajectory data in Figure 5.16 is in mostly accordance with the computed trajectory data in Figure 5.14.

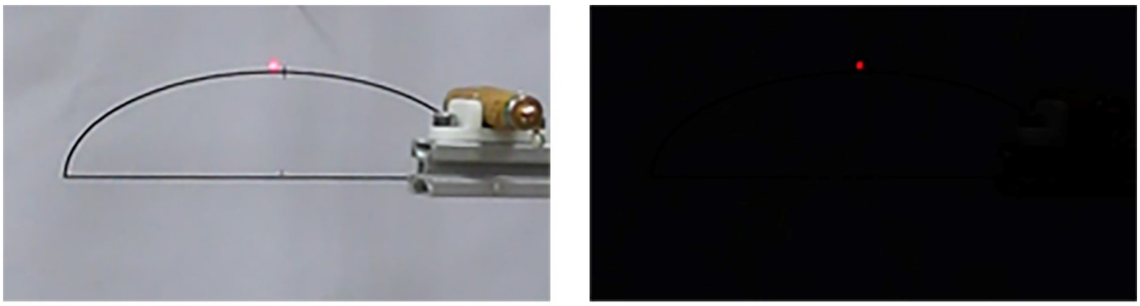

(a) (b)

Figure 5.15. Example of an image process (a) raw image, (b) processed image.

Figure 5.16. Trajectory of the foot point according to laser data.

CHAPTER 6

CONCLUSIONS

The objective of this thesis study is to propose novel cable-constrained parallel mechanisms to be used for static walking. Two different 3-dof translational parallel manipulators are proposed: (UPU-2Pa)-(UPU-2Pa) and (UU-2Pa)-P. The mechanism with anchored cables is selected for prototyping since the mechanical structure is simpler and more suitable for walking operation.

The position level kinematic analysis of the selected mechanism is performed. A CAD model is constructed and dynamic simulation with a human-like gait trajectory is carried out using SolidWorks® Motion Analysis toolbar. Once the computed actuator torques and forces found feasible, a first prototype is built to check the proposed solution. A second prototype of the (UU-2Pa)-P mechanism is built considering the identified problems in the first prototype. A slider-crank mechanism is used instead of a linear actuator in the second prototype. A 5^{th} order polynomial is used for the actuator inputs to obtain a smooth motion of the foot. Velocity profile control of the leg mechanism is performed using a real-time PCI controller and collected sensor data taken from magnetic encoders.

The mechanisms presented in this thesis is one of the few cable-constrained parallel manipulator designs in the literature. Such a manipulator design is used for a walking machine for the first time. The prototype and test results are quite satisfactory, so hopefully more detailed research can be conducted on this topic in the future.

This thesis study shows that the (UU-2Pa)-P mechanism has simple kinematic equations and is capable to accomplish human-like walking gait. A biped walking machine based on the proposed leg structure can be built, however, the stepper motors are used in the prototype are too heavy for a biped walking machine. DC motors and reducers with less weight should be used in future designs.

REFERENCES

Albus, James, Roger Bostelman, and Nicholas Dagalakis. "The NIST Robocrane." *Journal of Robotic Systems* 10, no. 5 (1993): 709-24.

Arai, Tatsuo, Kei Yuasa, Yahushi Mae, Kenji Inoue, Kunio Miyawaki, and Noriho Koyachi. "A hybrid drive parallel arm for heavy material handling." *IEEE robotics & automation magazine* 9, no. 1 (2002): 45-54.

Behzadipour, Saeed, and Amir Khajepour. "Cable-based robot manipulators with translational degrees of freedom." *Industrial Robotics: Theory, Modelling and Control*, (2006): 211-236..

Beomonte, Zobel, P. L., P. Di Stefano, and Terenziano Raparelli. "The design of a 3 dof parallel robot with pneumatic drives." *Proceedings of The International Symposium on Industrial Robots*, no. 27. International Federation of Robotics and Robotic Industries, (1996): 707-710.

Boztaş Sercan, Type Synthesis and Instantaneous Mobility Analysis of 3-UPU Parallel Manipulators. MSc. Thesis, İzmir Institute of Technology, (2017).

Callegari, Massimo, and Matteo Tarantini. "Kinematic analysis of a novel translational platform." *Journal of Mechanical Design* 125, no. 2 (2003): 308-315.

Callegari, Massimo, Matteo Palpacelli, and Marco Scarponi. "Kinematics of the 3-CPU parallel manipulator assembled for motions of pure translation." *Robotics and Automation*, Proceedings of the ICRA (2005): 4020-4025.

Carbone, Giuseppe, and Marco Ceccarelli. "Legged robotic systems." *Cutting Edge Robotics* (2005): 553-576.

Carricato, Marco, and Vincenzo Parenti-Castelli. "A family of 3-DOF translational parallel manipulators." *Journal of mechanical design* 125, no. 2 (2003): 302-307.

Ceccarelli, Marco. *Fundamentals of mechanics of robotic manipulation*. no. 27. Springer Science & Business Media, (2013).

Ceccarelli, Marco and Giuseppe Carbone. "A new leg design with parallel mechanism architecture." *Advanced Intelligent Mechatronics,* (2009): 1447-1452.

Clavel, Reymond. "Device for the Movement and Positioning of an Element in Space." U.S. Patent 4,976,582, issued December 11, 1990.

Pierrot, François, Vincent Nabat, and María de la O Rodríguez. "Schoen flies motion generator: A new non redundant parallel manipulator with unlimited rotation capability." *Robotics and Automation*, Proceedings of the ICRA (2005): 3250-3255.

Demirel, Murat, Giuseppe Carbone, Marco Ceccarelli, and Gökhan Kiper. "Design and simulation of a novel hybrid leg mechanism for walking machines." *New Advances in Mechanism and Machine Science*, Springer, (2018): 283-290.

Di Gregorio, Raffaele. "Kinematics of the translational 3-URC mechanism." *Journal of Mechanical Design* 126, no. 6 (2004): 1113-1117.

Gogu, Grigore. "Structural synthesis of fully-isotropic parallel robots with Schönflies motions via theory of linear transformations and evolutionary morphology." *European Journal of Mechanics*, no. 2 (2007): 242-269.

Honda Motor Co. Ltd., Asimo Technical Information, available online at http://asimo.honda.com/downloads/pdf/asimo-technical-information.pdf, (2007).

Joshi, Sameer, and Lung-Wen Tsai. "A comparison study of two 3-DOF parallel manipulators: One with three and the other with four supporting legs." *IEEE Transactions on Robotics and Automation* 19, no. 2 (2003): 200-209.

Kaneko, Kenji, Fumio Kanehiro, Mitsuharu Morisawa, Kanako Miura, Shin'ichiro Nakaoka, and Shuuji Kajita. "Cybernetic human HRP-4C." *Humanoid Robots,* 9th IEEE-RAS International Conference, (2009): 7-14.

Kato, Ichiro. "Development of WABOT 1." *Biomechanism* 2 (1973): 173-214.

Kim, Sung Mok, Wheekuk Kim, and Byung-Ju Yi. "Kinematic analysis and optimal design of a 3T1R type parallel mechanism." *Robotics and Automation,* Proceedings of the ICRA (2009): 2199-2204.

Kondo, Hideki, Akitoshi Morishima, Yu Ogura, Shimpei Momoki, Juri Shimizu, Hun-ok Lim, and Atsuo Takanishi. "Algorithm of pattern generation for mimicking disabled person's gait." *Biomedical Robotics and Biomechatronics,* 2nd IEEE RAS & EMBS International Conference (2008): 724-729.

Kong, Xianwen, and Clement M. Gosselin. "Kinematics and singularity analysis of a novel type of 3-CRR 3-DOF translational parallel manipulator." *The International Journal of Robotics Research* 21, no. 9 (2002): 791-798.

Kong, Xianwen, and Clément M. Gosselin. *Type synthesis of parallel mechanisms*. no. 33. Springer, (2007).

Li, Qinchuan, and Zhen Huang. "Mobility analysis of a 3-5R parallel mechanism family." *Robotics and Automation,* ICRA 2003, no. 2 (2003): 1887-1892.

Li, Yangmin, and Qingsong Xu. "Kinematic analysis and design of a new 3-DOF translational parallel manipulator." *Journal of Mechanical Design* 128, no. 4 (2006): 729-737.

Lohmeier, Sebastian, Thomas Buschmann, and Heinz Ulbrich. "Humanoid robot LOLA." *Robotics and Automation,* ICRA (2009): 775-780.

Lu, Yi, Yan Shi, Zhen Huang, Jianping Yu, Shihua Li, and Xingbin Tian. "Kinematics/statics of a 4-DOF over-constrained parallel manipulator with 3 legs." *Mechanism and Machine Theory* 44, no. 8 (2009): 1497-1506.

Mayhew, David, Benjamin Bachrach, W. Zev Rymer, and Randall F. Beer. "Development of the MACARM-a novel cable robot for upper limb neurorehabilitation." *Rehabilitation Robotics,* ICORR (2005): 299-302.

Merlet, Jean-Pierre. *Parallel robots*. no. 128. Springer Science & Business Media, 2006.

Mifflin, Houghton. "The American heritage college dictionary." *Houghton Mifflin (3rd ed)* (1993): 2014.

Ottaviano, Erika, Marco Ceccarelli, and Francesco Palmucci. "An application of CaTraSys, a cable-based parallel measuring system for an experimental characterization of human walking." *Robotica* 28, no. 1 (2010): 119-133.

Ottaviano, E., M. Ceccarelli, and M. De Ciantis. "A 4–4 cable-based parallel manipulator for an application in hospital environment." *Control and Automation,* Mediterranean Conference (2007)*:* 1-6.

Richard, Pierre-Luc, Clément M. Gosselin, and Xianwen Kong. "Kinematic analysis and prototyping of a partially decoupled 4-DOF 3T1R parallel manipulator." *Journal of Mechanical Design* 129, no. 6 (2007): 611-616.

Rocchi, Alessio, Enrico Mingo Hoffman, Edoardo Farnioli, and Nikos G. Tsagarakis. "A whole-body stack-of-tasks compliant control for the humanoid robot COMAN." IROS, (2015).

Romdhane, Lotfi, Z. Affi, and M. Fayet. "Design and singularity analysis of a 3-translational-DOF in-parallel manipulator." *Journal of Mechanical Design* 124, no. 3 (2002): 419-426.

Rose, Jessica. "Human walking." (1994).

Sato, Tatiana de Oliveira, Gert-Åke Hansson, and Helenice Jane Cote Gil Coury. "Goniometer crosstalk compensation for knee joint applications." *Sensors* 10, no. 11 (2010): 9994-10005.

Saunders J.B., Inman V. T., and Eberhart H.D. "The major determinants in normal and pathological gait." *JBJS* 35, no. 3 (1953): 543-558.

Sugahara, Yusuke, Tatsuro Endo, Hun-ok Lim, and Atsuo Takanishi. "Design of a battery-powered multi-purpose bipedal locomotor with parallel mechanism." *Intelligent Robots and Systems,* IEEE/RSJ International Conference no. 3 (2002): 2658-2663.

Tsai, Lung-Wen, Gregory C. Walsh, and Richard E. Stamper. "Kinematics of a novel three DOF translational platform." *Robotics and Automation,* IEEE International Conference no. 4 (1996): 3446-3451.

Vukobratović, Miomir, and J. Stepanenko. "On the stability of anthropomorphic systems." *Mathematical biosciences* 15, no. 1-2 (1972): 1-37.

Wang, M. F., and Marco Ceccarelli. "Design and simulation for kinematic characteristics of a tripod mechanism for biped robots." *22nd International Workshop on Robotics in Alpe-Adria-Danube Region, Portorož, Slovenia* no. 13, (2013): 124-131.

Yu, Zhangguo, Qiang Huang, Gan Ma, Xuechao Chen, Weimin Zhang, Jing Li, and Junyao Gao. "Design and development of the humanoid robot BHR-5." *Advances in Mechanical Engineering* 6 (2014).